Lappeenranta
University of Technology

Ari Vepsäläinen

HETEROGENEOUS MASS TRANSFER IN FLUIDIZED BEDS BY COMPUTATIONAL FLUID DYNAMICS

Thesis for the degree of Doctor of Science (Technology) to be presented with due permission for public examination and criticism in the Auditorium 1382 at Lappeenranta University of Technology, Lappeenranta, Finland on the 2nd of December, 2014, at noon.

Acta Universitatis
Lappeenrantaensis 605

Supervisor Professor Timo Hyppänen
Department of Energy Technology
Lappeenranta University of Technology
Finland

Reviewers Doctor Fabrizio Scala
Institute for Research on Combustion
National Research Council
Italy

Professor Filip Johnsson
Department of Energy and Environment
Chalmers University of Technology
Sweden

Opponent Doctor Fabrizio Scala
Institute for Research on Combustion
National Research Council
Italy

ISBN 978-952-265-688-9
ISBN 978-952-265-689-6 (PDF)
ISSN-L 1456-4491
ISSN 1456-4491
Lappeenrannan teknillinen yliopisto
Yliopistopaino 2014

Abstract

Ari Vepsäläinen
HETEROGENEOUS MASS TRANSFER IN FLUIDIZED BEDS BY COMPUTATIONAL FLUID DYNAMICS
Lappeenranta 2014
130 pages
Acta Universitatis Lappeenrantaensis 605
Diss. Lappeenranta University of Technology
ISBN 978-952-265-688-9, ISBN 978-952-265-689-6 (PDF), ISSN-L 1456-4491, ISSN 1456-4491

The main objective of this research is to estimate and characterize heterogeneous mass transfer coefficients in bench- and pilot-scale fluidized bed processes by the means of computational fluid dynamics (CFD). A further objective is to benchmark the heterogeneous mass transfer coefficients predicted by fine-grid Eulerian CFD simulations against empirical data presented in the scientific literature.
First, a fine-grid two-dimensional Eulerian CFD model with a solid and gas phase has been designed. The model is applied for transient two-dimensional simulations of char combustion in small-scale bubbling and turbulent fluidized beds. The same approach is used to simulate a novel fluidized bed energy conversion process developed for the carbon capture, chemical looping combustion operated with a gaseous fuel. In order to analyze the results of the CFD simulations, two one-dimensional fluidized bed models have been formulated. The single-phase and bubble-emulsion models were applied to derive the average gas-bed and interphase mass transfer coefficients, respectively.
In the analysis, the effects of various fluidized bed operation parameters, such as fluidization, velocity, particle and bubble diameter, reactor size, and chemical kinetics, on the heterogeneous mass transfer coefficients in the lower fluidized bed are evaluated extensively. The analysis shows that the fine-grid Eulerian CFD model can predict the heterogeneous mass transfer coefficients quantitatively with acceptable accuracy. Qualitatively, the CFD-based research of fluidized bed process revealed several new scientific results, such as parametrical relationships. The huge variance of seven orders of magnitude within the bed Sherwood numbers presented in the literature could be explained by the change of controlling mechanisms in the overall heterogeneous mass transfer process with the varied process conditions. The research opens new process-specific insights into the reactive fluidized bed processes, such as a strong mass transfer control over heterogeneous reaction rate, a dominance of interphase mass transfer in the fine-particle fluidized beds and a strong chemical kinetic dependence of the average gas-bed mass transfer. The obtained mass transfer coefficients can be applied in fluidized bed models used for various engineering design, reactor scale-up and process research tasks, and they consequently provide an enhanced prediction accuracy of the performance of fluidized bed processes.

Keywords: Combustion, Eulerian CFD, Fluidization, Heterogeneous mass transfer
UDC 66.021.3:519.6:004.942:697.326:517.581:66.096.5:544.45

Acknowledgements

First, I like to thank my family, parents Veikko and Rea Vepsäläinen, foster parents Erkki and Helena Björklund, brothers Reijo and Joni Vepsäläinen, and foster brothers Ari and Martti Björklund, for everything.

Considering the time and efforts spend on the research field of the thesis, acknowledgement is given for the supervisors of the work, professor Timo Hyppänen and associate professor Jouni Ritvanen. The research project with associated practical academic work has truly been a great academic adventure, and their various advices regarding scientific publishing, overall content, specific analysis methods and English grammar made my effort little comfortable during the long months of the research. Professor Timo Hyppänen earns a long and deep congratulation for giving an opportunity to work with such an interesting research topic, but also for providing funding for the research via sustainable-energy-production themed project of Academy of Finland and Fortum Oy.

The thesis benefits from the valuable help for the practical CFD related aspects shared within the research group, modeling of energy processes. Especially, I wish to thank doctor Srujal Shah and doctor Kari Myöhänen for the helpful advices and guidance given. Indeed, the Eulerian CFD simulation of the reactive fluidized beds is the main research method applied in the thesis. Also, co-operation with Petteri Peltola regarding the research of CLC process is appreciated. Here, I wish to gently stand up and send warm greetings also to the other members of the research team.

The reviewers, doctor Fabrizio Scala and professor Filip Johnsson, are acknowledged for their professional comments and guidance benefitting the content of the thesis. Also, Sinikka Talonpoika and Sari Silventoinen are appreciated for the proofreading that gave the text its final academic shine.

It is evident that the research owns much for the partners that funded it. I wish to express my polite greetings to the funding partners. These include (i) Academy of Finland, (ii) Fortum Oy, (iii) Technical University of Lappeenranta, and (iv) Research Foundation of Lappeenranta University of Technology. I hope you feel that the research with its numerous new practical and scientific results, and novel repeatable research methods is truly worth of your high expectations from the modern thesis work representing the highest academic degree.

Consequently, I wish to congratulate the teachers of the post-graduate courses I attended, especially professor Esa Vakkilainen and associate professor Payman Jalali. The studies provided both the deep academic knowledge and broad overview of trends in the commercial and technological development. I might also be pleased with the practical and beneficial professional know-how these studies offered i) helping in the practical research work and ii) gaining the import competence in the labour market.

It can be mentioned that the thesis would not had been possible to be designed to its hopefully-future-generations-inspiring structure without long- and short-term help of my former superiors, Arto Hotta and Ari Kettunen. Consequently, it is my honor and deep wish to send polite greetings to my other former superiors: professor Pertti Sarkomaa, Ragnar Lundgvist, Ilkka Venäläinen, Pertti Hätinen and Timo Jäntti. The above-mentioned gentlemen have been involved in pointing me diverse set of engineering tasks that have

helped in gaining practical know-how on the fluidized bed processes. Therefore, providing greater assets to focus the research to the most important aspects of the wide-ranged research field of the fluidized bed processes.
Now, I feel that also the former tacit and practical knowledge that inspired the focus of the research should be appreciated. Thus, I wish a fruitful life for the several inspiring professionals of the art with whom I have had opportunity to discuss considering the great mysteries of the fluidized bed processes during the years I was working in the Technology, and Research and development departments at Foster Wheeler. Daily social community of experts, field-testing visits to various operating research and industrial units, and meetings with diverse set of research professionals from the national and international research institutions have definitively influenced on the very essence of the thesis that tries to answer to a very practical engineering question with the modern computational research means.
I wish to point out, that there is a long list of true professionals, especially in the practical side of art, that deserve acknowledgement. Particularly, I wish to address my respectful greetings for few members of the professional community of fluidized bed combustion: Ossi Sippu, Toni Suutarinen, Marko Siitari, Eero Hälikkä, Tarmo Hatunen, Teemu Nevalainen and Esa Venäläinen. These gentlemen have certainly made difference on my philosophy, also with respect to the practically important aspects in the fluidized bed combustion process. In practice, there are many people I would like to thank. However, I settle here to share polite greetings for the people of Foster Wheeler I have worked with. I also send very warm wishes for the members of sporty community called KeSSi.
Sometimes, cold facts matter. Therefore, I may also express my gratitude to the IAET - the unemployment fund for members of the Confederation of Unions for Academic Professionals in Finland - for providing funding during the unemployment periods of my professional career, especially during the last one and half year before the doctoral dissertation. Thanks for providing the social safety web for the professionals-needed-no-more, and in-hunt for the next opportunity.
The thesis work was carried out mostly in the department of Energy Technology at Lappeenranta University of Technology between 2009 and 2013. I wish wellbeing, wise tolerance and enthusiastic attitude for all the academic members of LUT, LUT Energy and Energy Technology. I would especially like to mention the contribution of Juha Kaikko, Srujal Shah and Alexander Maximov for keeping the in-the-house spirit high during the daily coffee breaks. A special appreciation goes also to all nice people that participated with a true passion in their hearts to the various sport events of sport club SLUT - Sports by LUT - out of the intensive office hours. *No drop of sweat in vain, if shared with people in fair.*
I end by referring to miraculous words of William Blake for delight of everyone survived this far: *To see a World in a Grain of Sand.*

Ari Vepsäläinen
December 2nd 2014
Lappeenranta, Finland

Wether walking in a light rain
or heavy snowfall,
a windy day on a nice beach
or even the shores of Sahara,
I never lost the smallest thoughts
of the wonders of this research

with dedication

AV

Contents

List of publications

The thesis is presented in the form of a monograph, supported by the following peer-reviewed international journal and conference publications. The author of the thesis is the corresponding author and principal investigator in articles I - V.

Publication I
Vepsäläinen, A., Shah, S., Ritvanen, J. and Hyppänen, T. (2014). Interphase mass transfer coefficient in fluidised bed combustion by Eulerian CFD Modeling. *Chemical Engineering Science*, 106, pp. 30-38.

Publication II
Vepsäläinen, A., Shah, S., Peltola, P. and Hyppänen, T. (2013). Bed Sherwood number and chemical kinetic coefficient in a fuel reactor of chemical looping combustion by Eulerian CFD Modeling. In: *Proceedings of Fluidization XIV: From fundamentals to products, May 26-31, Noordwijkerhout, The Neatherlands*, pp. 275-282.

Publication III
Vepsäläinen, A., Shah, S., Ritvanen, J. and Hyppänen, T. (2013). Bed Sherwood number in Fluidised Bed Combustion by Eulerian CFD Modelling. *Chemical Engineering Science*, 93, pp. 206-213.

Publication IV
Vepsäläinen, A., Shah, S. and Hyppänen, T. (2012). Heterogeneous mass transfer characteristics in char combustion at fluidized bed reactor with laboratory to pilot size fluidization scaling approach - Eulerian multiphase CFD model study. In: *Proceedings of the 21^{st} International Conference on Fluidized Bed Combustion, Naples, Italy*, pp. 938-945.

Publication V
Vepsäläinen, A., Myöhänen, K., Hyppänen, T., Leino, T. and Tourunen, A. (2009). Development and validation of a 3-dimensional CFB furnace model. In: *Proceedings of the 20th International Conference on Fluidized Bed Combustion, Xian, China*, pp. 757-763.

Nomenclature

Latin alphabet

A	area, m^2
Ar	Archimedes number, $-$
a	surface area of active particle per volume, $\mathrm{m}^2/\mathrm{m}^3$
a_b	surface area of bubbles per volume, $\mathrm{m}^2/\mathrm{m}^3$
a_bub	surface area of single bubble, $\mathrm{m}^2/\mathrm{m}^3$
C	concentration, $\mathrm{mol}/\mathrm{m}^3$
C_D	particle drag coefficient, $-$
D	diffusion coefficient, m^2/s
$\bar{\bar{D}}$	strain rate sensor, s^{-1}
d	diameter, m
d_p^*	dimensionless particle diameter, $-$
e	restitution coefficient, $-$
f	general variable, $-$
f_s	slug shape factor, $-$
g	acceleration due to gravity, m/s^2
$g_{0,i}$	radial distribution function, $-$
H	reactor height, m
H_bed	bed height, m
h	dimensionless height, $-$
h_m	mass transfer coefficient, m/s
I	slug surface integral,
$\bar{\bar{I}}$	identity tensor, $-$
J	diffusion flux, $\mathrm{kg}/\mathrm{m}^2\mathrm{s}$
$K_{1,2,3,4}$	coefficients for granular temperature equation
K	momentum exchange coefficient, $\mathrm{kg}/\mathrm{m}^3\mathrm{s}$
K_bc	volumetric bubble-cloud interphase mass transfer coefficient, $1/\mathrm{s}$
K_be	volumetric bubble-emulsion interphase mass transfer coefficient, $1/\mathrm{s}$
K_ce	volumetric cloud-emulsion interphase mass transfer coefficient, $1/\mathrm{s}$
K_eff	volumetric effective reaction rate coefficient, $1/\mathrm{s}$
I	surface integral, $-$
k_sur	chemical kinetic rate coefficient, m/s
k_be	interphase mass transfer coefficient, m/s
k_eff	effective reaction rate coefficient, m/s
k_m	chemical kinetic rate coefficient per mass, $\mathrm{mol}/(\mathrm{kgbars})$
$\dot{n}$	molar flow rate, mol/s
q	molar mass transfer rate, $\mathrm{mol}/\mathrm{m}^3\mathrm{s}$
R	volumetric reaction rate, $\mathrm{mol}/\mathrm{m}^3\mathrm{s}$
R'	reaction rate, mol/s
r	specific reaction rate, $\mathrm{mol}/\mathrm{m}^2\mathrm{s}$
Re	Reynolds number, $-$

S	source term, $-$
Sh	Sherwood number, $-$
Sh_{bed}	bed Sherwood number, $-$
Sh_{e}	emulsion Sherwood number, $-$
Sc	Schmidt number, $-$
s_{NiO}	fraction of active NiO in oxygen carrier, $-$
U^*	dimensionless fluidization velocity, $-$
u	velocity, $\mathrm{m/s}$
u_{br}	bubble rising velocity, $\mathrm{m/s}$
V	volume, m^3
W	width of reactor, m
$X_{\mathrm{O_2}}$	oxidation degree, $-$
y_{c}	volume fraction of carbon within solids, $-$
$\langle x \rangle$	cross-section average of x
$\langle x \rangle_{20s}$	cross-section and time average (20 s) of x
$\bar{x}$	average value of x in bed
$\bar{x}^{\alpha_{\mathrm{s}}>0.15}$	average value of x in lower bed, $\langle \alpha_{\mathrm{s}} \rangle_{20s} > 0.15$
z	height coordinate, m

Greek alphabet

α	volume fraction of phase, $-$
κ	turbulent kinetic energy, $\mathrm{m}^2/\mathrm{s}^2$
ϵ	turbulent dissipation rate, $\mathrm{m}^2/\mathrm{s}^2$
λ_{s}	granular bulk viscosity, $\mathrm{kg/ms}$
λ_{g}	renewal frequency of gas, $1/\mathrm{s}$
κ	turbulent kinetic viscosity, $\mathrm{m}^2/\mathrm{s}^2$
μ	viscosity, $\mathrm{kg/sm}$
Φ	sphericity
ρ	density, $\mathrm{kg/m}^3$
θ	angle of internal friction, $^{\mathrm{o}}$
τ	shear stress, $\mathrm{N/m}^2$
Θ	granular temperature, $\mathrm{m}^2/\mathrm{s}^2$

Subscripts

a	active
B	gaseous species B
b	bubble phase
bed	average in bed
bub	bubble
C	char/carbon
col	collisional
e	emulsion phase

eff	effective
f	fluidization
fr	frictional
g	gas phase
i	general index/inert particle
kin	kinetic
lar	large
max	maximum
mf	minimum fluidization
p	particle
r	reactor
s	solid phase
sur	surface
t	time/terminal

Abbreviations

1D	one-dimensional
1.5D	one-and-half-dimensional core-annulus approach
2D	two-dimensional
3D	three-dimensional
BFB	bubbling fluidized bed
CCS	carbon capture and storage
CFB	circulating fluidized bed
CFD	computational fluid dynamics
CLC	chemical looping combustion
EMMS	energy minimization multiscale model
FCC	fluid-catalytic cracking
TGA	thermogravimetric analysis
MSMT	multiscale mass transfer model

1 Introduction

1.1 Background and field of research

1.1.1 Technological and environmental motivation

In the current millennium, the development of fluidized bed combustion technologies has been guided by two major themes: scale-up of technology and mitigation of carbon dioxide (CO_2) emission. Actual CO_2 emission reduction measures in solid fuel conversion processes can be divided into three main categories: development of carbon capture and storage (CCS) technologies, substitution of fossil fuels (coal) with biomass and increase of process efficiency. All these measures of developing sustainable heat and power generation technologies have their own path in the technological scale-up.

Driven by the market demands, global circulating fluidized bed (CFB) boiler manufactures have developed supercritical boiler technologies for higher capacity classes of 400 MW_e to 600 MW_e, where boiler plant net efficiency of about 45% can be reached (Hotta et al., 2008; Stamatelopoulos and Darling, 2008). The efficiency increase by the higher steam parameters and the increase of boiler plant size reduce the production cost of energy, and is a secondary measure for the reduction of CO_2 emissions. A similar unit size scale-up trend is continuously occurring in the biomass-fired bubbling and circulating fluidized bed boiler technology with recent achievements of 100 MW_e and 200 MW_e, respectively. Besides new biomass combustion units, the substitution of coal with biomass gains popularity as co-firing in CFB boilers. Co-firing of coal and biomass can also be executed by connecting a biomass gasifier to a coal-fired boiler as in the case of the recent scale-up achievement, CFB biomass gasifier of 140 MW_e replacing a remarkable share of coal fired in a pulverized coal unit it is attached (Basu, 2013).

Recently, three fluidized bed combustion technologies suitable for carbon capture and storage processes have been developed to a pilot unit or a demonstration plant scale as a part of the global combat against the climate change. In the oxygen combustion process, combustion air in the conventional combustion process is substituted by oxygen. The circulating fluidized bed oxygen combustion technology has reached the demonstration scale, and boiler manufactures guarantee capability to deliver utility size units (Anthony and Hack, 2013). The second process, chemical looping combustion (CLC), uses metal oxygen carriers to transport oxygen from the air reactor to the fuel reactor. The fluidized bed CLC process development has reached the pilot scale with plans for near future demonstration as discussed by Adanez et al. (2012) in a CLC technology development review. A similar technological status has been reached in the development of the fluidized bed calcium looping process, which utilizes limestone to capture carbon dioxide (Abdulally et al., 2012).

The relationship of the scale-up of fluidized bed solid fuel conversion technology and fluidized bed research environment is presented schematically in Fig. 1.1. The left side in Fig. 1.1 presents the state of art of fluidized bed energy conversion technologies as maximum proven capacities and planned near future development steps. It is essential to note that the process experiments related to the research and development of fluidized bed processes are primarily carried out in small fluidized bed reactors, either bench-scale de-

vices or pilot units. The reason for this originates from economical and practical issues. The operation of small-scale devices is far more cost-efficient than constructing a new commercial unit or even operating an existing unit under new operation conditions. In addition, accurate control and measurement of process conditions is practically possible only in small-scale fluidized beds. On the other hand, it is essential to have knowledge on the rate the phenomenon occurs in order to be able to design a fluidized bed, particularly in the case of a large scale-up unit or a new fluidized bed process, with a good performance for a wide range of operational conditions. However, there exists a contradiction between the required level of knowledge in phenomenology in a large unit versus the quality of phenomenology data, as well as the process performance knowledge obtained by experiments with small-scale fluidized beds. Here exists a fluidized bed process research field, which is here called scaling of the phenomenon. This research field creates a general level motivation for the thesis.

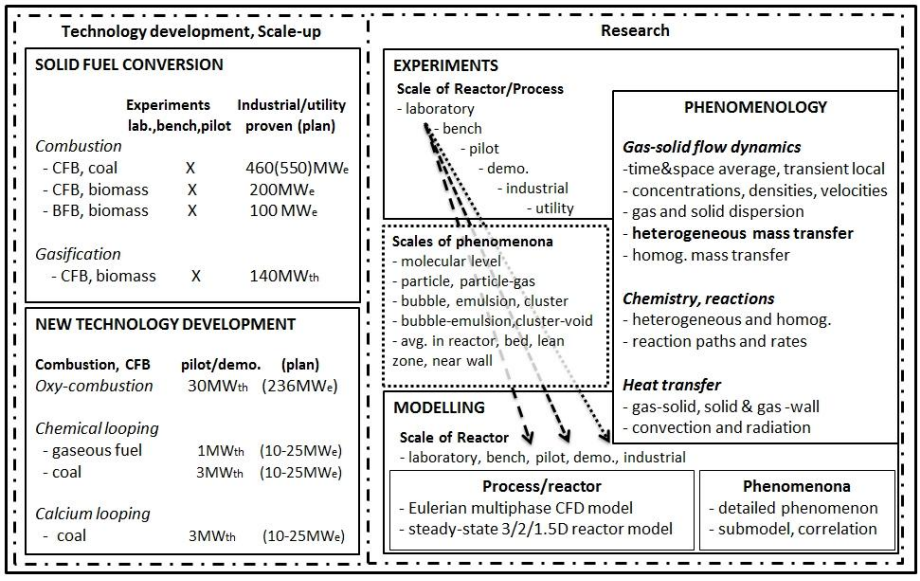

Figure 1.1: Scale-up status of fluidized bed solid fuel energy conversion technologies and scaling of the phenomenon point of view on the fluidized bed research environment.

1.1.2 From nature of fluidized beds into field of scaling of phenomenon

Fluidization provides a basis for a diversity of technologies from solid fuel energy conversion to chemical processes. The fluidized bed combustors are highly fuel flexible and suitable for co-combustion. The circulating fluidized beds operate on a wide range of solid fuels: anthracite, bituminous and brown coals, petroleum coke, peat, biomass and

various sorts of wastes. The bubbling bed technology is primarily utilized for the co-combustion of multiple sources of biomass, and is especially suitable for high moisture and low calorific value fuels. The phenomenology of fuel-flexible and versatile fluidized bed processes is formed by three cornerstones shown also in Fig. 1.1): (i) vigorous two-phase gas-solid flow dynamics, (ii) chemical reactions strongly coupled with gas-solid mixing and (iii) efficient heat transfer enhanced by solid convection. The basis for process performance is set by gas-solid flow dynamics, which provides an efficient gas-solid contact and mixing environment. Thus, the phenomenological characteristics of a specific fluidized bed process are defined by the operated fluidization regime: minimum fluidization, bubbling, slugging, and turbulent or fast fluidization.

The right side of Fig. 1.1 presents schematically the fluidized bed research environment from the point of view of the scaling of phenomenon. In principle, the research of fluidized bed processes is carried out by experimental and modeling efforts. As process testing in large, demonstration and industrial, units has its limits, the knowledge regarding the detailed process performance of large-scale units lies strongly on various fluidized bed process models. Besides fundamental mass and energy balances, a proper fluidized bed reactor model has sub-model descriptions for the fluidized bed phenomenology considering all the three cornerstones of the process: gas-solid flow dynamics, chemical reactions and heat transfer. Depending on the sophistication level of the fluidized bed model (Basu, 1999) a single phenomenon can have either a detailed physical description, empirical correlation or is not considered at all. The challenge with highly sophisticated models, with their detailed sub-models and required small discretization sizes, is the increased computational cost that is currently unpractical for the simulations of large-scale fluidized bed reactors (Myöhänen, 2011). While models with a lower level of sophistication or models with large discretization sizes are applied, information regarding the micro-scale, or even the meso-scale, solid flow structures is filtered. As solid flow dynamics has a dominating role in most of the phenomenona in fluidized beds, the result is a direct loss in the accuracy of process performance predictions.

The right side of Fig. 1.1 underlines that transferring the small-scale process performance to an accurate prediction of a larger scale reactor requires knowledge of the scales of solid flow structures where the modeled phenomenon occurs in both reactors, as discussed above. In practice, the main scales of flow structures that the models can describe are (i) single particle level, (ii) micro-, meso- and/or macro-scale bubble-emulsion and void-cluster structures and (iii) regions of fluidized bed reactors such as dense bed, lean upper zone and near wall regions. In general, more sophisticated models can be applied to produce knowledge on a particular phenomenon for models with a lower level of sophistication for example as descriptions of phenomenon models, semi-empirical correlations and rate coefficients. In this thesis, transient fine-grid CFD models are applied to produce refined information on heterogeneous mass transfer particularly for steady-state fluidized bed models with meso-scale discretization sizes. Besides understanding the importance of the sophistication level of the fluidized bed model and the related level of detail in phenomenon models, the research field of the scaling of the phenomenon has another main perspective. The other challenge origins from the different fluidization conditions prevailing in small-scale experiments compared to the large-scale reactors of interest. As

highlighted in the right side of Fig. 1.1, the accurate performance prediction of pilot, industrial or utility scale reactors would require knowledge on the scales in which the phenomena occur (particle, particle-gas, cluster, etc.) with respect to the discretization size applied in the modeling and the validity range of the phenomenon model applied in the performance prediction.

1.1.3 Focus on heterogeneous mass transfer

The fluidized bed offers an efficient gas-solid contact and mixing environment. However, the effective heterogeneous reaction rates in fluidized beds are under the influence of heterogeneous mass transfer (Kunii and Levenspiel, 1991). Thus, both the local thermal conditions and the chemical reaction paths are affected secondarily by the fluidization regime and the related heterogeneous mass transfer characteristics. Consequently, on the performance level of the fluidized bed reactor, heterogeneous mass transfer has a secondary impact on the combustion efficiency and the emission performance. Therefore, understanding the heterogeneous mass transfer and being able to define it under different fluidization regimes with a proper knowledge of the scale of phenomenon are keys to accurate predictions of fluidized bed processes. Thus, the research field described above is relevant for all fluidized bed reactor models and analyses of reactive fluidized bed processes. Especially, the scaling of heterogeneous mass transfer is important in the case of reactor scale-up related research and development of design.
The general validation range, as an available experimental or CFD-based research data, of heterogeneous mass transfer coefficients are shown in Table 1.1. The table highlights that almost all the available data is based on experiments at a bench or pilot scale reactor. The scope of the thesis covers the bubble-emulsion interphase and the average gas-bed mass transfer at the bubbling and turbulent bed regimes in bench- and pilot-scale reactors. Regarding the knowledge on heterogeneous mass transfer, particularly the turbulent regime lacks results of empirical research.

1.2 Research approach, objectives and scope

The first main, general level objective of the thesis is to benchmark heterogeneous mass transfer rate coefficients in fluidized bed combustors predicted by transient two-phase Eulerian CFD modeling against empirical data and correlations presented in the literature. In practice, CFD simulations are here applied to study the heterogeneous mass transfer phenomenon in bench-scale and pilot fluidized bed reactors under different fluidization regimes and operating conditions, which gives a proper perspective to the bench-to-pilot phenomenon scaling. The second general objective is to produce heterogeneous rate coefficients with an extended validity range from currently available experimental data that can be applied into steady-state reactor models or coarse-grid CFD simulations of fluidized beds. Particularly, the focus of the research is on the higher fluidization velocity range and large-particle size operating conditions, which exist in the lower bed region of large-scale fluidized bed combustors. In contrast, experimental research presented in the literature is carried out mostly with the fine particles and low fluidization velocities in

Table 1.1: Overview of the validation range of heterogeneous mass transfer coefficients: X = wide range of experiments available, x = limited number of experiments available, o = experiments not available, a = scope of the thesis. The experimental data is discussed in Chapter 2.1, research of interphase mass transfer is presented in Ch. 5, and research of average gas-bed mass transfer (bed Sherwood number) is discussed in Ch. 4,6 and 7.

Mass transfer mode	Bench	Pilot	Notes on type of experiments
In-emulsion convection			
- minimum fluidization	X	X	process types: (1) combustion, (2) all solids active
- bubbling	X	X	process types: (1) combustion, (2) all solids active
- turbulent	o	o	few CFD studies for over-cluster convection
Interphase mass transfer			
- bubbling	X,a	X,a	
- turbulent	x,a	o,a	only 3 reported experiments for fine (FCC) particles
Gas-bed mass transfer			(Bed Sherwood number)
- bubbling	X,a	X,a	only for processes where all solids are active
- turbulent	o,a	x,a	CFD-based for fine FCC particles

small-scale units, due to the inevitable fact that, in practice, accurate local measurements in the large industrial units are challenging.

1.2.1 Overview of methodology

The research is based on two-dimensional gas-solid phase Eulerian CFD modeling of bench- and pilot-scale fluidized bed reactors. Both the gas-solid flow dynamics and the heterogeneous combustion reactions have been simulated under bubbling and turbulent flow regimes with a relatively short time-step (0.001 s) and a fine mesh size (4 mm - 12.5 mm). Extensive time-dependent data recording of local conditions was carried out during the analysis period of simulations (10 s or 20 s) under stabilized conditions. Thermal effects, in-particle mass transfer mechanisms and particle size distributions were left out of the scope of this research.

In order to obtain heterogeneous mass transfer coefficients, two steady-state one-dimensional fluidized bed models were compiled, and were used to analyze the time and cross-section averaged axial profiles of the Eulerian CFD simulations. The average gas-bed mass transfer coefficients over the fluidized bed were derived, and presented as bed Sherwood numbers, with a one-phase steady-state model. The bubble-emulsion (or void-cluster) interphase mass transfer coefficients were obtained by fitting a steady-state fluidized bed model with two phases (bubble-emulsion) against the Eulerian CFD simulation results. Both the obtained bed Sherwood numbers and the interphase mass transfer coefficients were analyzed against experimental and modeling work based data, empirical correlations and theories presented in the literature. All models applied in the thesis were designed by author of the thesis. However, beneficial and practical help was provided by the research team for the CFD simulations, for example, in form of user defined functions (UDFs) that were used for recording the time dependent data and designing a reaction model.

1.2.2 Research process and main research questions

During the years 2006 to 2009, the author carried out an extensive validation process of a steady-state three-dimensional CFB combustor model (Hyppänen et al., 1991) as a part of the research and development activities of a global fluidized bed boiler manufacturer (Foster Wheeler). During the same time period, the author was also practically involved in field test periods focused on the furnace performance of industrial scale CFBs and a pilot-scale CFB (VTT, Technical Research Centre of Finland) operating with a wide range of fuels and load conditions. The first research question of the thesis resulted from the comparison of the furnace performance of a pilot-scale CFB reactor and a utility-scale CFB boiler combusting the same bituminous coal. The analysis with the three-dimensional CFB combustor model presented in Vepsäläinen et al. (2009) showed that the effective heterogeneous combustion reaction coefficients were different in the pilot and industrial size furnaces for the same bituminous coal at the same operation temperatures. A hypothesis was formed by author, stating that the gas-solid contact was different in the different size reactors even when operated with similar conditions. Consequently, the first research question was raised as

- What is the average gas-bed mass transfer coefficient, or bed Sherwood number, in the lower dense bed of bubbling and circulation fluidized bed combustors? In this thesis, the focus is particularly set on the heterogeneous mass transfer coefficients at the bubbling and turbulent fluidization regimes, as the bottom bed of a circulating fluidized bed is commonly considered either as a bubbling bed (Knoebig et al., 1999) or a turbulent one with a transition zone from the bubbling bed regime (Souza-Santos, 2010).

An answer to the research question could not be found in the existing scientific literature. The actual research for the thesis was carried out between 2010 and 2013 at Lappeenranta University of Technology. Knowledge regarding the Eulerian multiphase CFD modeling in the research group, Modeling of energy processes/LUT Energy, provided a research tool for the fluidized bed process phenomenology, and the versatile fluidized bed research activities of the research group supported the thesis. With a great possibility of utilizing an Eulerian CFD model for the scaling of the phenomenon research with a heterogeneous mass transfer focus, the second research question was naturally set as:

- Does the Eulerian multiphase CFD model predict correctly different mechanisms of heterogeneous mass transfer, qualitatively or quantitatively?

The different mechanisms and definitions of heterogeneous mass transfer applied in the thesis are presented in the literature review in Chapter 2. A logical continuation for the research questions above comes from i) the practical means of operation, design and control of CFB combustors, and ii) a literature review revealing the narrow validation range (Table 1.1) of the empirical heterogeneous mass transfer coefficients:

- What is the effect of the operation conditions (size of reactor and solid particles, fluidization regime and velocity, and type of process or fuel) on the different heterogeneous mass transfer coefficients: bed Sherwood number, bubble-emulsion interphase mass transfer coefficient and emulsion mass transfer coefficient?

After the main concepts and analysis methods of the thesis were defined and first results were achieved, also more specific research questions that had not been answered in the scientific literature could be raised up, particularly:

- What is the interphase mass transfer coefficient in a fluidized bed combustor operated under the turbulent regime? Does the interphase mass transfer control the rate of heterogeneous reactions?
- What is the average gas-bed mass transfer coefficient in the different type of processes? Particularly, the interest focused on a novel fluidized bed combustion process, the chemical looping combustion, utilized for methane combustion and operated with a fine particle bed.

1.2.3 Structure of the dissertation

The thesis consists of three main parts: (i) a theoretical review of the concepts of interest, heterogeneous mass transfer in fluidized beds (Chapter 2), (ii) a description of the applied research method, an Eulerian CFD model and its validation background together with the results of CFD simulations (Chapter 3), and (iii) an extensive discussive analysis on the executed model-based phenomenology research results (Chapter 4-7). The content of each chapter is briefly summarized below.

Chapter 2 provides the relevant theoretical background for the thesis. The chapter presents the current scientific knowledge regarding heterogeneous mass transfer in fluidized bed reactors, and gives the definitions of mass transfer mechanisms and coefficients applied in the thesis. The importance and relevance of heterogeneous mass transfer research is further highlighted by describing different heterogeneous mass transfer approaches in various steady-state bubbling and circulating fluidized bed combustor models published in the scientific literature.
Chapter 3 describes the two-dimensional fine-grid Eulerian two-phase CFD model applied in the research. It also discusses shortly the validation basis of the Eulerian CFD modeling of fluidized beds regarding the gas-solid momentum and mass transfer exchange. Finally, the fluid-dynamic and heterogeneous reaction characteristics of the twelve simulated bubbling and turbulent fluidized bed char combustion balances are described.
Chapter 4 presents the average gas-solid mass transfer coefficients, as bed Sherwood numbers, in the lower bed region of the bench- and pilot-scale fluidized bed combustors obtained from the executed CFD simulations. Particularly, the chapter highlights an important dimensionless relationship, the response of the bed Sherwood number to the particle Reynolds number for both the CFD-based results obtained here and the various empirical data presented in the literature with respect to the practical process conditions: fluidization velocity, particle and reactor size and chemical kinetics of the reactive solids.
Chapter 5 presents a continuation for the research presented in Chapters 3 and 4. In Chapter 5, the bubble-emulsion, or void-cluster, interphase mass transfer coefficients in the lower bed region are based on the CFD simulations of fluidized bed combustion balances presented in Chapter 3. The chapter introduces various new qualitative scientific

results regarding the dependence of the bubble-emulsion interphase mass transfer coefficient on the particle, reactor and bubble size, and particularly also on the fluidization velocity with the coarser, Geldart B and D solids. In the end, also the relation between the interphase mass transfer coefficient and the dimensionless particle Reynolds number is highlighted.
Chapter 6 shows a separate CFD study with the same fine-grid Eulerian CFD model as a case research of a methane fuel reactor in a pilot chemical looping combustion process applying the same modeling and analysis methods as described in Chapters 3 and 4. The results of the fine-particle chemical looping combustion simulations strongly underline the several orders-of-magnitude lower bed Sherwood numbers for the fine-particle fluidized bed processes, particularly, when all the solids are active.
Chapter 7 summarizes the learning of heterogeneous mass transfer regarding the bed Sherwood numbers obtained in the research presented in this thesis, and highlights several new process-specific, characteristic insights into the original bed Sherwood number theory of Kunii and Levenspiel (1968).
In the end, Chapter 8 concludes by presenting the scientific contributions of the thesis. The chapter also summarizes at a practical level the main uncertainties, assumptions made and limitations of the research approach. Furthermore, based on the strong experience regarding (i) the modeling of fluidized bed combustors, (ii) experimental process performance testing and (iii) deep theoretical knowledge on heterogeneous mass transfer established in this thesis, several recommendations for further activities in the research fields of various fluidized bed processes and process models are provided for science-, industry- and education-oriented readers.

2 Theoretical review and process modeling backgrounds

In the first part of this chapter, the different modes of heterogeneous mass transfer in fluidized beds and the level of related scientific knowledge are discussed in order to establish the research area of the thesis. In the second part of the chapter, the importance of the research field is highlighted by describing the main types of heterogeneous mass transfer sub-models in the steady-state and Eulerian CFD models of bubbling and circulating fluidized bed combustion presented in the literature. The content of this chapter forms a general view on the knowledge of heterogeneous mass transfer in fluidized beds. Even though the mechanisms of the phenomenon are well known, the empirical data is still limited primarily to bubbling bed conditions in small-scale equipment. The lack of accurate, process-specific knowledge of heterogeneous mass transfer rates results direct loss of accuracy in the prediction of effective reaction rates. This has a remarkable effect on the simulated total performance of a fluidized bed. Consequently, the limited knowledge regarding the heterogeneous mass transfer forms an important bottleneck, when fluidized bed engineering and research communities are reaching towards models capable for accurate thermal design and performance optimization tasks even in cases of process scale-up and novel fluidized bed processes.

2.1 Heterogeneous mass transfer in fluidized beds

The average gas-bed mass transfer in a fluidized bed consist two modes of heterogeneous mass transfer: an interphase and emulsion mass transfer. Both modes contain a convective and a diffusive component of mass transfer. Consequently, there are two different ways of defining the heterogeneous mass transfer coefficients in heterogeneous fluidized bed systems as highlighted by Hou et al. (2010):

- Multi-phase model: the flow dynamic model, consisting typically of separate bubble and emulsion phases, provides a possibility to describe the heterogeneous mass transfer modes separately with the related interphase and emulsion mass transfer coefficients.
- Single-phase model: the gas-solid flow in a calculation cell is described as a plug flow and the average conditions and properties of the gas and solid phases in the cell are applied. The heterogeneous gas-bed mass transfer is described with the average gas-bed mass transfer coefficient that includes the effects of both interphase and emulsion mass transfer.

In this chapter, three commonly applied definitions related to heterogeneous mass transfer in fluidized beds are discussed: (1) emulsion mass transfer, (2) average gas-bed mass transfer and (3) interphase mass transfer. In the discussion, the different heterogeneous mass transfer characteristics between two main types of fluidized bed processes are highlighted. The two main types of fluidized bed processes are

- Process type A: Fluidized bed consisting of only active particles: e.g. catalytic processes and chemical looping combustion for gaseous fuels.

- Process type B: Fluidized bed containing both active and inert particles: e.g. combustion and gasification processes.

Characteristics of heterogeneous mass transfer are most likely remarkably different between the process types A and B. Besides the active particle concentration in bed, main reasons for the differences are caused by particle sizes and chemical kinetics as described in Chapter 7 summarizing the results of this research.

2.1.1 Emulsion mass transfer

Among the different heterogeneous mass transfer modes, emulsion gas-solid mass transfer has the best established theory. Numerous proven empirical correlations with relatively wide validity ranges have been presented in the literature for the emulsion mass transfer coefficients. These are discussed below.
Emulsion mass transfer refers most often to the average gas-bed mass transfer in a minimum fluidization condition. Figs. 2.1a-b presents schematically the minimum fluidization regime for the above discussed process types: (A) fluidized bed consisting of only active particles and (B) fluidized bed containing both active and inert particles. Fig. 2.1c shows the bubbling bed regime for a bed consisting of both inert and active particles (process type B). According to the two-phase theory (Davidson and Harrison, 1963) the emulsion phase at the bubbling bed regime is in the minimum fluidization condition. However, even Davidson and Harrison (1963) stated that the voidage of the emulsion phase can be slightly higher. At the turbulent bed regime (Fig. 2.1d), large fractions of the emulsion phase in the dense bed region and smaller clusters of solid particles have most of the time a higher gas volume fraction than the minimum fluidization voidage proposes. In the dense bed region, a small fraction of the solid particles is also dispersed as single particles in the gas flow within the bubbles at the bubbling bed regime and the vigorous voids at the turbulent regime.
The emulsion gas-solid mass transfer theory originates from the theory of convection mass transfer over a single sphere. A typical emulsion Sherwood number correlation is a modification of Frössling's equation (Frössling, 1938) for convection mass transfer between gas and surface of a single sphere:

$$Sh = 2 + 0.69 Re^{1/2} Sc^{1/3}. \tag{2.1}$$

The Sherwood number $Sh = h_{\mathrm{m}} d_{\mathrm{p}} / D_{\mathrm{g}}$ is the dimensionless transferring gas species concentration gradient at the particle surface. The first term of 2 represents pure diffusion to the surface of the sphere. Frössling's Sherwood number equation for gas flow over a single sphere has been accurately validated up to Reynolds number of 2000. The constant 0.69 is based on later experimental work of Rowe et al. (1965), while the original constant presented by Frössling (1938) was 0.522. The interest here is particularly in the emulsion mass transfer at fluidized beds containing active and inert particles. For this type of fluidized beds, La Nauze and Jung (1982) were the first to consider the effect of emulsion voidage in both terms of the Frössling's type correlation (Table 2.1):

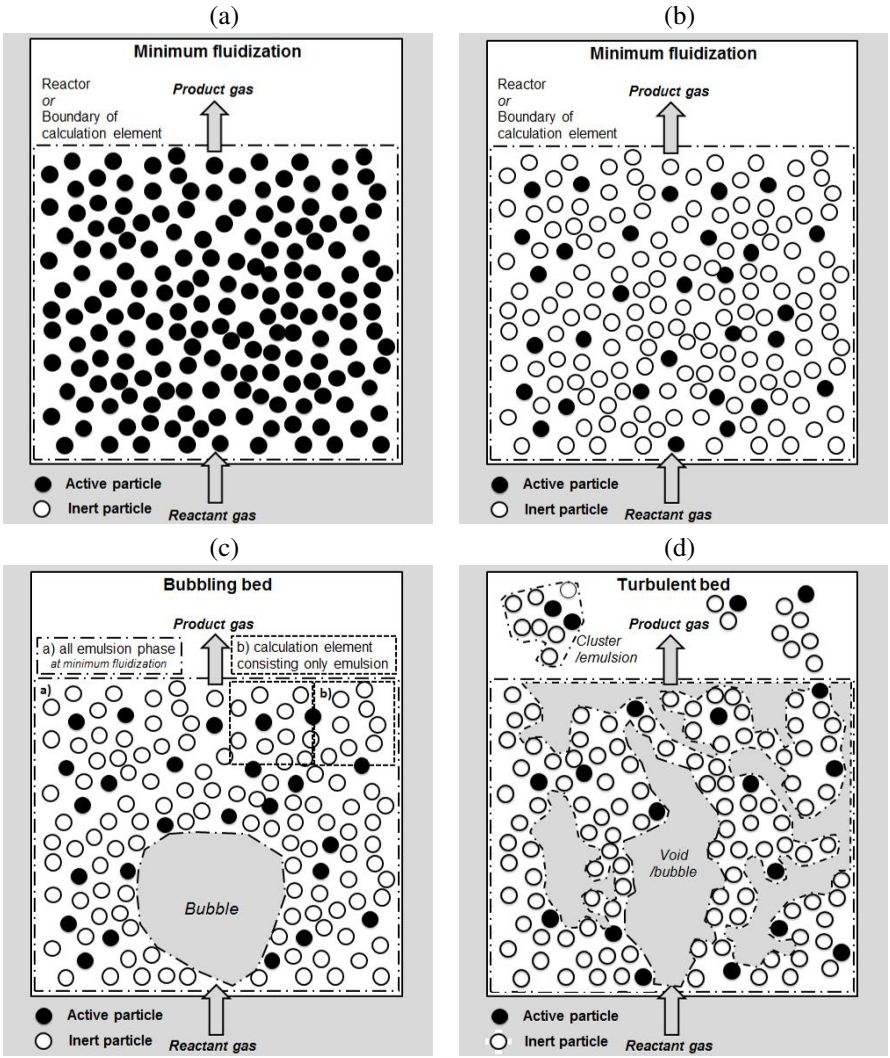

Figure 2.1: Schematics of different gas-solid contact conditions in a small-diameter fluidized bed reactor or in a calculation cell of a fluidized bed reactor model: (a) minimum fluidization condition with only active particles, (b) minimum fluidization condition with inert and active particles, (c) bubbling bed regime with inert and active particles present and (d) turbulent regime with inert and active particles.

- first term: $2\alpha_{\mathrm{g}}$ - pure diffusion to the surface of a particle is restricted by the presence of inert solids Avedesian and Davidson (1973) and
- second term: Re/α_{g} - convection transfer to the surface of a particle is enhanced by the velocity increase caused by the volume of solids.

A comprehensive review of the emulsion Sherwood number Sh_e correlations for active particles in a fluidized bed of inert particles has been introduced by Scala (2007). Table 2.1 shows examples of the emulsion Sherwood number correlations for the fluidized bed combustion and gasification processes presented in the literature. When using the emulsion Sherwood number correlations, it is important to consider carefully, how the conditions (Re, u, α_g) are defined, as the minimum fluidization conditions presenting the actual conditions in the emulsion or as superficial and average ones. Fig. 2.2 shows that the emulsion Sherwood numbers Sh_e are very close to, or between, the single sphere (Frössling, 1938) and the fixed bed (Ranz and Marshall, 1952) ones (Table 2.1). The emulsion Sherwood number correlation of Ranz and Marshall (1952) is based on tests of an evaporating water droplet (d_p= 0.3-11 mm, $6 < Re < 40$). The fitting of the tests and other earlier experiments resulted as a constant of 0.6 to the Frössling type correlation.

Table 2.1: Single sphere, fixed bed and in-emulsion Sherwood number correlations

Frössling (1938)	
- Single sphere	$Sh = 2 + 0.69 Re^{1/2} Sc^{1/3}$
Ranz and Marshall (1952)	
- Fixed bed	$Sh = 2 + 1.8 Re^{0.5} Sc^{0.33}$
- BFB, emulsion	$Sh_\mathrm{e} = 2 + 0.6 Re^{0.5} Sc^{0.33}$
La Nauze and Jung (1983b)	
- BFB, emulsion	$Sh_\mathrm{e} = 2\alpha_\mathrm{g,mf} + 0.69 (Re/\alpha_\mathrm{g,mf})^{1/2} Sc^{1/3}$
La Nauze et al. (1984)	
- BFB, emulsion	$Sh_\mathrm{e} = 2\alpha_\mathrm{g,mf} + \frac{4\alpha_\mathrm{g,mf} d_p (U_{mf}/\alpha_\mathrm{g,mf} + u_b)}{\pi D_\mathrm{g}}^{1/2}$
Gunn (1978)	
- BFB, emulsion	$Sh_\mathrm{e} = (7 - 10\alpha_\mathrm{g} + 5\alpha_\mathrm{g}^2)(1 + 0.7 Re^{0.2} Sc^{1/3}) + (1.33 - 2.4\alpha_\mathrm{g} + 1.2\alpha_\mathrm{g}^2) Re^{0.7} Sc^{1/3}$
Li and Wang (2002)	
- BFB, emulsion	$Sh_\mathrm{e} = 2\alpha_\mathrm{g} + 0.69 \frac{Re}{\alpha_\mathrm{g}}^{0.5} Sc^{0.3}$
Hayhurst and Parmar (2002)	
- BFB, emulsion	$Sh_\mathrm{e} = 2\alpha_\mathrm{g,mf} + 0.61 Re^{0.48} Sc^{1/3}$
Scala (2007)	
- BFB, emulsion	$Sh_\mathrm{e} = 2\alpha_\mathrm{g,mf} + 0.7 (\frac{Re_\mathrm{mf}}{\alpha_\mathrm{g,mf}})^{0.5} Sc^{1/3}$
Prins et al. (1985)	
- BFB, emulsion	$Sh_\mathrm{e} = (0.1 + 1.5(\frac{d_\mathrm{p,a}}{d_\mathrm{p,i}})^{-1.05})(\frac{d_\mathrm{p,a}}{d_\mathrm{p,i}})(\frac{1-\alpha_\mathrm{g,mf}}{\alpha_\mathrm{g,mf}}) Re_\mathrm{mf,i}^{1-m} Sc^{1/3}$ $Re_\mathrm{mf,i} = \frac{\rho_\mathrm{g} u_\mathrm{mf,i} d_\mathrm{p,i}}{(1-\alpha_\mathrm{g,mf})\mu_\mathrm{g}}$ $m = 0.35 + 0.29(\frac{d_\mathrm{p,a}}{d_\mathrm{p,i}})^{-0.5}$

The emulsion Sherwood number correlation of Gunn (1978) is based on the analytical solution of a theoretical gas-solid heat transfer description, where the analogy of heat and mass transfer is then applied further. The correlation is intended for single particles, fixed beds and fluidized beds ($20 < Re < 1000$). However, the radiation heat transfer has not an analogical mechanism in gas-solid mass transfer processes, which in practice means

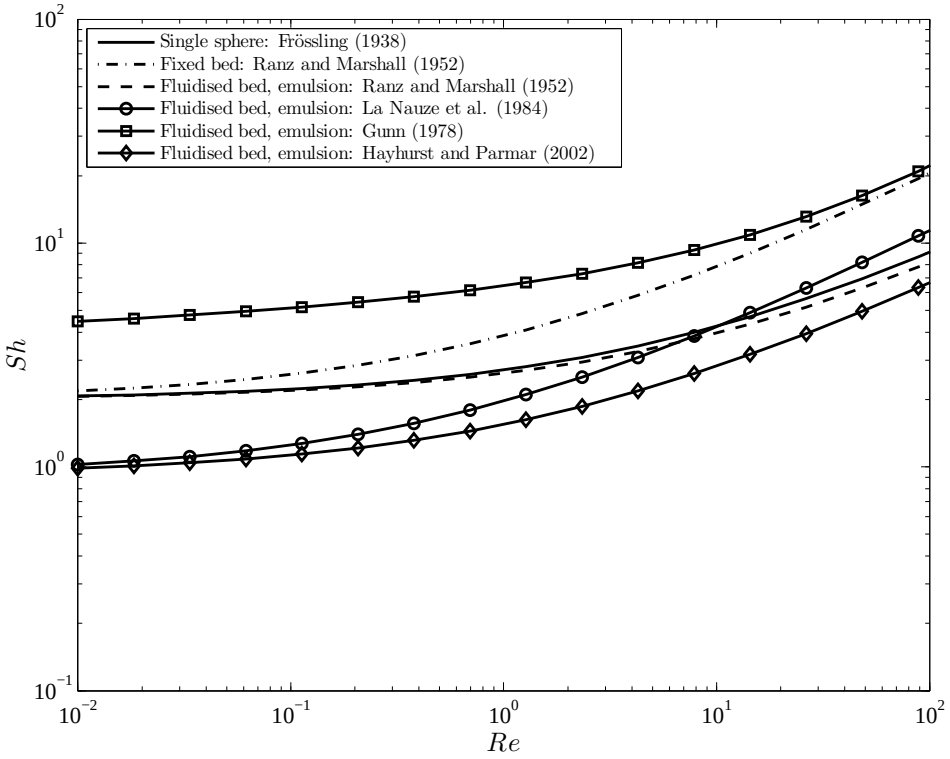

Figure 2.2: Single sphere, fixed bed and emulsion Sherwood number correlations

that the analogy is not valid for the higher temperature fluidized bed conditions. La Nauze and Jung (1982) have proposed a modification to Frössling's equation to account for the found decrease of Sherwood number with the size decrease of a burning petroleum coke particle size by introducing the voidage of bed α_{g} to both terms of Sherwood number correlation as follows

$$Sh = 2\alpha_{\mathrm{g}} + 0.69(Re/\alpha_{\mathrm{g}})^{1/2} Sc^{1/3}. \tag{2.2}$$

Later (La Nauze and Jung, 1983b), the term α_{g} was substituted by the term $\alpha_{\mathrm{g,mf}}$ presenting the minimum fluidization conditions expected in the particle dense emulsion phase. The authors (La Nauze et al., 1984) have also developed a Sherwood number correlation (Table 2.1) based on the surface penetration theory, considering also particle packet convection. In the related experimental work, char of petroleum coke (active particle size $d_{\mathrm{p,a}} > 0.2$ mm) was combusted in a fluidized bed of sand particles (inert particle size $d_{\mathrm{p,i}}$= 0.65-0.925 mm). The correlation was developed for the large active particles in a

bed of smaller inert solids. The emulsion mass transfer mechanisms between the process types of (A) fluidized bed consisting of only active particles and (B) fluidized bed containing both active and inert particles differs, for example, due to particle packet convection, which is an enhanced fresh gas convection to the surface of a large active particle inside a cluster of small inert particles as discussed by La Nauze et al. (1984). The authors also proposed that the gas velocity in the emulsion phase should be considered higher than the minimum fluidization velocity due to the enhancing effect of bubble-emulsion interphase mass transfer.

Fairly recently, two experimental research works applying the technique where carbon particles are combusted in an inert bed by Hayhurst and Parmar (2002) and Scala (2007) recommended a La Nauze-type of correlation (La Nauze and Jung, 1983b) for emulsion mass transfer. The experiments were carried out at the bubbling bed regime with large active particle diameters ($d_{\mathrm{p,a}} =$ 1-12 mm) compared to the inert particle diameter. Hayhurst and Parmar (2002) concluded also that the term, $\alpha_{\mathrm{g,mf}}$, should be replaced by 2, if the active particles are small compared to the inert particles ($d_{\mathrm{p,a}} << d_{\mathrm{p,i}}$). The reason for this is that larger active particles do not affect the convective boundary layer of very small active particles. Both the above mentioned works, Hayhurst and Parmar (2002) and Scala (2007), also highlight that the emulsion mass transfer is fairly independent on the fluidization velocity, but is strongly a function of minimum fluidization velocity. As a consequence, both researches recommended appling the minimum fluidization voidage α_{mf} and Reynolds number Re_{mf} in a La Nauze-type of correlation. The correlation of Prins et al. (1985) is based on the sublimation of naphthalene particles in a fluidized bed of inert particles. The correlation takes into account the sizes of both the active and inert particle size ($d_{\mathrm{p,a}}/d_{\mathrm{p,i}}$= 3-200). Later, Prins (1987) confirmed the correlation with the experimental technique of burning single graphite particles in a fluidized bed of inert solids. Also the experiments of Scala (2007) fit with the correlation of Prins et al. (1985), but only for the inert particle sizes of $d_{\mathrm{p,i}} <$ 0.7 mm.

The La Nauze -type correlation could be assumed to apply as a description of the emulsion mass transfer coefficient, at least qualitatively, also at the turbulent regime. Even though there is no experimental evidence for this, the described semi-empirical formulation of the emulsion Sherwood number correlations provides additional qualitative confidence regarding the actual physics of the diffusion and convection processes. The local conditions, voidage α_{g} and gas velocity u_{g}, in the emulsion phase should then be applied in the correlations.

As a summary, the range and Reynolds number response of the emulsion Sherwood number are well known. On the other hand, some variance from the presented correlations can occur, as in the case where the voidage of the emulsion phase is remarkably higher than the minimum fluidization condition proposes (in practice: at the turbulent beds), as the experimental work has been mostly carried out with the emulsion phase being close to the minimum fluidization conditions and at the bubbling bed regime operation. Similarly, a small variance in the emulsion Sherwood number from correlations presented in the literature can occur depending on whether the correlation is validated for the particular active to inert particle diameter sizes. However, the variance from correlations presented in the literature is not expected to be great, as e.g. the effect of voidage is considered in

most of the correlations. It is worth mentioning also that the emulsion Sherwood numbers for beds of only active particles have not been researched so extensively as gas-solid mass transfer to large active particles in an inert bed, which leaves room for further discussion regarding the accurate formats of the diffusive and convective terms in the associated emulsion Sherwood number correlation as discussed by Scala (2013).

2.1.2 Average gas-bed mass transfer

The overall theory describing the behavior of the average gas-bed mass transfer coefficient as a bed Sherwood number Sh_{bed}=$\bar{h}_{\mathrm{m}} d_{\mathrm{p}}/D$ was well-established by Kunii(1968). In principle, the theory explains the higher bed Sherwood numbers for the high Reynolds number ($Re_{\mathrm{p}} = u_{\mathrm{f}}\rho_{\mathrm{g}} d_{\mathrm{p}}/\mu$) range ($>$100) and the drop of bed Sherwood number at the smaller Reynolds numbers ($<$100). However, specific bed Sherwood numbers for the various practical fluidized bed processes in the real, mostly high temperature, process conditions do not exist. Furthermore, the experimental bed Sherwood numbers for circulating fluidized beds are in a range of seven orders of magnitude as discussed in a review by Breault (2006). In fact, the primary objective of the thesis, defining the average mass transfer coefficients (bed Sherwood numbers) for bubbling and circulating fluidized bed combustion in bench-to-pilot size reactors, originates from the practical needs of analyzing the pilot-to-industrial size circulating fluidized bed combustion processes. Vepsäläinen et al. (2009) showed that the combustion of the same bituminous coal in the pilot and utility size circulating fluidized beds resulted as a relevantly higher volumetric reaction rate in the pilot reactor than in the large utility reactors. As the temperature conditions in the reactors were similar, the difference strongly indicates remarkably different average gas-bed mass transfer rates. A comprehensive literature review revealed that the average gas-bed mass transfer coefficients in the conditions prevailing in the fluidized bed combustion process cannot be evaluated on the basis of the so far published experimental or theoretical data.

In the still valid bed Sherwood number theory, Kunii and Levenspiel (1968) showed that the bed Sherwood numbers for large particle beds of active particles with high Reynolds numbers ($>$100) were between the fixed bed and single particle ones in a $Sh-Re$ chart (Fig 2.3). The experimental work of Chu et al. (1953) was carried out in a reactor with the diameter of 10.2 cm and with coarse naphthalene coated solids having diameters in the range of 0.71-1.98 mm. Thodos and Ricetti (1961) measured bed Sherwood numbers with coarse solids having diameters in the range of 1.8 mm to 3.1 mm in reactors with diameters from 3.8 cm to 11.3 cm. Similar high Reynolds number results were obtained by (Richardson and Szekely, 1961) in a shallow (up to 5 particle diameter deep) small diameter reactor (d_{r}= 3 cm) by the adsorption process (d_{p}= 0.088-2.58 mm) for the higher Reynolds number range ($Re>$ 10). The shallow bed was used in order to control the fluidization conditions carefully and to avoid the bubbling phenomenon in the bed. In the lower Reynolds number range ($Re<$ 100), the controlling mechanism of the average gas-bed mass transfer seems to change (Fig 2.2). Kunii and Levenspiel (1968) highlighted the steeper exponential relation of the bed Sherwood and Reynolds numbers for the small Reynolds number range based on earlier experimental mass transfer studies for beds of

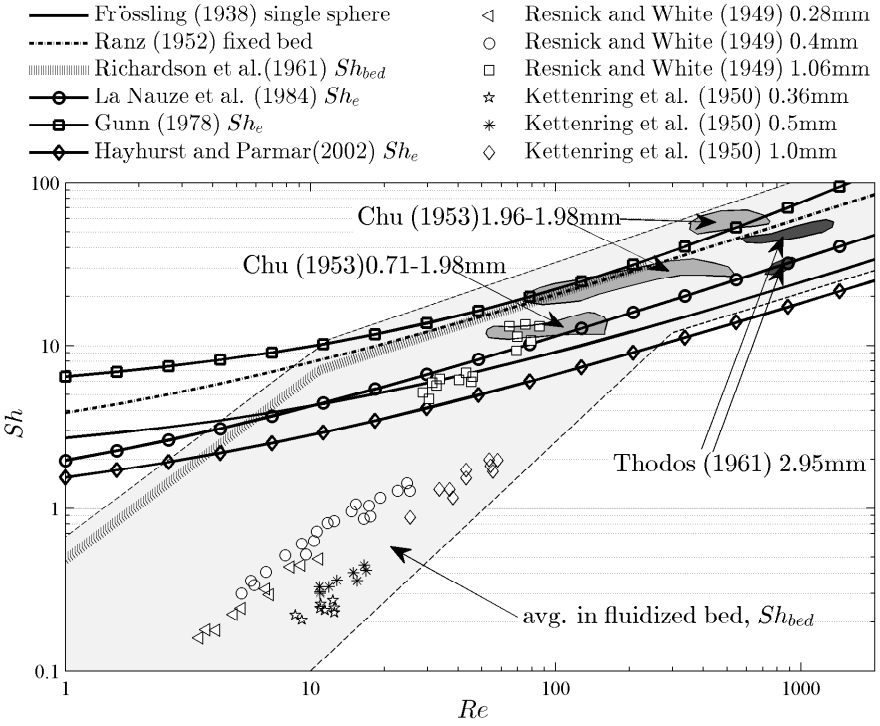

Figure 2.3: Bed Sherwood numbers (experimental data of Resnick and White (1949) and Kettering et al. (1950) is adapted from Kunii and Levenspiel (1968))

active particles. Resnick and White (1949) derived the bed Sherwood numbers by the technique of naphtalene sublimation in small diameter bubbling bed reactors (d_r= 2.2, 4.4 cm). The results showed that the bed Sherwood number was dependent on the particle size (d_p= 0.28-1.06 mm), as well as the Reynolds number. The bubbling bed experiments of Kettering et al. (1950) showed a similar decrease of the bed Sherwood numbers with a decrease of particle diameter (d_p= 0.36-1 mm). A vaporization of water mass transfer measurements technique in a slightly wider reactor (d_r= 5.9 cm) was used in the experiments. The experiments of Richardson and Szekely (1961) for the small Reynolds number range ($Re < 10$) showed the same exponential relation of the bed Sherwood and Reynolds number as the studies of Resnick and White (1949) and Kettering et al. (1950). It is also worth noting that the experiments were carried out at the ambient conditions in the bubbling bed regime, which approached the slugging regime at the higher fluidization velocities. Also the theoretical approach for fine particle beds with large bubbles presented by Kunii and Levenspiel (1968) explained the decrease of bed Sherwood number

with the decreasing particle diameter. The particle size dependence was be related to the ratio of the bubble-emulsion gas interphase mass transfer and absortion (reaction) rate. All the experimental data of Resnick and White (1949) and Kettering et al. (1950) could be correlated by a form of bed Sherwood number equation derived from the basic species conservation equations of the fluidized bed system with heterogeneous reactions. The correlation has the general form of

$$Sh_{\mathrm{bed}} = A \times Re + B. \tag{2.3}$$

However, the correlation applies only for a certain particle size, reactor diameter and chemical reaction. It is evident that the dimensionless group of the particle Reynolds number cannot alone describe the combined effects of the interphase mass transfer, the emulsion mass transfer and the chemical kinetic reaction rate to form a general bed Sherwood number correlation. Figs. 2.4a-b show the principle of the conditions the average gas-bed mass transfer coefficient (Sh_{bed}) concerns at the bubbling and turbulent fluidization regimes. At minimum fluidization, the average gas-to-bed mass transfer coefficient is certainly the same as the average in-emulsion mass transfer coefficient. Taking account of the discussed experimental and theoretical results, it is also evident that at the bubbling bed regime in the lower Reynolds number range, there occurs convective bypass of gases in the bubbles and the bubble-emulsion interphase mass transfer is a limiting mechanism in the total gas-bed mass transfer process. At the higher Reynolds numbers the bed Sherwood number follows the single, fixed bed and emulsion Sherwood numbers, thus the interphase mass transfer is not the controlling mechanism in these large particle beds as concluded by Kunii and Levenspiel (1991).

The theoretical review presented above concerns mainly the bubbling bed fluidization regime. However, the theoretical aspects of the controlling mechanisms in the average gas-bed mass transfer could be extended also to the turbulent regime. Of course, the structure of the voids and clusters are more complicated as underlined in Fig. 2.4b. In a review of gas-solid mass transfer coefficient correlations in the circulating fluidized beds, Breault (2006) highlights a wide range (from 10^{-5} to 200) of Sherwood numbers presented in the literature. After the elimination of a few experiments from the analysis due to a different fluidization regime or non-appropriate measurements, the bed Sherwood number in the circulating fluidized bed risers was ranged to a region from 0.01 to 10. The review also suggested a clarification of the fluidization regime with mass transfer research conducted in order to establish a distinct classification of the results. Subsequently, Breault (2009) has presented a thin film analogy method to estimate gas-solid mass transfer over a cluster in the core-annular and fast fluidization regimes of a circulating fluidized bed reactor. The model could predict the few available experimental mass transfer coefficients. Later, Breault et al. (2010) have incorporated the thin film analogy to Eulerian CFD simulations and showed the Sherwood number over a cluster in a circulating fluidized bed that was in the same range as the experimental data of Resnick and White (1949), and relevantly smaller than proposed by the emulsion Sherwood number correlation (Gunn, 1978) used as a default in the CFD simulations of heterogeneous reactions. At the clus-

tering core regime, the heterogeneous mass transfer is mostly referred to a gas-solid mass transfer over a cluster. Wang et al. (2009) have shown by means of CFD modeling that the average gas-solid Sherwood number can be overestimated up to five times, if the local, remarkably lower gas velocities inside a cluster are not used when estimating the gas-solid mass transfer over the cluster with the emulsion Sherwood numbers (Table 2.1). The CFD study of Wang et al. (2009) quantified the effect of the cluster voidage and the superficial gas velocity on the cluster Sherwood number.

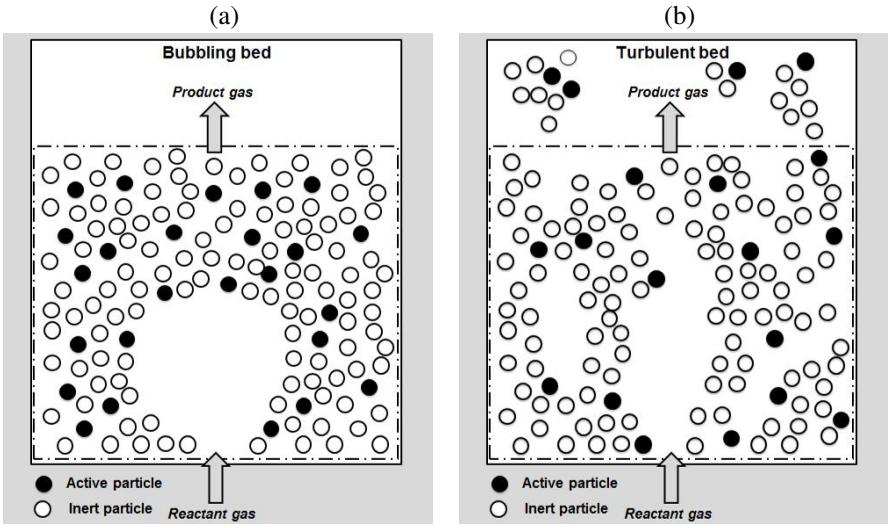

Figure 2.4: Schematics of different gas-solid contact conditions in a small-diameter fluidized bed reactor or in a calculation cell of a fluidized bed reactor model: (a) bubbling bed with inert and active particles, (b) turbulent bed regime with inert and active particles.

In recent years, couple of research studies, where CFD simulations of very fine particle fluidized bed systems has been used to derive bed Sherwood numbers, have been presented. Chalermsinsuwana et al. (2009) derived bed Sherwood numbers for the fluid-catalytic cracking (FCC) process (d_p= 76 μm) by means of Eulerian CFD modeling of a fast fluidized bed (u_f= 5.2 m/s) in a pilot scale reactor (d_r= 20 cm, H= 14.2 m) of the ozone decomposition process. The obtained bed Sherwood numbers were between 0.0044 and 0.006 in the lower part of the reactor. Additionally, axial variation was shown, as the bed Sherwood numbers in the lower dense bed were slightly higher than in the upper clustering part of the reactor. The CFD-based bed Sherwood numbers were one to two orders of magnitude lower than the earlier presented Sherwood numbers. Similar fine FCC particles (d_p= 75 μm) were used by Kashyap and Gidaspow (2010) in an experimental mass transfer research with a shallow pilot scale ozone decomposition reactor (W= 30.5 cm, D=5cm, H=140cm). Kashyap and Gidaspow (2010) report on experimental bed Sherwood numbers between 0.00005 and 0.00011 for the Reynolds number of 1.57. The lower bed was under the bubbling bed regime and above the dense bubbling

bed a clustering regime was observed. The bed Sherwood number was about 0.0001 at the bottom of the bed and at the clustering region, while it dropped to a half at the upper parts of the bubbling bed. Chalermsinsuwan and Piumsomboon (2011) have used the Eulerian CFD model to simulate the bubbling bed operation (Re=1.57) of the same pilot ozone decomposition reactor with fine FCC particles. Two-dimensional simulations resulted in average bed Sherwood numbers in the reactor in the range of 0.0004 to 0.0008. As a conclusion, the bed Sherwood numbers for the very fine particle fluidized bed processes, as the fluid catalytic cracking, seemed to be several orders of magnitude lower than the earlier presented experimental results for larger particles showed.
As a summary of this chapter, the bed Sherwood numbers for fluidized bed processes with an inert and active particle bed, e.g. combustion and gasification, at high temperature conditions are not available in the literature. Furthermore, a general empirical bed Sherwood number correlation that is valid for a wide Reynolds number range and for different types of fluidized bed processes, does not exist. On the other hand, the basic behavioral principles at the high and low Reynolds numbers are known.

2.1.3 Interphase mass transfer

When describing heterogeneous gas-solid mass transfer in bubbling bed reactors, the bubble-emulsion interphase and emulsion gas-solid mass transfer rates are usually considered separately. For the bubbling bed regime, the bubble-emulsion mass transfer phenomenon is well known, and also related and validated coefficient correlations can be found. On the other hand, for the slugging and turbulent regimes, only a few bubble-emulsion (or void-emulsion) interphase mass transfer coefficient experiments and correlations have been presented in the literature.
Figs. 2.5a-b show schematically a convective flow of gas within a dilute bubble (or void) phase and interphase mass transfer to a solid-dense emulsion (or cluster) phase at the bubbling bed and turbulent regimes. The interphase mass transfer rate is usually described as follows

$$q_{\mathrm{B,be}} = K_{be}(C_{\mathrm{B,b}} - C_{\mathrm{B,e}}), \tag{2.4}$$

where q_{B} is the molar transfer rate of gaseous species B from the bubble to the emulsion phase, and $C_{\mathrm{B,b}}$ and $C_{\mathrm{B,e}}$ concentrations of species B in the bubble and emulsion phases, respectively. The interphase mass transfer coefficient can be expressed also as

$$K_{be}[s^{-1}] = k_{\mathrm{be}} a_{\mathrm{b}}, \tag{2.5}$$

where a_{b} [$\mathrm{m}^2/\mathrm{m}^3_{\mathrm{bed}}$] describes the surface area of bubbles/voids and k_{be} [$\mathrm{m/s}$] is the interphase mass transfer coefficient presented per surface area of the bubble surface area given. Fig. 2.5 highlights the fact that at the turbulent regime the interphase mass transfer is enhanced by the increased specific surface area of the voids a_{b}. However, at the turbulent regime, an exact experimental determination of the specific surface area of the voids is more challenging. The importance of the rate of interphase mass transfer is that it

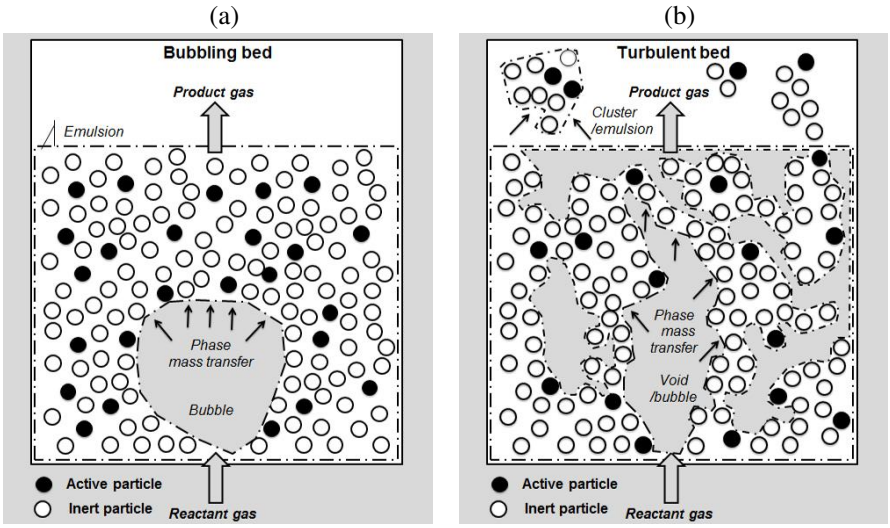

Figure 2.5: Schematics of phase mass transfer in a small-diameter fluidized bed reactor or in a calculation cell of a fluidized bed reactor model. (a) bubbling bed regime with inert and active particles and (b) turbulent regime with inert and active particles.

can have a dominant role in the chemical reactions occurring in fluidized beds, as it controls the reactant gas concentrations between the solid rich emulsion and the dilute bubble phases. Table 2.2 shows a set of empirical correlations of the interphase mass transfer coefficient for the bubbling, slugging and turbulent fluidization regimes.
In order to understand the interphase mass transfer in bubbling beds, a basic classification of bubbles in the fine and coarse particle beds is necessary. In the bubbling bed of fine solids, fast clouded bubbles are formed as described by the Davidson model (Davidson and Harrison, 1963) for gas flow in the bubbles. In the large particle beds (Geldart D), bubbling results as slow cloudless bubbles. The criterion for the formation of fast bubbles is related to bubble rise velocity in relation to the gas velocity in the emulsion as $u_{\mathrm{br}} > u_{\mathrm{e}} \approx u_{\mathrm{mf}}/\alpha_{\mathrm{g,mf}}$. The bubble rising velocity can be estimated from $u_{\mathrm{br}} = 0.711(gd_{\mathrm{b}})^{1/2}$ (Davidson et al., 1959). In principle, the fast bubble rises with a higher velocity than the surrounding emulsion gas. Inside the fast bubble, the gas flows upward until it convectively penetrates the roof of the bubble. Above the bubble, the gas flow turns downwards and recirculates back to the bubble from the bottom of it. The circulation region is called a cloud and it is characterized by a higher voidage than the surrounding emulsion due to the circulating convective interphase mass transfer around the bubble. On the other hand, when a bubble rises with a same, or lower, velocity than the surrounding emulsion gas ($u_{\mathrm{e}} \geq u_{\mathrm{br}}$), the bubble is called a slow cloudless bubble. These are typical for large particle beds. In the slow bubbles, the emulsion gas flows convectively through the bubble from the bottom to the roof. The slow bubble has also a circulation flow, but beside the bubble, not around it. It is worth of noting that the transition between the fast and slow bubbles is smooth and intermediate (rising velocity) bubbles

Table 2.2: Interphase mass transfer correlations

Author		Fluidization mode
		Bubbling bed
Davidson and Harrison (1963)	$K_{\mathrm{bc}} = 4.5(\frac{u_{\mathrm{mf}}}{d_{\mathrm{b}}} + 5.85(\frac{D_{\mathrm{g}}^{1/2} g^{1/4}}{d_{\mathrm{b}}})$	Bubble-cloud
Patridge and Rowe (1966)	$k_{\mathrm{be}} = D_{\mathrm{g}}/d_{\mathrm{c}}(2 + 0.6Re_{\mathrm{c}}^{0.5} Sc^{0.33})$	Bubble-cloud-emulsion
	$Re_{\mathrm{c}} = \frac{(u_{\mathrm{c}} - u_{\mathrm{e}}) d_c \rho_{\mathrm{g}}}{\mu_{\mathrm{g}}}$	
Kunii and Levenspiel (1968)	$1/K_{\mathrm{be}} = 1/K_{\mathrm{bc}} + 1/K_{\mathrm{ce}}$	Fast bubble with thin cloud
	$K_{\mathrm{bc}} = 4.5(\frac{u_{\mathrm{mf}}}{d_{\mathrm{b}}} + 5.85(\frac{D_{\mathrm{g}}^{1/2} g^{1/4}}{d_{\mathrm{b}}})$	Bubble-cloud
	$K_{\mathrm{ce}} = 6.77(\frac{D_{\mathrm{g}} \alpha_{\mathrm{g,mf}} u_{\mathrm{br}}}{d_{\mathrm{b}}})^{1/2}$	Cloud-emulsion
Sit and Grace (1981)	$k_{\mathrm{be}} = u_{\mathrm{mf}}/3 + 2(\frac{D_{\mathrm{g}} \alpha_{\mathrm{g,mf}} u_{\mathrm{br}}}{\pi d_{\mathrm{b}}})$	2D freely bubbling bed
	$a_{\mathrm{b}} = 6/d_{\mathrm{b}}$	
Chiba and Kobayashi (1970)	$K_{\mathrm{be}} = 11/d_{\mathrm{bub}}$	Single bubbles
Hatano and Ishida (1986)	$k_{\mathrm{be}} = 0.127 D_{\mathrm{g}}^{1/3} g^{1/3} (\frac{\alpha_{\mathrm{g,mf}} u_{\mathrm{br}}}{u_{\mathrm{f}}})^{0.22}$	Single and paired bubbles
Hovmand and Davidson (1971)	$k_g = u_{\mathrm{mf}} + \frac{16 \alpha_{\mathrm{mf}} I}{1+\alpha_{\mathrm{mf}}} (\frac{D_{\mathrm{g}}}{\pi})^{1/2} (\frac{g}{d_r})^{1/4}$	Slugging bed
	$a_{\mathrm{b}} = 1/(d_{\mathrm{r}} f_s)$	
		Turbulent bed
Foka et al. (1996)	$K_{\mathrm{be}} = k_{\mathrm{be}} a_{\mathrm{b}} = 1.631 Sc^{0.37} u_{\mathrm{f}}$	Bubbling and turbulent bed
Miyauchi et al. (1980)	$K_{\mathrm{be}} = k_{\mathrm{be}} a_{\mathrm{b}} = 3.7(\frac{D_{\mathrm{g}}^{1/2} \alpha_{\mathrm{b}}}{d_{\mathrm{b}}^{5/4}})$	Turbulent bed
Zhang and Qian (1997)	$k_{\mathrm{be}} = 1.74 \times 10^{-4} Sc^{0.81} D_{\mathrm{g}}/d_{\mathrm{p}}$	Turbulent bed

with a large cloud region exists between the two major bubble classifications. The generally accepted bubble flow theory is introduced in detail in Davidson and Harrison (1963). Kunii and Levenspiel (1991) also describe the bubble flow model theory and discuss the characteristics of bubbles in dense bubbling beds comprehensively including the bubble interaction (coalescence, splitting), shape, size, frequency and slugging phenomenona.
The first interphase mass transfer coefficient correlation in Table 2.2, the bubble-cloud mass transfer correlation of Davidson and Harrison (1963), is based on theoretical analysis of the Davidson bubble model. The convective term in the interphase mass transfer correlation originates from the throughflow equation of Murray (1965), which relates the convective throughflow to the minimum fluidization velocity as $k_{\mathrm{be}} = u_{\mathrm{mf}}/\pi$. The diffusion term is derived by the penetration model of Higbie (1935) with the assumption of a thin diffusive cloud around the bubble. The second correlation, the bubble-emulsion interphase mass transfer coefficient correlation of Patridge and Rowe (1966) relies on the analogy to gas-solid convective mass transfer over a sphere in gas flow. The origi-

nal theory assumes that the cloud and bubble are one perfectly mixed single phase, and the correlation applies the single particle Sherwood number correlation, where the cloud Reynolds number is defined with the diameter of the cloud and the relative velocity difference of the bubble and emulsion gases. Kunii and Levenspiel (1968) have presented an interphase mass transfer coefficient correlation for thin clouded fast bubbles (fine particle, Geldart A bed). The correlation has the bubble-cloud convective throughflow and diffusive terms (Davidson and Harrison, 1963) and a cloud-emulsion diffusive mass transfer term. The diffusive mass transfer term is based on the penetration model of Higbie (1935). The experiments by Stephens et al. (1967) and Chiba and Kobayashi (1970) with the single bubble injection method showed that the volumetric interphase mass transfer coefficient of the fast clouded bubbles drops with the increase of the bubble diameter (Fig. 2.6).

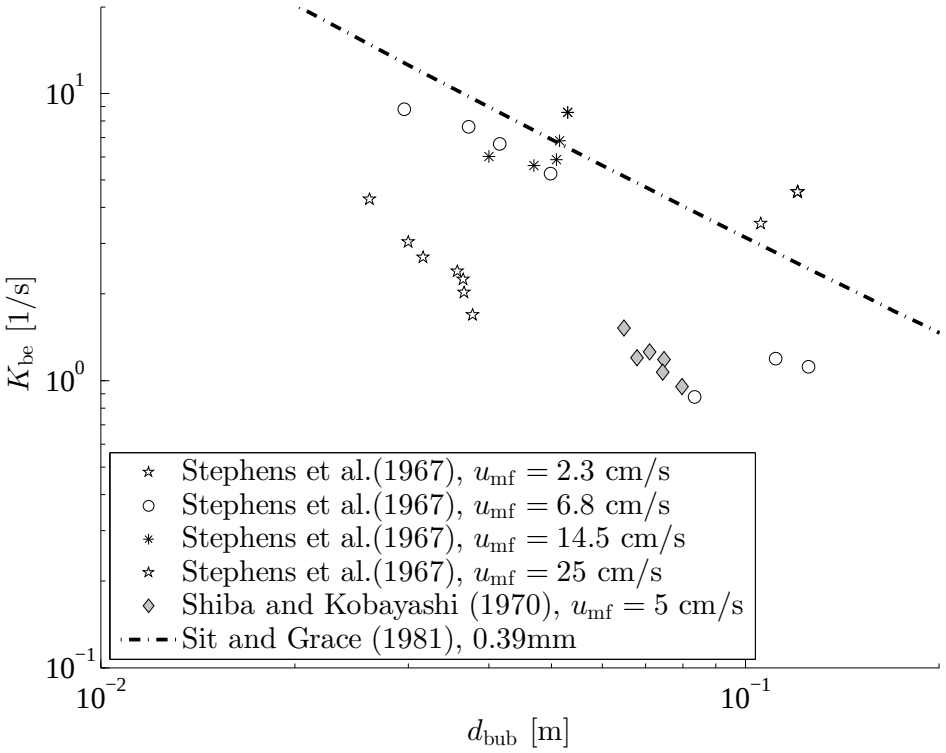

Figure 2.6: Volumetric interphase mass transfer coefficients against bubble diameters; the experimental single injected bubble method data (Stephens et al., 1967; Chiba and Kobayashi, 1970) is adapted from Kunii and Levenspiel (1991).

The interphase mass transfer coefficient correlations presented above were defined for a single rising bubble. The correlation of Sit and Grace (1981) takes account of the enhance-

ment of convective throughflow in interphase mass transfer due to bubble interaction and is validated for the coarser, Geldart B (0.39 μm) particle bed. The correlation (Table 2.2) has both throughflow and diffusive terms. It has been defined by experiments conducted in a two-dimensional freely bubbling bed (W=59 cm, d_r=0.9 cm). It is worth noting that in the experiments the fluidization velocities were kept close to the minimum fluidization velocity of 0.112 m/s. In the coarser particle beds, bubbling occurs as slow cloudless bubbles or bubbles with thick clouds (intermediate particle sizes) that both have a remarkable rate of convective throughflow. Actually, this correlation is comparable to the bubble-cloud interphase mass transfer correlation of Kunii and Levenspiel (1968) as discussed in Ho (2003a). In general, in a fine particle bed, the diffusive term controls the rate of interphase mass transfer, while in a coarser particle bed, the convective throughflow dominates (Sit and Grace, 1981). The correlation of Hatano and Ishida (1986) is defined for single rising bubbles. However, their experimental research suggested the same correlation for paired bubbles contrary to the findings of Sit and Grace (1981). However, Sit and Grace (1981) conclude that the bubble interaction enhancement of the convective throughflow term increased with the increase of particle sizes.

Hovmand and Davidson (1971) have introduced interphase mass transfer coefficient correlation also for the slugging regime (Table 2.2). Even though the slugging regime is not a normal operation mode for fluidized bed reactors, it can occur in very small diameter bench and pilot reactors with a sufficient bed height. In general, slugging can occur when the maximum bubble size exceeds 60 percent of the reactor diameter. The slugging criteria presented by Stewart and Davidson (1967) state that slugging can occur, if $u_\mathrm{f} - u_\mathrm{mf} > 0.07(gd_\mathrm{r})^{1/2}$.

For the turbulent regime, only a few empirical interphase mass transfer coefficient correlations have been reported in the literature (Bi et al., 2000) due to the difficulty of definition and experiments. This originates from the characteristics of turbulent fluidization as a strict interface between the emulsion/cluster and bubble/void may not exist (Fig. 2.5b). The local voidage can vary from one to the voidage at the minimum fluidization conditions. Table 2.2 presents the turbulent bed interphase mass transfer correlations of Miyauchi et al. (1980), Foka et al. (1996) and Zhang and Qian (1997). The interphase mass transfer coefficient K_be correlation of Miyauchi et al. (1980) is based on experiments in a turbulent bed (d_r=8 cm) of very fine particles (d_p = 53 μm) The fluidization velocity was varied from 0.2 $\mathrm{m/s}$ to 0.4 $\mathrm{m/s}$ and the resulted interphase mass transfer coefficients were in the range of 0.8-0.93 s^{-1}. The interphase mass transfer coefficients showed remarkable dependence on the diffusion coefficient, which suggests that the diffusive component is remarkable also in fine particle turbulent beds similar to the case of fine particle bubbling beds. The interphase mass transfer correlation K_be of Foka et al. (1996) has the widest validity range. The experimental work covered both bubbling and turbulent regimes in 10 cm and 20 cm diameter fluidized beds. The particle diameter range was 75-196 μm, and fluidization velocity up to 2.6 $\mathrm{m/s}$ was applied in the experiments. The interphase mass transfer coefficients were between 0.19 s^{-1} and 4.6 s^{-1} and showed remarkable dependence on the fluidization velocity contrary to the fine particle experiments. In the experimental work of Zhang and Qian (1997), fine particles with a diameter of 77 μm in a 20 cm diameter turbulent bed were used, and fluidization velocities

up to 1 $\mathrm{m/s}$ were applied. The interphase mass transfer coefficient k_{be} correlation was given as a function of the Reynolds number and was close to the structure of the common emulsion Sherwood number correlations.

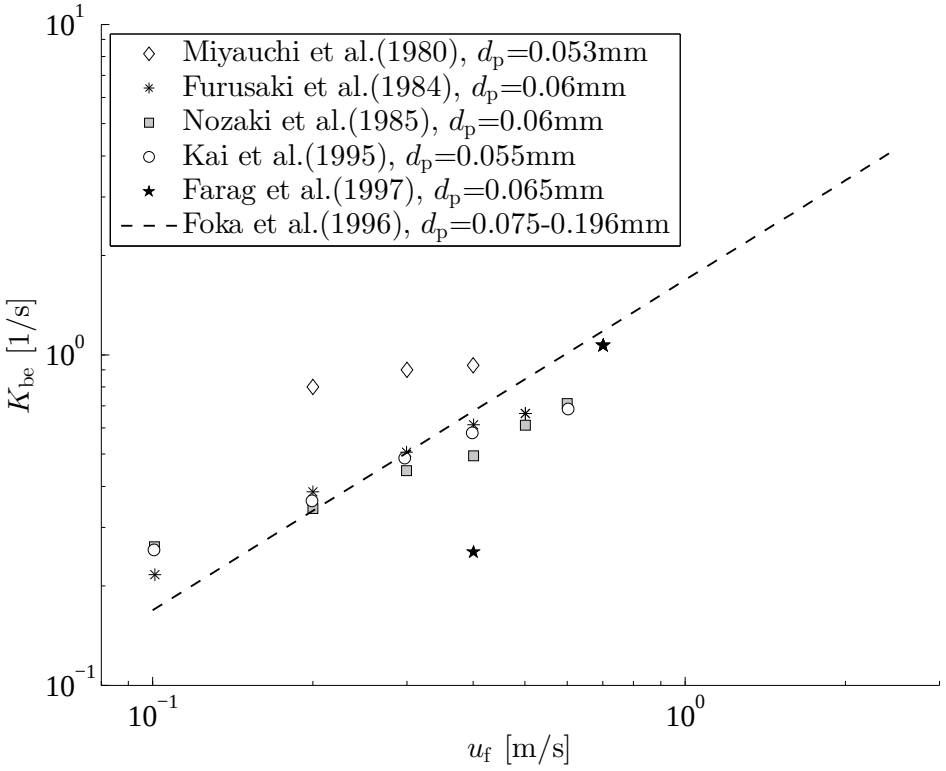

Figure 2.7: Volumetric interphase mass transfer coefficients against fluidization velocity in fine particle turbulent beds. Data of Furuzaki et al. (1984) and Nozaki et al. (1985) has been adapted from Kai et al. (1995), and data of Miyauchi et al. (1980) from Bi et al. (2000).

Besides the turbulent bed correlations discussed above, also some experimental studies focusing on the interphase mass transfer coefficients, mostly with very fine particle beds, has been conducted. In principle, all experimental fine particle (55 μm - 65 μm) turbulent bed interphase mass transfer coefficients K_{be} of Furuzaki et al. (1984), Nozaki et al. (1985), Kai et al. (1995) and Farag et al. (1997) show dependence on the fluidization velocity as highlighted in Fig. 2.7. The same dependence was already shown in the experiments of Miyauchi et al. (1980). The experiments of Furuzaki et al. (1984) were conducted in a fluidized bed reactor having the diameter of 19.5 cm with fluidization velocities up to 0.5 $\mathrm{m/s}$. Nozaki et al. (1985) found similar interphase mass transfer behavior in a fluidized bed reactor having the diameter of 10 cm. Also, the experimen-

tal work of Kai et al. (1995) in a 5 cm turbulent fluidized bed reactor showed the same fluidization velocity response. Kai et al. (1995) showed also that the increase of the volumetric interphase mass transfer coefficient K_{be} resulted from the increase of the specific bubble surface area a_{b} [$\mathrm{m}^2/\mathrm{m}^3_{\mathrm{bed}}$] with the fluidization velocity, while the interphase mass transfer coefficient k_{be} was independent of the fluidization velocity (constant k_{be} of 0.013 $\mathrm{m/s}$ in their experiments). The fine particle interphase mass transfer coefficients (d_{r}=50 cm) obtained by Farag et al. (1997) differed slightly from the other fine particle turbulent bed experiments regarding the fluidization velocity response.
In addition to the fluidization regime dependent dense bed interphase mass transfer, also region-vise variation of interphase mass transfer in a fluidized bed occurs. The effect of void-cluster interphase mass transfer to the cluster Sherwood number at the core region of the core-annular and fast fluidized circulating fluidized beds is discussed in Chapter 2.2.2. Furthermore, the presence of jets brought by the primary air feeding nozzles and the secondary air nozzles, enhances the interphase mass transfer dramatically. For example, in the grid region the interphase mass transfer coefficient has been reported to be 40 to 60 times greater than in the bed region (Ho, 2003b). In the present work, the focus is, however, on the interphase mass transfer in the lower dense bed region of fluidized beds.
As a conclusion, the bubble-emulsion interphase mass transfer coefficient correlations for fast bubbles with clouds and for slow cloudless bubbles at the bubbling bed regime are theoretically well-established and are also validated for the Geldart A and B particles. On the other hand, the fluidization conditions in the experiments have mostly been close to the minimum fluidization condition. Considering the turbulent regime, almost all the interphase mass transfer coefficient correlations are defined for fine (Geldart A) particle fluidized beds for fluidization velocities lower than 1 $\mathrm{m/s}$. On the other hand, the fluidization velocity response for fine particle bed conditions is well-known.

2.2 Heterogeneous mass transfer in fluidized bed models

In practice, the chemical conversion and thermal performance of large industrial size bubbling and circulating fluidized bed combustors can be estimated by steady-state semi-empirical or coarse-grid multiphase Eulerian CFD models (Myöhänen, 2011; Shah, 2012). In order to relate the knowledge regarding heterogeneous mass transfer in fluidized beds to the prediction accuracy of the heterogeneous reactions of the fluidized bed models, different heterogeneous mass transfer models applied in the models are described in this chapter. A basic classification of circulating fluidized bed reactor models based on the level of their sophistication can be done according Basu (1999):

I One-dimensional plug flow model with simple mass and energy balances

II Core-annulus (1.5D) model with semi-empirical sub-models of combustion and other processes

III Three-dimensional model with Navier Stokes equations for fluid dynamics, and detailed semi-empirical sub-models for chemical kinetics and individual physical processes

In recent decades, the focus in the development of CFB reactor models have moved from simple plug flow models of level I to core-annulus reactor models (level II), which are still the models applied in the engineering design of fluidized bed reactors. This has been followed by a development of an increasing number of two- and three-dimensional circulating fluidized bed reactor models. On the other hand, fine- and coarse-grid Eulerian gas-solid CFD modeling of fluidized beds (level III) has been under intensive development recently, and it has been applied to validation studies of a variety of different fluidized bed processes.
In order to fundamentally classify the fluidized bed models, it is worth noting that the real fluidized bed processes are transient. Besides being time dependent, the fluidized bed process is always characterized by three-dimensional flow structures, such as the round shape of bubbles, clusters, voids and streamers, regardless of the size scale of the reactor. Thus, understanding these basic features of the fluidized bed models and acknowledgement of the consequent capacities to predict detailed process performance are the keys for the proper classification of the fluidized bed model. In general, fluidized bed models can be classified with the following main features: i) time dependence, ii) number of space dimensions, iii) number of phases and iv) space discretization.
The models concerned in this thesis have two different approaches regarding the time dependence in the process.

- First, the empirical models are steady-state models. These models consider only time-averaged conditions, properties and rates in a calculation cell. Thus, they lose the information on the transient three-dimensional flow structures.

- Secondly, the Eulerian CFD models applied in this work apply the time discretization of 0.001 s. These CFD models are able to solve the time-dependent behavior of important flow structures, such as formation and growth of bubbles, and the vigorous movement of meso-scale streamers and cluster above the dense bed.

However, the type of time resolving is not enough to describe the basic characteristic of the model. For example, the steady-state empirical models with three dimensions try to describe the time-averaged solid and gas concentration, reaction rate and temperature profiles. Even though the solid density profiles are most likely based on one-dimensional semi-empirical correlations, the model acknowledges also the lateral locations of important sources, such as fuel and air feedings. Therefore, three-dimensional models presented in Tables 2.5 and 2.6 predict a process performance that is time-averaged and three-dimensional. In the case of empirical two-dimensional models, the third space-dimension, usually the depth of reactor, is not described, and thus the properties, conditions and rates in the calculation cells present also space-average over the dimension that is not discretized. With respect to the three-dimensional models, most importantly the information on the local sources, such as the penetration of secondary air jet and fuel feeding streams, are filtered. In the one-dimensional models, the space-averaging is applied also to the last lateral dimension, and only the axial performance is predicted according to the lateral- and time-average conditions, properties and rates within the calculation cells.

Besides the time resolving and number of space dimensions, the empirical models have additional important fundamental feature: the number of phases. Here, the phase refers commonly to the solid-rich emulsion phase and gas-rich bubble phase. Above the dense bed, these phases are usually called clusters and voids. In the case where one gas-solid phase in calculation cell is concerned, the model assumes that all solids and gas species are evenly distributed within the calculation cell. The other applied option is to define two phases: solid-rich emulsion and gas-rich bubbles. In this approach, the conditions and rates are constant within the phase inside the calculation cell. A benefit of the latter approach is that it can describe some of the time-dependent and space-averaged features of the fluidized bed process. This is possible even if the two-phase model were a steady-state projection of the process into the axial direction. Naturally, such transient phenomena as the size distribution of bubbles, voids and clusters cannot be fully described, and only average sizes of flow structures can be modeled.

Finally, there is one more main feature of fluidized bed models worth discussing here: the space discretization. Myöhänen and Hyppänen (2011) presented a classification of fluidized bed models based on the time and space scales and highlighted that typically, the steady-state empirical models apply macro-scale space discretization from 0.1 m to even 50 m. In contrast, the Eulerian CFD models apply also the meso-scale space discretization varying usually from 0.1 mm to the maximum of few meters. The level of details in flow structures and consequent local reaction performance that a fluidized bed model can describe depends on the size of space discretization. For example, the transient Eulerian CFD model applied in this thesis for the research of the heterogeneous mass transfer phenomenon applies the space discretization between 1.25 mm and 30 mm. The applied CFD model is considered to have fine-grid capable of resolving the meso-scale flow structure of bubbles, clusters and voids, which is very important for the process performance, and also defines the rate of local average heterogeneous mass transfer that is a main research focus in the thesis. Even though two-dimensional approach in the CFD simulations is applied, the relevant meso-scale structures are assumed to be predicted with acceptable accuracy as only small-scale reactors are concerned. The applied fine-grid two-fluid CFD model is presented in Chapter 3 in details.

The above discussion forms the basis why the average gas-bed and interphase mass transfer coefficients derived from the transient Eulerian CFD simulations with fine-grids presented in Chapter 3 can be applied to the steady-state semi-empirical or coarse-grid multiphase CFD models. In the following, the steady-state empirical and transient Eulerian CFD models of BFB and CFB reactors presented in the literature are discussed with respect to the above defined fundamental features.

2.2.1 Empirical bubbling bed models

Almost all steady-state bubbling bed models have a fluidization model, and thus belong to the group of sophistication level II. The fluidization model can have either one, two or three phases, and the definition of the phase is different from the traditional gas, fluid and solid description. The one-phase bubbling bed model assumes a homogeneous dense gas-solid suspension as a bed where a plug flow of gas occurs. As one-phase models

have been shown to be inadequate for an accurate prediction of the bubbling bed processes, most bubbling bed models describe a meso-scale (10 mm - 0.1 m) two-phase flow structure. The two phases are a gas-rich bubble and a solid-dense emulsion phase. The original two-phase theory of Toomey and Johnstone (1952) stated that all gas flow excess to the minimum fluidization velocity flows through the bed as bubbles and all the solids are in the dense emulsion, where a plug flow of gas at a minimum fluidization velocity occurs. The Davidson-Harrison bubble model (Davidson and Harrison, 1963) still forms the basic understanding of the bubble behavior, as it can predict the slow bubbles with upward throughflow of gas and the fast bubbles surrounded by circulating gas flow called cloud. The characteristics of the cloud phase and clouded bubble behavior were discussed in Chapter 2.1.3 above. Kunii and Levenspiel (1968) extended the model to a three-phase, bubble-cloud-emulsion, bubbling bed model, where also the presence of solids in a bubble and different gas flow behavior characteristics in a dense emulsion were considered. The bubble assemblage model (Kato and Wen, 1969) has also bubble-cloud-emulsion phases and it additionally considers the bubble size growth with the distance from the fluidization gas distributor. Other often referred bubbling bed models are the counter-current back-mixing model of Fryer and Potter (1972) and the bubbling bed model of Werther (1980), which takes particularly account of the bubble size distribution and the expansion of the bubbling bed. A bed expansion model of Johnsson et al. (1991) applies a simple principle of constant pressure drop over a fluidized bed, and is also a derivation from the two-phase flow theory (Toomey and Johnstone, 1952). The bubbling bed flow theory seems to be well-established, as all recently presented models, e.g. those presented by Gómez-Barea and Leckner (2010) and Jain et al. (2013), combine the structures of the earlier presented models, while they still may apply an updated knowledge in their semi-empirical correlations. For example, Gómez-Barea and Leckner (2010) apply in their bubbling bed model for BFB and CFB gasification estimates the single bubble rising velocity according to Davidson and Harrison (1963), bubble velocity from Kunii and Levenspiel (1968), the bubble growth and voidage in the emulsion phase from Delvosalle and Vanderschuren (1985), and the interphase mass transfer coefficient from Sit and Grace (1981) as presented in Table 2.2. In contrast, Jain et al. (2013) have presented a bubbling bed model that describes the bubble growth similarly to the bubble assemblage model of Mori and Wen (1975), while it estimates the interphase mass transfer with the Kunii and Levenspiel (1968) correlation shown in Table 2.2. The bubble assemblage model (Kato and Wen, 1969) originally applies the interphase mass transfer correlation of Chiba and Kobayashi (1970) given in Table 2.2. Most bubbling bed models have been developed for fine-particle catalytic processes, but they have already been applied in models of solid fuel conversion processes as well (Gómez-Barea and Leckner, 2010).

As a conclusion, the bubbling bed fluidization models most importantly describe the fraction of gas in the bubbles, the size and velocity of the bubbles, the voidage and gas velocity in the emulsion, and of course interphase mass transfer. In order to describe the heterogeneous gas-solid mass transfer, the one-phase bubbling bed model should use the bed Sherwood number, and the bubble-emulsion models require both the interphase and within-phase gas-solid mass transfer coefficients. Further, the three-phase models have two interphase mass transfer coefficients, the bubble-cloud and cloud-emulsion coeffi-

cients as shown in Table 2.2. Besides the selection of the fluidization model, particular attention should be paid to the validity range (e.g. particle size, fluidization velocity, reactor size) of the empirical correlation applied in the bubbling bed models. A good practice for developing a suitable model for a particular type of process has been presented by Jain et al. (2013), who have performed a model validation study for five different chemical catalytic conversion processes in the bubbling bed with Geldart B solids, and compared the prediction performance of their model with the bubbling bed models of Kunii and Levenspiel (1968) and Kato and Wen (1969).
In addition to the fluidization and heterogeneous mass transfer models, the heterogeneous reaction rate prediction in bubbling and circulating fluidized bed models are affected by the particle reaction and population models as well as the solid and gas mixing models. The particle models can be divided into uniform combustion, shrinking particle and shrinking core models. Particle population balance usually describes the reacting particle size distribution by taking account of fragmentation, attrition and size reduction due to the reactions. The increase of dimensions in the fluidized bed models offers an opportunity to describe both lateral and axial solid fuel segregation with point-wise fuel feeding and limited fuel mixing by the dispersion mechanism. However, as these are secondary aspects regarding the heterogeneous mass transfer focus of the thesis, they are only shown in Tables 2.3, 2.4, 2.5 and 2.6 presenting different circulating fluidized bed models for the following discussion regarding heterogeneous mass transfer in CFB combustor models.

2.2.2 Empirical CFB combustor models

The circulating fluidized bed combustor models are macroscale (discretization size: 0.1m -1m) models that describe the solid flow dynamics by semi-empirical axial solid density profiles, while the meso-scale flow structures, such as clusters, streamers and voids, are not modeled (Myöhänen and Hyppänen, 2011). The circulating fluidized bed models can be classified by two of their main features: (1) number of dimensions and (2) type of fluidization model as (a) one-phase homogeneous suspension, (b) bubble-emulsion phase description or (c) bubble-cloud-emulsion phases. Tables 2.3 and 2.4 present a selection of core-annulus CFB combustor models, Tables 2.6 and 2.5 show two- and three-dimensional CFB combustor models presented in the literature. The models are described according to the principle of their fluid dynamic model and aspects related to the heterogeneous mass transfer and reaction rates. There are two main procedures to describe the bottom bed of a circulating fluidized bed. The first approach (i) assumes a turbulent bottom bed with a constant voidage and a plug flow of gas and a perfect dispersion of solids in a calculation cell. The second approach (ii) applies a bubbling bed model with bubble and emulsion phases for the lower bed region.
As an example, the semi-empirical core-annulus circulating fluidized bed combustor models of Adanez et al. (1995), Wang et al. (1999) and Hua et al. (2004) apply the first approach (type i) for fluidization in the lower bed as shown in Table 2.3. Adanez et al. (1995) were able to show the effect of carbon particle size, bed temperature, air ratio and fluidization velocity to the carbon combustion efficiency in a pilot CFB combustor by the 1.5D core-annulus CFB model that resulted in a proper fit to the experimental data with

three types of coals without applying any fitting parameters. Wang et al. (1999) presented validation for their 1.5D core-annulus CFB model with a small 12 MW CFB boiler with a good correspondence to the experimental results. Hua et al. (2004) showed the importance of radial and axial solid distribution by their core-annulus CFB model by highlighting the higher fraction of coarser particles at the wall layer of a circulating fluidized bed boiler and the tendency of particle size decrease with the height of the furnace. The two first models apply the average gas-to-solid mass transfer coefficient in the lower bed, and especially Adanez et al. (1995) referred to the correlation of Halder et al. (1993). However, Hua et al. (2004) applied the emulsion bed Sherwood number correlation of La Nauze and Jung (1983b) for the dilute and lower bed regions.

On the other hand, the circulating fluidized bed combustor models of Huilin et al. (2000) and Souza-Santos (2010) deploy a bubbling bed model for the bottom bed fluid dynamics as shown in Table 2.4. The core-annulus model of Huilin et al. (2000) has been developed for the prediction of the axial and radial gas and char concentration, as well as the temperature profiles of a small coal-fired CFB boiler. The bubbling bed model has been modified from the two-phase theory with bubble and emulsion properties estimated by the empirical correlation of Mori and Wen (1975) and Saraiva et al. (1993). The interphase mass transfer coefficient of Sit and Grace (1981) is applied in their model. The empirical one-dimensional fluidized bed model of Souza-Santos (2010) has been developed for the performance prediction of both bubbling and circulating fluidized beds. Gómez-Barea and Leckner (2010) have classified their fluidization model as an advanced. The bottom bed is considered as a normal bubbling bed till the first turbulent limit, where the decreasing of the bubble sizes with the fluidization velocity is considered as a turbulent bed behavior. Further, when a second turbulent limit is exceeded with the increased fluidization velocity, the fluidization model assumes a fast bed operation with disappearance of the bubble phase. In addition, the model gives the user a set of optional empirical correlations to apply. For example, the modeler can choose between three interphase mass transfer coefficients in the lower bed: those of Chiba and Kobayashi (1970), Kunii and Levenspiel (1968) or, as recommended, Sit and Grace (1981). However, published validation studies with the fluidized bed model of Souza-Santos (2010) concern mostly only bubbling bed processes.

The higher dimension CFB combustor models with a homogeneous turbulent suspension bottom bed fluidization model (type i) are presented in Table 2.6. The CFB combustor model of Hyppänen et al. (1991) is the first three-dimensional CFB model presented in the literature. There are several published validation studies (Myöhänen et al., 2003, 2005, 2006; Vepsäläinen et al., 2009) about its development path and the current model structure is reported in Myöhänen (2011). Vepsäläinen et al. (2009) have presented the validation scope of the three-dimensional CFB model considering eight large-scale coal combusting CFB boilers and several peat, wood, biomass and waste fired CFB boilers, and the range of validations cover capacities up to 370 $\mathrm{MW_{th}}$ and furnace depths of over 10 m. The validations were focused particularly on the experimental horizontal and axial temperature, and combustion gas and nitrogen emission profiles inside the furnace, and additionally the performance of pilot and industrial size furnaces were compared with model-based analysis. The analysis showed that the effective heterogeneous combustion

reaction rate coefficients were considerably different for the pilot and industrial size furnaces combusting the same bituminous coal at the same operational bed temperatures. The three-dimensional CFB combustor model of Pallares and Johnsson (2008) applies also constant voidage to describe the turbulent fluidization in the bottom bed region, and the model even calculates the bubble parameters at the lower bed. However sub-grid continuity mass and energy balances are solved only for one homogeneous phase. The model of Pallares and Johnsson (2008) applies the average mass transfer coefficients in the dense lower and dilute upper fluidized bed regions, but the exact correlations are not reported.
Finally, two semi-empirical CFB models that apply a bubbling bed model are shown in Table 2.5. The first one, the two-dimensional model of Gungor and Eskin (2008) was validated against experiments a 50 kW pilot and 160 MW industrial-scale CFB coal-fired combustors. The CFB model uses the empirical correlations of Horio (1997) and Mori and Wen (1975) for two-phase bubbling bed fluidization model, and applies the interphase coefficient of Chiba and Kobayashi (1970) given in Table 2.2 and the emulsion Sherwood number of La Nauze and Jung (1983b). The last model discussed is the three-dimensional CFB combustor model of Knoebig et al. (1999), which uses the shallow bubbling bed model of Werther and Wein (1994) that has been extrapolated for higher fluidization velocities. Validation of the model against a 12 $\mathrm{MW_{th}}$ coal-fired CFB boiler has been presented by Luecke et al. (2004) with a special focus on fuel misdistribution due to limited dispersion particularly in the shallow bottom bed. The model estimates the interphase mass transfer coefficient in the lower bed with the correlation of Preto (1986) and in the upper lean region according to the cluster mass transfer coefficient of Schoenfelder et al. (1996). In the shallow bed, the emulsion Sherwood number is defined according to Ross and Davidson (1981) and in the lean clustering region with the correlation of La Nauze and Jung (1983b).

2.2.3 Eulerian CFD models

The fine grid CFD simulations of fluidized beds, where the mesh sizes are about 10 times the particle diameter, can describe the average gas-solid mass transfer with the emulsion mass transfer coefficient correlations presented in Table 2.1. However, only coarse-grid simulations are currently practical for the modeling of large-scale fluidized bed reactors due to the very high computational times caused by the exponentially increased number of calculation cells in fine-grid CFD simulations. The coarse-grid Eulerian CFD models of large industrial fluidized bed combustors can describe a rough meso-scale (0.1-1 m) bubble-emulsion or cluster-void flow structure. On the other hand, as stated by Dong et al. (2008a) the flow structure is also fine meso-scale and micro-scale dependent and dynamic by nature, particularly in gas-solid risers. Consequently, the sub-grid heterogeneity of the solid flow structure should be considered in the coarse grid CFD simulations of fluidized beds.
Even though extensive research efforts have been focused on the heterogeneous flow structure related sub-grid solid-gas drag exchange in the coarse-grid CFD simulations (Agrawal et al., 2001; Zhang and van der Heyden, 2002; Yang et al., 2003; Andrews et al., 2005b; Kallio, 2005; Qi et al., 2007; Igci et al., 2008), the same concept regarding

gas-solid mass transfer has been mostly neglected. However, two approaches worth mentioning have recently been presented in the literature. Wang and Li (2007) have applied an energy-minimization multi-scale (EMMS) model (Li, 1994) for the sub-grid level calculation of flow dynamic structure dependent gas-solid drag coefficient in a two-dimensional Eulerian CFD simulation of solid flow dynamics in a 10 m high circulating fluidized bed of the fluid catalytic cracking (FCC) process. In practice, the approach scales down the gas-solid drag coefficient with a heterogeneity index (0-1), which is calculated according to the energy-minimization principle based on the gas and solid velocities, the voidages, the specific cluster diameter and the inertial terms in the sub-grid dense and dilute phases. As the approach requires total solution time increasing iteration, Li (1994) also present an EMMS/matrix model that pre-solves the heterogeneity index matrix for the process conditions used in the CFD simulations. Since its development, the sub-grid structure-dependent EMMS drag coefficient correction has been commonly applied for the coarse-grid Eulerian CFD simulations of gas-solid risers (Zhang et al., 2010; Wang and Liu, 2010; Nikolopoulos et al., 2010). As an extension of the EMMS drag coefficient correction model, Dong et al. (2008a) have presented an EMMS-based sub-grid mass transfer model. Moreover, they compare the performance of two sub-grid mass transfer models. In the first approach (i), the sub-grid is divided to a gas-rich dilute and a solid-rich dense phase, while the interfacial area is calculated on the basis of the parameters of the EMMS model and the interphase mass transfer rate has a surface penetration theory -originated sub-model that treats the cluster of particles as a big particle. In the second sub-model (ii), the sub-grid gas-solid mass transfer is estimated with an average/effective gas-solid mass transfer coefficient calculated on the basis of the parameters of the so-called EMMS/matrix. By simulations of two different fine-particle CFB processes, Dong et al. (2008a) show that the first approach (i) resulted in a more accurate prediction of conversion performance at the dense suspension conditions, and that both sub-grid gas-solid mass transfer models were accurate at the dilute fluidization conditions. Even more importantly, they highlight that the straightforward homogeneous plug flow mass transfer approach failed totally in the prediction of axial chemical conversion performance. Additionally, they underline that the simulated sub-grid bed Sherwood numbers corresponded well with the bed Sherwood numbers presented in the experimental studies that were simulated. Later, Dong et al. (2008b) compared three modeling methods to the experimental conversion performance in a CFB reactor. The approach that applied both the structure dependent drag and mass transfer model resulted closest to the experimental performance predictions compared to approaches that used only the structure dependent EMMS drag model or only a traditional fine-grid uncorrected drag model.

In a further quest of searching for a mesh-independent heterogeneous mass transfer model, also another sub-grid mass transfer model has been presented. Hou et al. (2010) have derived a multiscale mass transfer (MSMT) model, which also applies the local flow structure parameters for the sub-grid dilute and dense phases calculated based on the EMMS model interconnected to the Eulerian two-phase CFD model. They compared the conversion prediction performance of the MSTM model by applying the local parameters to the typical two-fluid model assuming the homogeneous local flow structure, the traditional theory-book plug flow model and the MSTM model applying the average flow

structure parameters in the fluidized bed. The simulations of two different fast fluidized bed process experiments reported in the literature showed that the multi-scale mass transfer applying the sub-grid dilute and dense phase flow structure parameters results clearly the most accurate conversion performance. Interestingly, both the above sub-grid mass transfer models describes the interphase mass transfer between dilute and dense phases with the penetration theory originated equation presented by Higbie (1935):

$$k_{\mathrm{be}} = 2\frac{D_{\mathrm{g}}\alpha_{\mathrm{gc}}}{d_{\mathrm{c}}} + (\frac{4D_{\mathrm{g}}\alpha_{\mathrm{gc}}\lambda_{\mathrm{g}}}{\pi})^{1/2}. \tag{2.6}$$

As a conclusion to the above discussion, if a sub-grid gas-solid mass transfer model is not applied to a coarse-grid CFD simulation, the average gas-solid mass transfer coefficients estimated by the bed Sherwood number should be used in the dense lower bed region, and the single sphere or over-cluster Sherwood numbers would be proper in the lean upper region. However, only limited number of publications exist about process-specific bed Sherwood numbers, particularly for fluidized bed combustion and gasification processes, as discussed in Chapter 2.1.2 above.

Table 2.3: Empirical 1.5D core-annulus CFB combustor models with a single-phase lower bed fluidization model, and their heterogeneous mass transfer and combustion sub-models

	Core-annulus CFB model	**Adanez et al. (1995)**
Bottom bed		
Fluidization model	constant voidage with plug flow of gas	
Heterogeneous MT coef.	Sh_{bed}	Halder et al. (1993)
Dilute region		
Fluidization model	exponential decay model	Kunii and Levenspiel (1990)
Heterogeneous MT coef.	Sh_{e}	La Nauze and Jung (1983b)
Combustion model		
Volatiles	uniform devolatilization in dense bottom bed	
Char	shrinking particle model with chemical kinetic and external gas convection control	
Char population balance	considers char combustion, but not fragmentation and attrition	

	Core-annulus CFB model	**Wang et al. (1999)**
Bottom bed		
Fluidization model	constant voidage with plug flow of gas	Hannes et al. (1995)
Heterogeneous MT coef.	average h_m (Sh_{bed})	Not specified
Dilute region		
Fluidization model	exponential decay model	
Heterogeneous MT coef.	average h_m (Sh_{bed})	Not specified
Combustion model		
Volatiles	uniform devolatilization in dense bottom bed	
Char	i) dual shrinking-core (high ash) ii) shrinking-core, (low ash) iii) uniform (fine particles)	
Char population balance	char combustion and attrition (instant fragmentation in fuel feeding port)	

	Core-annulus CFB model	**Hua et al. (2004)**
Bottom bed		
Fluidization model	constant voidage with plug flow of gas	
Heterogeneous MT coef.	Sh_{e}	La Nauze and Jung (1983b)
Dilute region		
Fluidization model	core-annulus model with exponential decay model, radial solid concentration assumed constant in core and annulus	solid profile according to Johnsson and Leckner (1995), and thickness of annulus according to Harris et al. (2002)
Heterogeneous MT coef.	Sh_{e}	La Nauze and Jung (1983b)
Combustion model		
Volatiles	uniform devolatilization in dense bottom bed	
Char	shrinking-particle model	
Char population balance	char combustion, fragmentation and attrition	

Table 2.4: Empirical core-annulus and one-dimensional CFB combustor models with a two-phase lower bed fluidization model, and their heterogeneous mass transfer and combustion sub-models

	Core-annulus CFB model	**Huilin et al. (2000)**
Bottom bed		
Fluidization model	bubbling bed as modified two-phase theory	parameters according to Mori and Wen (1975) and Saraiva et al. (1993)
Heterogeneous MT coef.	K_{be}	Sit and Grace (1981)
Dilute region		
Fluidization model	core-annulus structure with exponential decay model	Kunii and Levenspiel (1990), and radial solid profile according to Rhodes et al. (1992)
Heterogeneous MT coef.	average h_m (Sh_{bed})	Not specified
Combustion model		
Volatiles	uniform devolatilization in dense bottom bed	
Char	shrinking-particle model	
Char population balance	yes	
	One-dimensional CFB model	**Souza-Santos (2010)**
Bottom bed		
Fluidization model	bubbling bed as modified two-phase theory, bubble size decrease starts at turbulent regime and bubble phase disappears at fast bed regime	applies combination of earlier stated empirical correlations as descibed in Souza-Santos (2010)
Heterogeneous MT coef.	K_{be}	Chiba and Kobayashi (1970), Kunii and Levenspiel (1968) or as recommended: Sit and Grace (1981)
	Sh_{e}	La Nauze and Jung (1983b)
Dilute region		
Fluidization model	not specified	
Heterogeneous MT coef.	not specified	
Combustion model		
Volatiles	devolatilization near fuel feeding port, region user defined	
Char	i) shrinking-core model or ii) shrinking-particle model	
Char population balance	combustion and attrition	

Table 2.5: Semi-empirical three-dimensional CFB combustor models with a single phase lower bed fluidization model, and their heterogeneous mass transfer and combustion sub-models

	3-dimensional CFB Model	**Hyppänen et al. (1991)**
Bottom bed		
Fluidization model	constant voidage with plug flow of gas	
Heterogeneous MT coef.	included in the effective combustion rate coefficient	(Myöhänen, 2011)
Dilute region		
Fluidization model	exponential decay model with a wall layer	solid profile: Johnsson and Leckner (1995), wall layer: Myöhänen and Hyppänen (2011)
Heterogeneous MT coef.	included in the effective combustion rate coefficient	(Myöhänen, 2011)
Combustion model		
Volatiles	devolatilization region is propotional to the rate of devolatilization and solid mixing/dispersion	Myöhänen (2011)
Char	uniform combustion model with effective rate coefficient	
Char population balance	combustion and comminution	
	3-dimensional CFB Model	**Pallares and Johnsson (2008)**
Bottom bed		
Fluidization model	constant voidage and pressure loss over bed with plug flow of gas and dispersion of solids	
Heterogeneous MT coef.	Sh_{bed}	not specified
Dilute region		
Fluidization model	exponential decay model with cluster and lean gas phases	modified Johnsson and Leckner (1995)
Heterogeneous MT coef.	not specified	
Combustion model		
Volatiles	devolatilization region is propotional to the rate of devolatilization and solid mixing/dispersion	
Char	uniform combustion with chemical kinetic and external gas convection control	
Char population balance	not specified	

Table 2.6: Semi-empirical two- and three-dimensional CFB combustor models with a bubbling bed fluidization model, and their heterogeneous mass transfer and combustion sub-models

	Two-dimensional CFB model	**Gungor and Eskin (2008)**
Bottom bed		
Fluidization model	bubbling bed as modified two-phase theory	parameters from Horio (1997) and Mori and Wen (1975)
Heterogeneous MT coef.	K_{be}	Chiba and Kobayashi (1970)
	Sh_{e}	La Nauze and Jung (1983b)
Dilute region		
Fluidization model	core-annulus model with exponential decay model	solid profile according to Smolders and Baeyens (2001), and thickness of annulus according to Werther and Wein (1994)
Heterogeneous MT coef.	Sh_{e}	La Nauze and Jung (1983b)
Combustion model		
Volatiles	devolatilization in the emulsion phase of a dense bottom bed with a rate propotional to solid mixing	
Char	dual shrinking-core model	
Char population balance	combustion, fragmentation and attrition	
	3-dimensional CFB Model	**Knoebig et al. (1999)**
Bottom bed		
Fluidization model	shallow bubbling bed as modified two-phase theory	bubbling bed model of Werther and Wein (1994) extrapolated to turbulent bed
Heterogeneous MT coef.	K_{be}	Preto (1986)
	Sh_{e} =3.5	Ross and Davidson (1981)
Dilute region		
Fluidization model	exponential decay model with cluster and void phases	
Heterogeneous MT coef.	K_{be} =$K_c\alpha_{\mathrm{e}}(1-\alpha_{\mathrm{e}})$	Single cluster transfer coefficient $K_c = 0.3s^{-1}$ according to Schoenfelder et al. (1996)
	Sh_{e}	La Nauze and Jung (1983b)
Combustion model		
Volatiles	devolatilization region is propotional to the rate of devolatilization and solid mixing/dispersion	
Char	shrinking-particle model	
Char population balance	combustion, fragmentation	

3 Eulerian CFD model for heterogeneous chemical conversion in fluidized beds

The main research method applied in the thesis is presented in this chapter. First, the chapter describes the transient two-dimensional Eulerian CFD model with gas and solid phases applied in the research. After this, the validation background of this CFD modeling approach in the prediction of the fluidized bed processes is discussed with respect to the relevant phenomenona, solid flow dynamics and heterogeneous mass transfer. In the end, the characteristics of the solid flow dynamics and the chemical conversion resulting from the fine-grid Eulerian CFD simulations of heterogeneous char combustion in a fluidized bed are presented to provide relevant process condition information for the heterogeneous mass transfer research presented in Chapters 4-5.

3.1 Modeling approach

All the CFD simulations in this thesis are based on the same two-dimensional Eulerian approach of modeling fluid dynamics in a fluidized bed. As a primary approach, the heterogeneous combustion of char particles in an inert fluidized bed of sand is simulated in a bench and a pilot scale combustor. In Chapter 6, the same CFD modeling approach is applied to a pilot scale fuel reactor of a chemical looping combustion process consisting of only active nickel-oxide oxygen carrier particles. Only the applied heterogeneous reaction model is slightly modified according to a primary combustion reaction of the process. In this chapter, the principle of the Eulerian CFD model with gas-solid phases and the applied char combustion reaction model are presented with the reactor and mesh design, the material properties and the boundary conditions applied in the simulations used in the derivation of the heterogeneous mass transfer coefficients for fluidized bed combustion.

3.1.1 Governing equations and main sub-models

The two-phase Eulerian CFD simulations presented in the thesis were performed with Ansys Fluent 14. The two-dimensional form of the continuity and momentum conservation equations for the gas and solid phases are presented in Table 3.1. The closure models for the solid phase follow the kinetic theory of granular flow with algebraic equation of granular temperature (Syamlal et al., 1993). The gas phase turbulence is described by the modified $\kappa - \epsilon$ model with additional terms that include the interphase momentum exchange.

The species transport within a phase was modeled by considering a turbulent diffusivity term with the turbulent Schmidt number of 0.7. The approach was successfully applied in the assessment of Eulerian CFD models to predict a reactive fluidized bed system, a fuel reactor of chemical looping combustion, as presented by Cloete et al. (2012). The minimum fluidization voidage of 0.38 was selected for all the simulated balances.

In order to find the heterogeneous mass transfer coefficients, the model of char combustion was executed as simply as possible. Thus, only one primary combustion reaction was considered:

Table 3.1: Conservation equations and main closure models used in Eulerian two-phase CFD model.

Gas phase - continuity and momentum equations

$$\frac{\partial}{\partial t}(\alpha_{\mathrm{g}}\rho_{\mathrm{g}}) + \nabla\cdot(\alpha_{\mathrm{g}}\rho_{\mathrm{g}}\vec{u}_{\mathrm{g}}) = \alpha_{\mathrm{g}}S_{\mathrm{g}}$$

$$\frac{\partial}{\partial t}(\alpha_{\mathrm{g}}\rho_{\mathrm{g}}\vec{u}_{\mathrm{g}}) + \nabla\cdot(\alpha_{\mathrm{g}}\rho_{\mathrm{g}}\vec{u}_{\mathrm{g}}\vec{u}_{\mathrm{g}}) = -\alpha_{\mathrm{g}}\nabla p + \nabla\cdot\bar{\bar{\tau}}_{\mathrm{g}} + \alpha_{\mathrm{g}}\rho_{\mathrm{g}}\vec{g} + K_{\mathrm{sg}}(\vec{u}_{\mathrm{s}} - \vec{u}_{\mathrm{g}})$$

Solid phase - continuity and momentum equations

$$\frac{\partial}{\partial t}(\alpha_{\mathrm{s}}\rho_{\mathrm{s}}) + \nabla\cdot(\alpha_{\mathrm{s}}\rho_{\mathrm{s}}\vec{u}_{\mathrm{s}}) = \alpha_{\mathrm{s}}S_{\mathrm{s}}$$

$$\frac{\partial}{\partial t}(\alpha_{\mathrm{s}}\rho_{\mathrm{s}}\vec{u}_{\mathrm{s}}) + \nabla\cdot(\alpha_{\mathrm{s}}\rho_{\mathrm{s}}\vec{u}_{\mathrm{s}}\vec{u}_{\mathrm{s}}) = -\alpha_{\mathrm{s}}\nabla p + \nabla\cdot\bar{\bar{\tau}}_{\mathrm{s}} - \nabla p_{\mathrm{s}} + \alpha_{\mathrm{s}}\rho_{\mathrm{s}}\vec{g} + K_{\mathrm{gs}}(\vec{u}_{\mathrm{g}} - \vec{u}_{\mathrm{s}})$$

Species i conservation within phase (p)

$$\frac{\partial}{\partial t}(\alpha_{\mathrm{p}}\rho_{\mathrm{p}}y^{\mathrm{i}}_{\mathrm{p}}) + \nabla\cdot(\alpha_{\mathrm{p}}\rho_{\mathrm{p}}\vec{u}_{\mathrm{p}}y^{\mathrm{i}}_{\mathrm{p}}) = -\nabla\alpha_{\mathrm{p}}J^{\mathrm{i}}_{\mathrm{p}} + r_{i,p}$$

Algebraic equation of granular temperature ($K_{1,2,3,4}$ according Syamlal et al. (1993))

$$\Theta_{\mathrm{s}} = \left[\frac{-K_1\alpha_s tr(\bar{\bar{D}}_{\mathrm{s}}) + \sqrt{K_1^2\alpha_s^2 tr^2(\bar{\bar{D}}_{\mathrm{s}}) + 4K_4\alpha_s\left[K_2 tr^2(\bar{\bar{D}}_{\mathrm{s}}) + 2K_3 tr(\bar{\bar{D}}_{\mathrm{s}}\right]}}{2\alpha_s K_4}\right]^2$$

Interphase momentum exchange coefficient: gas (g) - solid (s) (Gidaspow et al., 1992)

when $\alpha_{\mathrm{g}} > 0.8$, $K_{\mathrm{gs}} = \frac{3}{4}C_{\mathrm{D}}\frac{\alpha_{\mathrm{s}}\alpha_{\mathrm{g}}\rho_{\mathrm{g}}\left|\vec{u}_{\mathrm{s}} - \vec{u}_{\mathrm{g}}\right|}{d_{\mathrm{s}}}\alpha_{\mathrm{g}}^{-2.65}$,

where $C_{\mathrm{D}} = \frac{24}{\alpha_{\mathrm{g}}Re}\left[1 + 0.15(\alpha_{\mathrm{g}}Re)^{0.687}\right]$ and $Re = \frac{\rho_{\mathrm{g}}|\vec{u}_{\mathrm{s}} - \vec{u}_{\mathrm{g}}|d_{\mathrm{s}}}{\mu_{\mathrm{g}}}$

when $\alpha_{\mathrm{g}} \leq 0.8$, $K_{\mathrm{gs}} = 150\frac{\alpha_{\mathrm{s}}\left(1-\alpha_{\mathrm{g}}\right)\mu_{\mathrm{g}}}{\alpha_{\mathrm{g}}d_s^2} + 1.75\frac{\rho_{\mathrm{g}}\alpha_{\mathrm{s}}\left|\vec{u}_{\mathrm{s}} - \vec{u}_{\mathrm{g}}\right|}{d_{\mathrm{s}}}$

Phase stress-strain tensors

$$\bar{\bar{\tau}}_{\mathrm{g}} = \alpha_{\mathrm{g}}\mu_{\mathrm{g}}\left(\nabla\vec{u}_{\mathrm{g}} + \nabla\vec{u}_{\mathrm{g}}^{\mathrm{T}}\right) - \frac{2}{3}\alpha_{\mathrm{g}}\mu_{\mathrm{g}}\nabla\cdot\vec{u}_{\mathrm{g}}\bar{\bar{I}}$$

$$\bar{\bar{\tau}}_{\mathrm{s}} = \alpha_{\mathrm{s}}\mu_{\mathrm{s}}\left(\nabla\vec{u}_{\mathrm{s}} + \nabla\vec{u}_{\mathrm{s}}^{\mathrm{T}}\right) + \alpha_{\mathrm{s}}\left(\lambda_{\mathrm{s}} - \frac{2}{3}\mu_{\mathrm{s}}\right)\nabla\cdot\vec{u}_{\mathrm{s}}\bar{\bar{I}}$$

Solids shear viscosity, $\mu_{\mathrm{s}} = \mu_{\mathrm{s,col}} + \mu_{\mathrm{s,kin}} + \mu_{\mathrm{s,fr}}$

$$\mu_{\mathrm{s}} = \frac{4}{5}\alpha_{\mathrm{s}}\rho_{\mathrm{s}}d_{\mathrm{s}}g_{0,\mathrm{ss}}(1+e_{\mathrm{ss}})\left(\frac{\Theta_{\mathrm{s}}}{\pi}\right)^{1/2} + \frac{\alpha_{\mathrm{s}}\rho_{\mathrm{s}}d_{\mathrm{s}}\sqrt{\Theta_{\mathrm{s}}\pi}}{6(3-e_{\mathrm{ss}})}\left[1 + \frac{2}{5}(1+e_{\mathrm{ss}})(3e_{\mathrm{ss}}-1)\alpha_{\mathrm{s}}g_{0,\mathrm{ss}}\right] + \frac{p_{\mathrm{s}}\sin\theta}{2\sqrt{I_{2\mathrm{D}}}}$$

Granular bulk viscosity

$$\lambda_{\mathrm{s}} = \frac{4}{3}\alpha_{\mathrm{s}}\rho_{\mathrm{s}}d_{\mathrm{s}}g_{0,\mathrm{ss}}(1+e_{\mathrm{ss}})\left(\frac{\Theta_{\mathrm{s}}}{\pi}\right)^{1/2},$$

radial distribution function $g_{0,\mathrm{ss}} = \left[1 - \left(\frac{\alpha_{\mathrm{s}}}{\alpha_{\mathrm{s,max}}}\right)^{1/3}\right]^{-1}$

Solids pressure

$$p_{\mathrm{s}} = \alpha_{\mathrm{s}}\rho_{\mathrm{s}}\Theta_{\mathrm{s}} + 2\rho_{\mathrm{s}}(1+e_{\mathrm{ss}})\alpha_{\mathrm{s}}^2 g_{0,\mathrm{ss}}\Theta_{\mathrm{s}}$$

$$\mathrm{C(s)} + \mathrm{O_2(g)} \Rightarrow \mathrm{CO_2(g)}. \tag{3.1}$$

The chemical kinetic char combustion rate is defined with the first-order rate function as

$$R_\mathrm{C} = a_\mathrm{C} r_\mathrm{C} = a_\mathrm{C} k_{eff} C_{O_2}, \tag{3.2}$$

where the surface area of char per reactor volume is calculated from

$$a_\mathrm{C} = 6\alpha_\mathrm{s} y_\mathrm{C} / d_\mathrm{p} \tag{3.3}$$

and the effective reaction rate coefficient is defined as

$$k_\mathrm{eff} = \frac{1}{1/k_\mathrm{C,sur} + 1/h_\mathrm{m}}, \tag{3.4}$$

where $k_\mathrm{C,sur}$ is the chemical kinetic reaction rate coefficient given as per surface area of a char particle. The local convection mass transfer coefficient h_m is calculated with the emulsion Sherwood number correlation (Table 2.1: La Nauze et al. (1984)) given by

$$Sh_\mathrm{e} = 2\alpha_\mathrm{g} + 0.69(Re/\alpha_\mathrm{g})^{1/2} Sc^{1/3}, \tag{3.5}$$

where the local voidage and particle Reynolds number are applied.

3.1.2 Reactor and mesh design, boundary conditions and properties

A two-dimensional fluidized bed reactor with a height-to-width ratio of 10 was designed for the simulations. First, for the pilot scale simulations, a representative width of 0.2 m was selected, which resulted in the height of 2 m with the selected height-to-width ratio. For this reactor design, the fine mesh size of $5 \times 5\ \mathrm{mm^2}$ was selected. The mesh design had totally 16000 cells, 40 in width and 400 in height. The design of the reactor is presented in Fig. 3.1. The design of the bench scale reactor was obtained by scaling the pilot scale reactor with the size factor of 0.25, which resulted in the reactor having the width of 0.05 m and height of 0.5 m. With the same design of the mesh, the bench scale reactor model had the mesh size of $1.25 \times 1.25\ \mathrm{mm^2}$. The fine-grid mesh designs of the pilot and bench reactors are presented in Tables 3.2 and 3.3, respectively. The tables show also an important parameter, cell width-to-particle diameter ratio, for the executed two-phase Eulerian CFD simulations, which is further discussed in Chapter 3.3.4 concerning grid independence in the simulations. In addition, a grid independence study for the CFD modelling was executed, where one pilot reactor balance was simulated with a finer ($2.5 \times 2.5\ \mathrm{mm^2}$) and a coarser ($10 \times 10\ \mathrm{mm^2}$) grid size.

The boundary conditions of the simulations were defined as follows. All the fluidization air is fed through the primary air feeding. The primary air feeding is defined as the constant velocity inlet. At the walls, no slip boundary condition is applied for the gas and

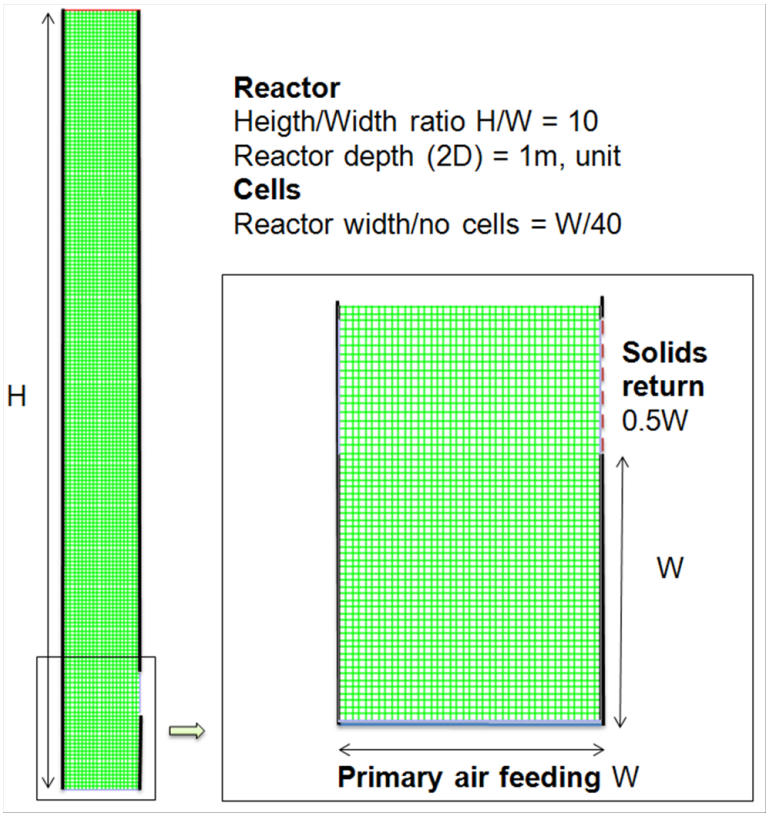

Figure 3.1: Pilot scale reactor design and grid sizes

Table 3.2: Design of fine-grid meshes, pilot reactor

	Unit	Pilot, small d_p	Pilot, large d_p
d_p	mm	0.5	1.25
$d_\mathrm{r} \times H$	mm	200×2000	200×2000
no. cells		40×400	40×400
size of mesh	mm × mm	5×5	5×5
mesh width/d_p		10×10	4×4

Table 3.3: Design of fine-grid meshes, bench reactor

	Unit	Bench 1	Bench 2 and 3	Bench 4
d_p	mm	0.1	0.35	0.5
$d_\mathrm{r} \times H$	mm	50×500	50×500	50×500
no. cells		40×400	40×400	40×400
size of mesh	mm × mm	1.25×1.25	1.25×1.25	1.25×1.25
mesh width/d_p		12.5×12.5	3.6×3.6	2.5×2.5

solid phases. The solids that flow from the top exit of the reactor are re-circulated to the reactor from the solid return. The gas and particle temperatures are defined as constant 850 °C, and all the gas properties (Table 3.4) are defined at this temperature. The solid particles are spherical, and the solid density is 2500 $\mathrm{kg/m^3}$. The char is defined as a mass fraction of the solids (Table 3.5 and 3.6). The applied chemical kinetic reaction rate coefficient of $k_{\mathrm{C,sur}} = 0.1\ \mathrm{m/s}$ represents the char of wood (Rangel and Pinho, 2011). In order to evaluate the effect of chemical kinetics to the average mass transfer coefficients also faster kinetic coefficient of $k_{\mathrm{C,sur}} = 1\ \mathrm{m/s}$ was applied for the Geldart group D balances as discussed in later in Chapters 4 and 5.

Table 3.4: Gas properties

Gas density	$0.31\ \mathrm{kg/m^3}$
Gas viscosity	$45 \times 10^{-6}\mathrm{kg/ms}$
Oxygen diffusivity	$132 \times 10^{-6}\mathrm{m^2/s}$

3.1.3 Solution strategy and procedure

In a solution, the first order implicit method is used for the time discretization and the first order upwind method for the space discretization. Forty iterations per each time step were used as the solution procedure and the convergence criteria for the continuity and velocity residuals were checked in preliminary calculations to stabilize with this solution strategy.

In all simulations, the time step size has been 0.001 s, which is selected based on previous Eulerian CFD modeling research in bubbling (Hulme et al., 2005) and circulating (Shah et al., 2012) beds.
All simulations were executed with the same procedure. The procedure included two sequential steps. First, 5 s of fluidized bed operation was simulated to reach a stabilized fluidization condition from the constant initial solid volume fraction of 0.12. The stabilized state of fluidization was confirmed from the time-averaged axial solid volume fraction profiles, which are presented in Figs. 3.4, 3.5 and 3.6. However, the stabilization considers only the time-averaged conditions, while the real conditions in a fluidized bed are always locally transient as highlighted in Fig. 3.11. The figure shows two simulated 2 s time-series of local solid volume fractions from one calculation cell. The simulation of 5 s stabilization period was followed by a simulation of an analysis period of 20 s fluidized bed operation. Data monitoring was carried out during the analysis period: (1) time-averaging of the data in the calculation cells and (2) storing of instant solid volume fraction in all calculation cells with the frequency of 20 1/s. The later data was used for the bubble size analysis presented in Chapter 5.

3.2 Validation background of flow dynamics and heterogeneous mass transfer

The Eulerian CFD modeling strategy of fluidized beds is well-established with known limiting factors related to the size of the reactor concerned, or the size of the mesh and time step. Eulerian modeling with the granular kinetic theory has been successfully applied to simulate gas-solid flow in pilot scale fluidized beds (Benyahia (2012), Shah et al. (2012), (Hulme et al., 2005)). A complete description of the Eulerian two-phase flow theory regarding bubbling and turbulent fluidized beds has been presented by Enwald et al. (1996). A notable validation of the time-averaged axial and horizontal solid volume fractions and solid fluxes in the fluid catalytic cracking (FCC) process has been presented by Benyahia et al. (2000). Shah et al. (2012) have presented a successful comparison of time-averaged axial and horizontal solid volume fractions against measurements in a cold pilot-scale CFB reactor with a relevant study on the effects of the different mesh and time step sizes. The same Eulerian principles have been applied in simulations of a bubbling fluidized bed with validation against measurements of bubble frequencies and diameters, and average solid volume fractions (Hulme et al., 2005).
The time-averaged axial and horizontal density profiles and solid fluxes have been the main interests in the validation process of Eulerian CFD modeling. However, also some Eulerian CFD-based evaluations of heterogeneous mass transfer in fluidized bed processes have been published recently. On the other hand, the flow dynamic conditions in these studies focusing on fine-particle fluidized beds have not been similar to the combustion of solid fuels in a circulating or bubbling fluidized bed reactor. Chalermsinsuwana et al. (2009) have presented Eulerian CFD based heterogeneous mass transfer research for the fast fluidization regime with a small particle diameter of 76 μm. In their work, the bed Sherwood numbers derived for FCC particles and heterogeneous mass transfer characteristics were presented against the height of the reactor and the chemical kinetic coefficient

of an ozone decomposition catalyst. Chalermsinsuwan and Piumsomboon (2011) have presented bed Sherwood numbers also for a thin bubbling bed operated with similar FCC particles by means of two-phase Eulerian CFD modeling. In addition, Cloete et al. (2012) have recently presented multi-phase Eulerian CFD simulation of chemical looping combustion at the bubbling fluidization regime. The CFD simulated axial gas conversion profiles corresponded well with the measured profiles, which suggests that the heterogeneous mass transfer was correctly predicted by the fine-grid Eulerian CFD simulations. On the other hand, the particle size in the CLC process was very small compared to the combustion processes and the actual heterogeneous mass transfer coefficients were not presented.

A closely related research field to the fundamental research of heterogeneous mass transfer in fluidized beds is the development of heterogeneous mass transfer models for coarse grid CFD simulations. The principle is similar to a drag correction development targeting at a faster CFD solution of solid flow dynamics by means of modeling mesoscale flow structures in coarser than microscale grids. Shah (2012) has reviewed the status of the methods used in mesoscale drag correction modeling. Dong et al. (2008a) have developed a multiscale mass transfer model for the prediction of thevsub-grid heterogeneous mass transfer rate. The mass transfer model assesses sub-grid heterogeneous flow structure with separate dilute and dense phases similarly to the energy minimization multiscale (EMMS) model for the mesoscale drag coefficient of Wang and Li (2007). In a review of multiscale CFD for gas-solid CFB modeling, Wang et al. (2010) have presented sub-grid bed Sherwood numbers calculated from a multiscale mass transfer model (Dong et al., 2008a) for a wide operating condition range of Reynolds numbers and voidages based on the multiscale fluid dynamic CFD simulations (EMMS). A similar approach has been presented by Hou et al. (2010). Their CFD simulations of a reactive fast fluidized bed applied a sub-grid heterogeneous mass transfer model that was coupled with a solution of solid flow dynamics. The sub-grid heterogeneous mass transfer model requires an assessment of the heterogeneous flow structure in a calculation cell: dispersed solids in the voids, the interface of a void and cluster phases and solids in the dense cluster phase. In this thesis, both the grid size and the calculation time step have been defined small enough, so that drag or heterogeneous mass transfer sub-grid corrections should not be required. On the other hand, the interphase mass transfer coefficients presented in Chapter 5 provides knowledge also for the evaluation of sub-grid heterogeneous mass transfer in the Eulerian CFD simulations of fluidized bed combustion processes.

3.3 Simulated fluidized bed combustion balances

The overall research approach of the thesis is to simulate fluidized bed heterogeneous combustion of wood char by the means of Eulerian CFD modeling. In the simulations of bench and pilot scale reactors, chemical kinetic coefficients and particle sizes are varied, as well as the fluidization regime from bubbling bed to turbulent operation.

3.3.1 Simulation matrix, Geldart classification and flow regime

Twelve fluidization balances presented in Tables 3.5 and 3.6 were simulated. The pilot reactor (W=0.2 m) balances were simulated with two particle sizes, a large particle diameter of 1.25 mm and a smaller particle diameter of 0.5 mm. The bench-size reactor (W=0.05 m) balances were at the bubbling bed regime, where fine particle diameters of 0.1 mm, 0.35 mm and 0.5 mm were studied. The Geldart particle classification for the particles used in the simulations is shown in Fig. 3.2. The finer particles with diameters of 0.1 mm, 0.35 mm and 0.5 mm belong to Geldart group B, and even the finest particle size of 0.1 mm is very close to group A, aeratable behavior of fluidized solids. The largest particles with a diameter of 1.25 mm are Geldart D solids. The particle diameter, the fluidization velocity and the minimum fluidization velocity of the simulated balances are shown in Tables 3.5 and 3.6. The minimum fluidization velocity is calculated from $u_{\mathrm{mf}} = ((28.7^2 + 0.0494Ar)^{0.5} - 28.7)\mu_{\mathrm{g}}/(d_{\mathrm{p}}\rho_{\mathrm{g}})$ (Grace, 1986b). In all balances, solid loading is a result of the same average initial solid volume fraction of 0.12. Char loading is given as a volume fraction within the solids y_{c}, and is shown in Tables 3.5 and 3.6. In the large particle (1.25 mm) pilot balances, the char loading was increased with the fluidization velocity in order to maintain the average exit oxygen at the same level between the balances. On the other hand, the oxygen level was allowed to change in the fine particle pilot balance, while keeping the char loading constant with increased fluidization velocity. The principle is shown in Figs. 3.7 and 3.8, which present the average axial oxygen concentration profiles of these simulations.

Table 3.5: Fluidization balance matrix for pilot reactor simulations

	Unit	Pilot, large d_{p}	Pilot, small d_{p}
d_{p}	mm	1.25	0.5
u_{f}	$\mathrm{m/s}$	2, 3.5, 5, 7	1, 2, 3, 4
u_{mf}	$\mathrm{m/s}$	0.67	0.12
y_{c}		0.1, 0.12, 0.13, 0.14	0.01

Table 3.6: Fluidization balance matrix for bench reactor simulations

	Unit	Bench 1	Bench 2	Bench 3	Bench 4
d_{p}	mm	0.1	0.35	0.35	0.5
u_{f}	$\mathrm{m/s}$	0.05	0.25	0.5	0.5
u_{mf}	$\mathrm{m/s}$	0.005	0.06	0.06	0.12
y_{c}		0.0001	0.0025	0.0025	0.01

The Geldart particle classification for the particles used in the simulations is presented in Fig. 3.2. The finer particles with diameters of 0.1 mm, 0.35 mm and 0.5 mm belong

to Geldart group of B, sand-like particles. Generally, fluidized beds formed by Geldart B particles are expected to form bubbles as soon as the minimum fluidization velocity is exceeded. The bubble sizes typically increase with the excess gas velocity $u_\mathrm{f} - u_\mathrm{mf}$ and with the distance above the air feeding (Kunii and Levenspiel, 1991). The coarsest particle size of 1.25 mm seems to belong onto the Geldart group D, even though the characteristics are relevantly close to group B particles as shown in Fig. 3.2. Similarly, the finest particle size of 0.1 mm is close to group A, an aeratable behavior of solids. The fluidization with Geldart group D particles results mostly in large bubble sizes that rise with a slower velocity than a gas penetrating through the denser emulsion phase . In the case of Geldart group A and B, aeratable and sand-like solids, the gas bubbles are expected to rise faster than the gas flowing through the emulsion phase (Kunii and Levenspiel, 1991).

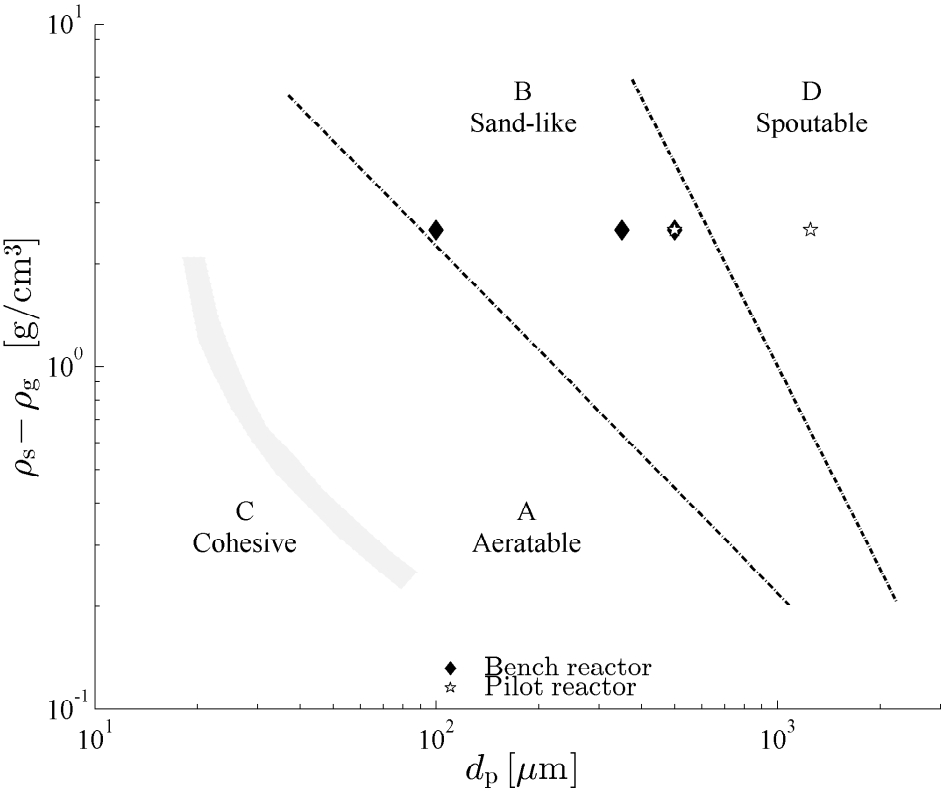

Figure 3.2: Geldart classification of solids used in bench and pilot reactor simulations. The classification is adopted from Kunii and Levenspiel (1991).

The fluid dynamic regime of the balances is shown by a flow regime chart of Grace (1986a), which is formed based on the dimensionless particle diameter $d_\mathrm{p}^* = Ar^{1/3}$ and the dimensionless fluidization velocity $U^* = Re_\mathrm{p}/Ar^{1/3}$. In the pilot size reactor simulations, the two lowest fluidization velocity balances with group B and D solids are in the

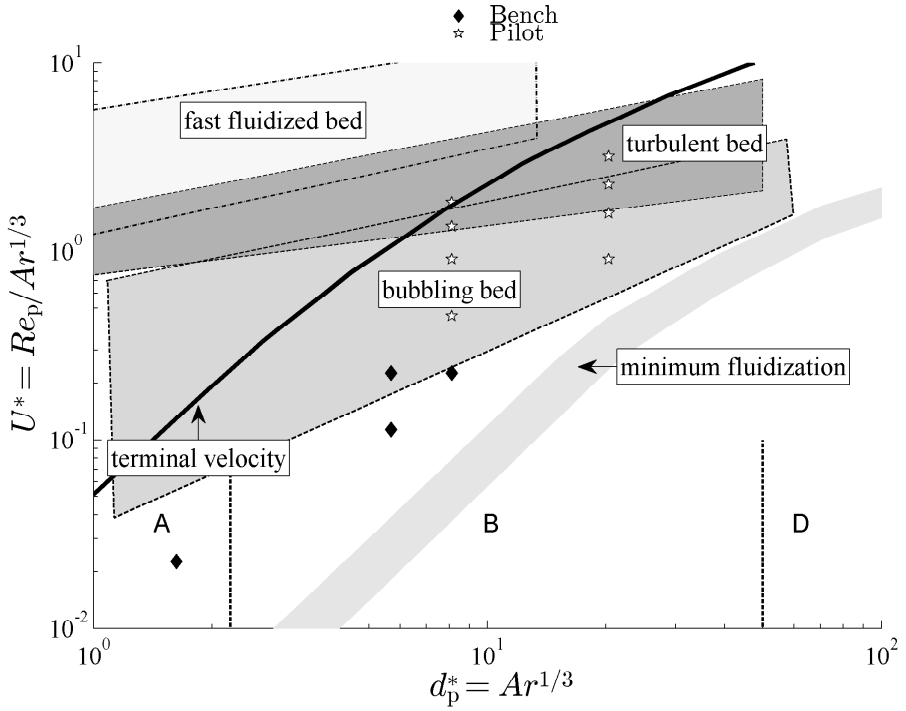

Figure 3.3: Flow regime chart of Grace (1986a) for the simulated bench and pilot reactor balances. The regimes are adopted from Kunii and Levenspiel (1991), except for the turbulent regime that is adopted from Abba et al. (2003)

bubbling bed regime. For the two higher velocity balances, the turbulent regime could be expected. The bench reactor balances are above the minimum fluidization velocity, and even the flow regime proposes that the flow regimes could be under the bubbling bed regime observed in the simulations. While recognizing the guidance given by the flow regime chart, the term turbulent fluidization, in this thesis, refers to any non-regular and vigorous movement of solids and gases in the fluidized bed at the higher fluidization velocities than at the bubbling bed regime. The bubbling bed regime is recognized from the round and regular shape of bubbles, and from the clear interface between bubble and emulsion.

3.3.2 Axial solid and oxygen conversion profiles

The bubbling and turbulent bed regimes described above are also shown by the time and horizontally averaged axial solid volume fractions $\langle \alpha_s \rangle_{20s}$ of the pilot reactor simulations, which are presented in Figs. 3.4 and 3.5. In the case of large particle (1.25 mm) pilot

balances, the fluidization velocity of 2 $\mathrm{m/s}$ represents the bubbling bed regime, 3.5 $\mathrm{m/s}$ the vigorously bubbling bed regime, 5 $\mathrm{m/s}$ the early turbulent regime and 7 $\mathrm{m/s}$ the turbulent regime, respectively. Similarly, for small particle (0.5 mm) pilot balances, the fluidization velocity of 1 $\mathrm{m/s}$ and 2 $\mathrm{m/s}$ represents the bubbling bed regime, 3 $\mathrm{m/s}$ the transition to the turbulent bed regime, and $4\mathrm{m/s}$ the turbulent regime. Fig. 3.6 shows the averaged axial solid volume fractions for the bench reactor simulations. As suggested by the fluid regime chart (Fig. 3.3), the averaged axial solid volume fractions show that the bench reactor balances are clearly at the bubbling bed regime.

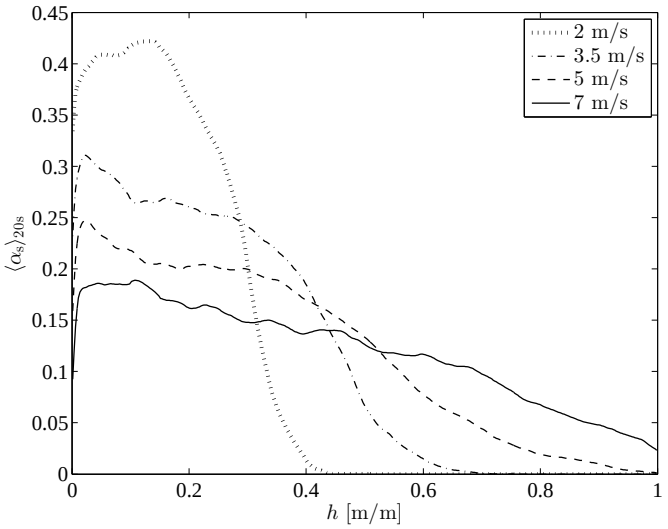

Figure 3.4: Averaged axial solid volume fractions in pilot, $d_\mathrm{p} = 1.25$ mm, simulations.

The char volume fraction (Tables 3.5 and 3.6) has been chosen for the lowest fluidization velocity balance so that the volume fraction of oxygen in a gas phase at the exit of reactor would preferably be between one and five percent. In all the simulated balances, the time-averaged volume fraction of oxygen in a gas phase at the exit of the reactor is between 1 $\mathrm{mol/m^3}$ and 8 $\mathrm{mol/m^3}$. The reason for controlling the exit oxygen was ensuring that the gas concentration conditions in the emulsion and bubble phase would be comparable between the tests, even though the analysis method (Chapter 4.1.3) of heterogeneous mass transfer coefficient already considers the effect of axial concentration profiles. Figs. 3.7, 3.8 and 3.9 presents the simulated average axial oxygen concentrations $\langle C_{\mathrm{O}_2} \rangle_{20\mathrm{s}}$.

3.3.3 Multiphase flow and reaction characteristics

The actual flow structures in bubbling and turbulent beds are very heterogeneous with bubbles, voids, clusters and streamers of different sizes, although the time-averaged axial solid density profiles described above are, as typical for all fluidized bed processes,

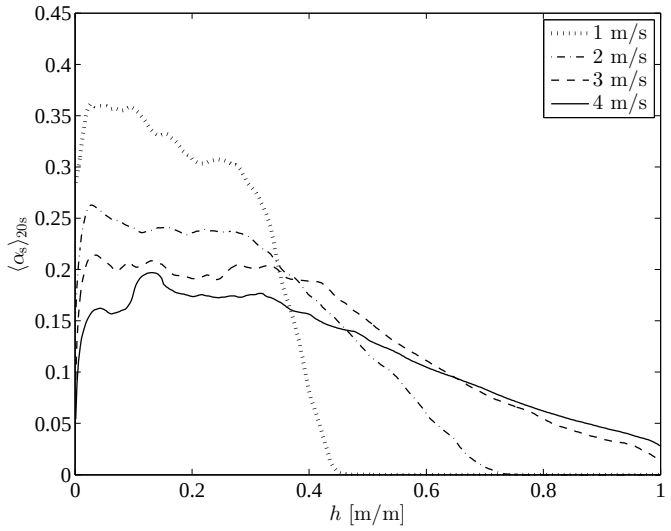

Figure 3.5: Averaged axial solid volume fractions in pilot, $d_p = 0.5$ mm, simulations.

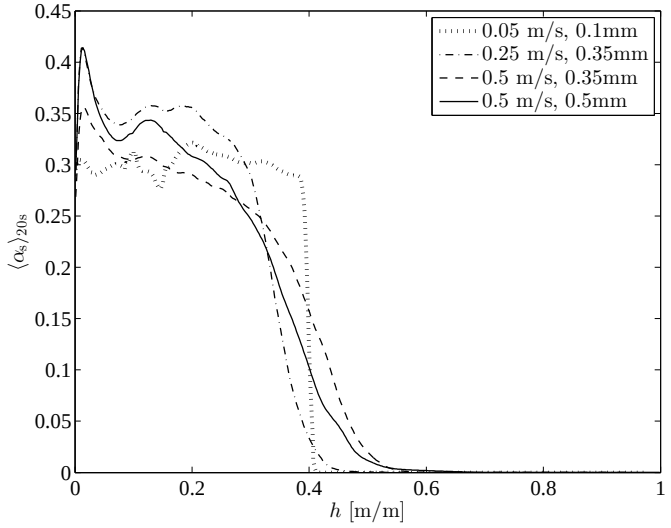

Figure 3.6: Averaged axial solid volume fractions in bench simulations.

very smooth and stable in particular process condition. This can be clearly seen in Fig. 3.10, which shows the instant solid volume fractions contours for the pilot balances with Geldart B solids. The fluidization velocity of 1 $\mathrm{m/s}$ results as a bubbling bed with small

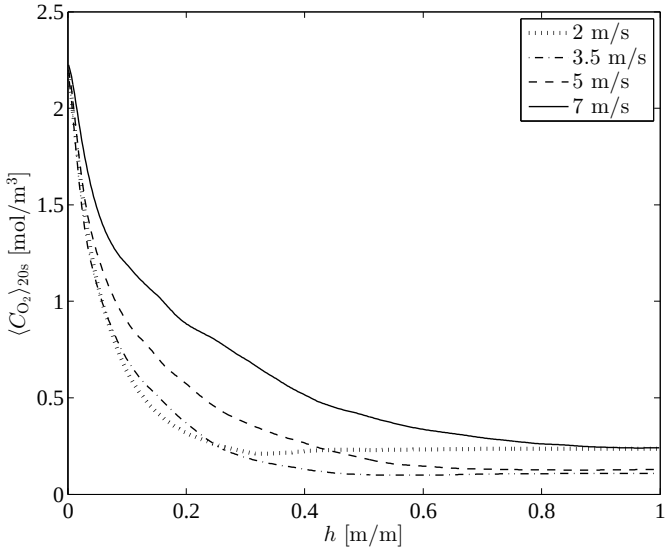

Figure 3.7: Averaged axial oxygen concentrations in the pilot, $d_\mathrm{p} = 1.25$ mm, simulations.

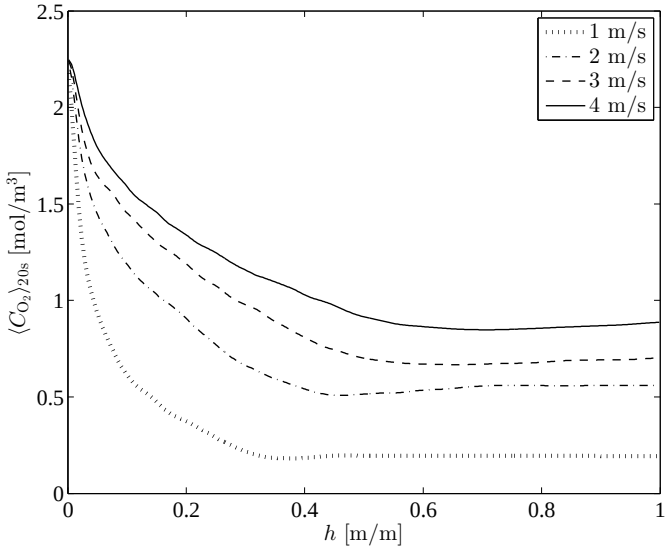

Figure 3.8: Averaged axial oxygen concentrations in the pilot, $d_\mathrm{p} = 0.5$ mm, simulations.

bubbles near the air distributor, which then grow and coalesce while rising in the bed (Fig. 3.10a). Similar bubble behavior occur in the case of the fluidization velocity of 2

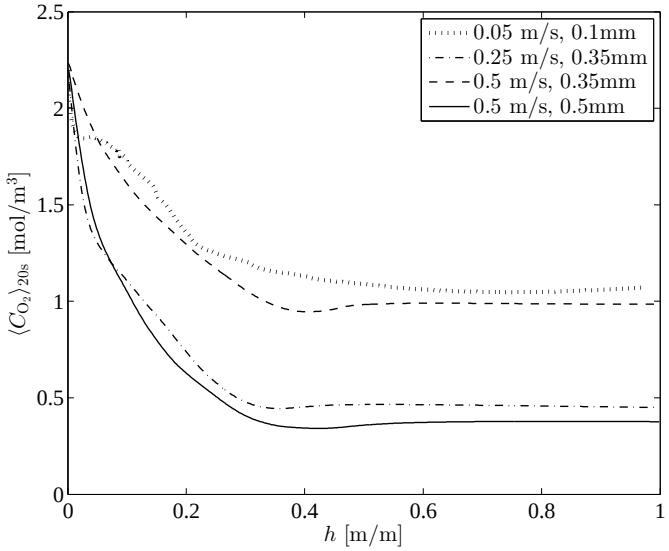

Figure 3.9: Averaged axial oxygen concentrations in the bench simulations.

$\mathrm{m/s}$ (Fig. 3.10b), except that bubbles are larger and the bed height is expanded. Transition to the turbulent regime occurs when moving to the fluidization velocity of 3 $\mathrm{m/s}$ (Fig. 3.10c). Bubbles or voids are formed more frequently at the lower bed than in the bubbling bed balances, which then burst the solids to the upper parts of the reactor as axial, and even wall, slugs. In the upper part of the reactor, extensive channeling of gas flow occurs. The solids flow preferably back to the dense bed area as downward-dropping large clusters near the walls. The back-flow of solids, a wall layer, forms also in the case of the fluidization velocity of 4 $\mathrm{m/s}$ (Fig. 3.10d). In this balance, also a small solid re-circulation flow is formed as some solids are transported out from the top exit of the reactor. The fluid dynamic behavior discussed above occurred also in the case of pilot balances with group D particles.

The differences between bubbling and turbulent bed flow structures are shown in Fig. 3.11. The figure presents, as an example, two simulated 2 s time-series of local solid volume fractions from one calculation cell located 50 cm above the air distributor. The bubbling bed simulation of the pilot reactor with fine solids and the fluidization velocity of 2 $\mathrm{m/s}$ results in a very steep and clear boundary between the dense emulsion very close to the minimum fluidization velocity and the low-solid bubble. On the other hand, the turbulent bed pilot simulation with the coarse solids and the fluidization velocity of 7 $\mathrm{m/s}$ shows more frequent peaks of solid-rich clusters that have lower solid volume fraction than the minimum fluidization voidage suggests. However, in these turbulent conditions, the local solid volume fraction has a wide operation range essentially at the low and middle solid-rich conditions.

Multiphase reaction characteristics in the fluidized beds are highlighted in Figs. 3.12a and

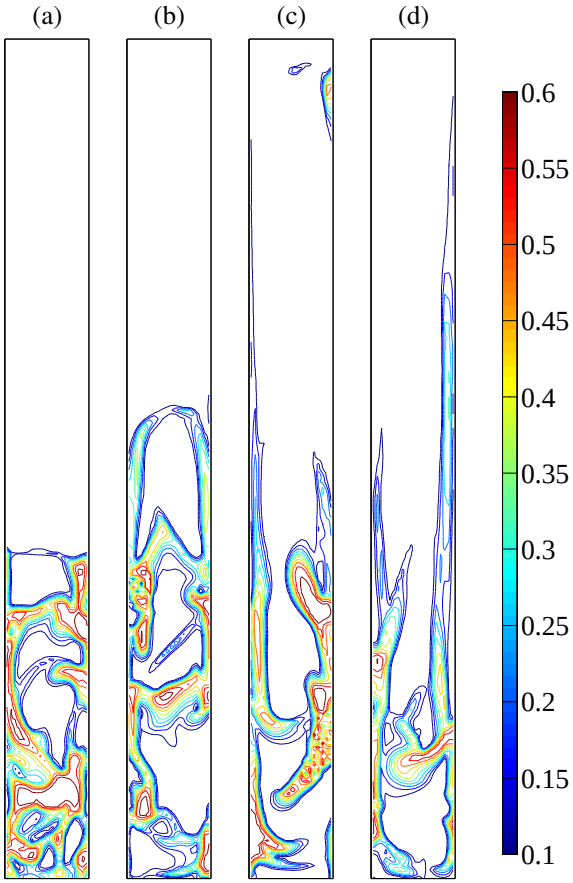

Figure 3.10: Instant solid volume fraction contours for pilot balances with small particles, and fluidization velocities of (a) $1\mathrm{m/s}$, (b) $2\mathrm{m/s}$, (c) $3\mathrm{m/s}$ and (d) $4\mathrm{m/s}$.

b. Fig. 3.12a shows the instant volume fraction of solids in the lower bed in the $2\ \mathrm{m/s}$ fine-particle pilot balance and Fig. 3.12b shows the corresponding instant concentration of oxygen in gas in the same balance at the same time. The solid lean bubbles are marked with (1) in the figures and the regions of solid-dense emulsion with (2), respectively. Extensive channeling of oxygen-rich gas flow occurs in all fluidized bed balances. The main flow-reaction characteristics of the multiphase system are high concentration of oxygen in the solid lean bubbles and very low oxygen conditions in the solid-dense emulsion.

3.3.4 Grid independence

The tightest mesh size selection criteria that have been reported in the literature vary from three (Wang et al., 2009) to ten/twenty (Andrews et al., 2005a; Benyahia, 2012) particle diameters. Andrews et al. (2005a) present that the fluidized bed risers contain

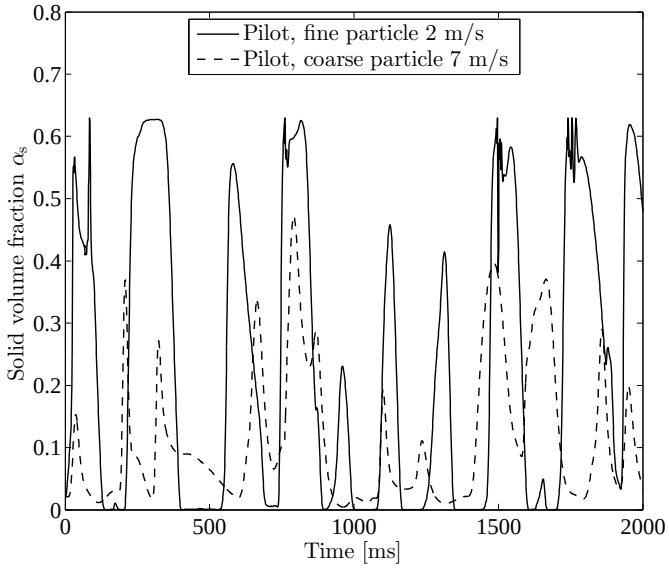

Figure 3.11: Time-series (2 s) of local solid volume fraction from one calculation cell located at the height of 50 cm above the air feeding grid for bubbling and turbulent bed pilot balances.

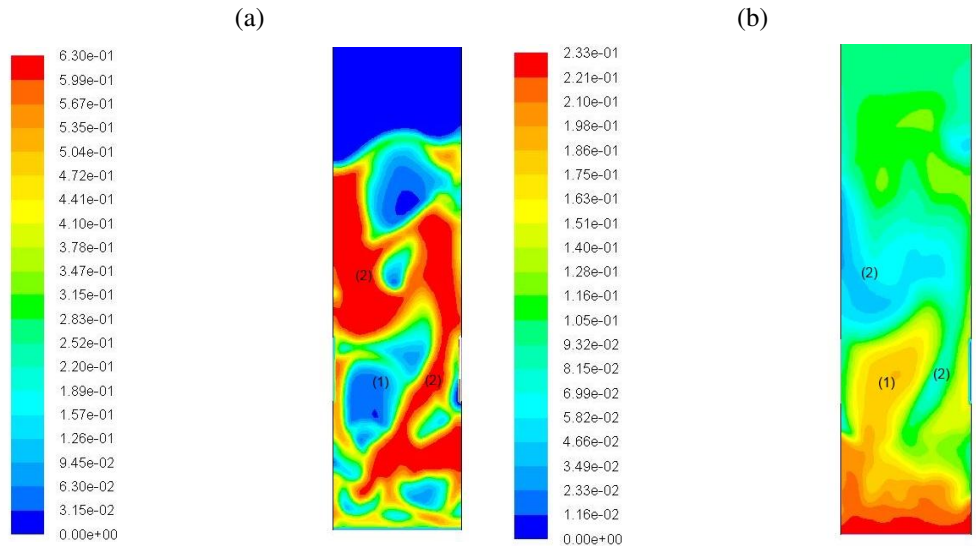

Figure 3.12: Instantaneous (a) volume fractions of solids and (b) concentration of oxygen in the bottom bed of the pilot reactor during 2 $\mathrm{m/s}$ fine particle balance.

mesoscale structures (bubbles, clusters and streamers) with the length scale of the order of 10 particle diameters. Thus, the criterion for the maximum grid size to use in a gas-solid CFD simulation is often set to less than 10 particle diameters, if no sub-grid closure correction models are used.

A grid independence study was also carried out to ensure that the best achievable Eulerian CFD simulations had been executed. In order to recognize the effect of the mesh size to the resulted solid flow dynamic and heterogeneous mass transfer characteristics, a finer and a coarser mesh size were tested. The pilot reactor balance with $d_\mathrm{p} = 0.5$ mm and $u_\mathrm{f} = 3$ m/s solved with a mesh of 5×5 mm^2, was also simulated with a fine (2.5×2.5 mm^2) and a coarse (10×10 mm^2) grid size. Tables 3.2 and 3.3 presents the cell width to particle diameter ratios for the executed CFD simulations. The pilot, small d_p, balances had the highest cell width and close to highest cell width to particle diameter ratio of 10. Consequently, grid independence in the all simulations could be assumed to be fulfilled with practical accuracy.

Fig. 3.13 shows that the coarse grid (10×10 mm^2) simulations result as a changed solid flow dynamics compared to the finer grid simulations. In practice, the clusters were not properly resolved with the coarse mesh. The fine (2.5×2.5 mm^2) grid and the grid size applied in the simulations of the thesis (5×5 mm^2) resulted as a similar time-averaged solid volume fraction profile. The bed Sherwood numbers presented in Chapter 4 were stabilized already with the grid size of 5×5 mm^2 as shown in Table 3.7. Thus, this mesh design (40×400 cells) is considered to be proper to capture the essential features of the transient gas-solid flow dynamics and the related heterogeneous mass transfer mechanisms with a practical accuracy.

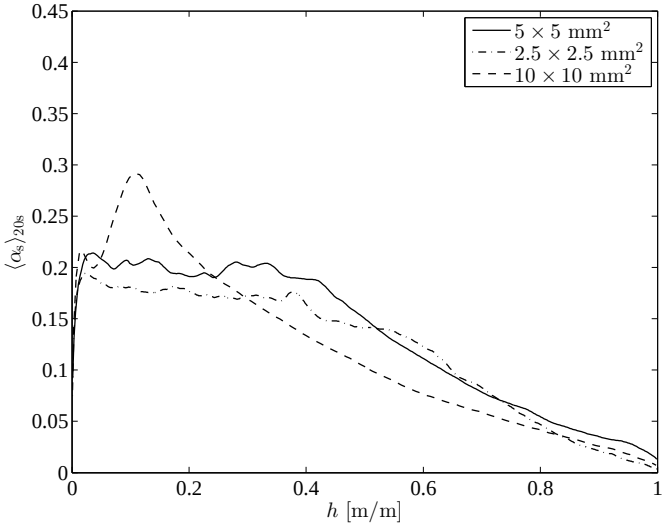

Figure 3.13: Averaged axial solid volume fractions in grid independence simulations.

Table 3.7: Grid independence: Pilot, $d_\mathrm{p} = 0.5$ mm, $u_\mathrm{f} = 3$ m/s

Mesh	Sh_bed
10×10 mm^2	0.3
5×5 mm^2	1.2
2.5×2.5 mm^2	1.3

4 Bed Sherwood numbers in bench and pilot scale fluidized bed combustors

This chapter presents average gas-bed mass transfer coefficients as bed Sherwood numbers derived from the Eulerian CFD simulations discussed in Chapter 3. As experimental data of bed Sherwood numbers for fluidized bed combustion is not available in the literature, the bed Sherwood numbers are compared with experimental data of fluidized beds consisting of only active particles operated at the same Reynolds number range. As a result of heterogeneous mass transfer analysis, a generalized behavior of average gas-bed mass transfer in fluidized bed combustion is presented in a dimensionless $Sh_{\mathrm{bed}} - Re$ diagram with discussion on the effect of the operational parameters: fluidization velocity, particle diameter, reactor width and chemical kinetic coefficient. Also the axial behavior of cross-section- and time-average gas-solid mass transfer is described.

4.1 Research approach and method of analysis

The objective of the research presented in this chapter is to benchmark the bed Sherwood numbers predicted by the Eulerian two-phase CFD model in bench and pilot scale fluidized bed combustors operated under bubbling and turbulent conditions. Furthermore, the derived bed Sherwood numbers are compared and analyzed against the available empirical data of only active particle beds. This is due to the fact that any experimental data on the bed Sherwood numbers for the active particles in bed of inert solids was not found for this study. The similarities in the heterogeneous mass transfer between the two main process types, the beds of only active solids and the beds of inert solids with active particles, found in this thesis are concluded in Chapter 7.

4.1.1 Eulerian CFD modeling

The overall research approach is to simulate the heterogeneous combustion reaction of a wood char in fluidized bed by means of the Eulerian CFD modeling with varied chemical kinetic coefficients and particle sizes under the bubbling and turbulent fluidization regimes. The governing equations, main sub-models, reactor and mesh design, boundary conditions and properties, solution procedure, and resulted solid flow dynamics and chemical conversion of the Eulerian two-phase CFD modeling applied in the research work presented in this chapter are described in Chapter 3.

4.1.2 Time- and space-averaging

Different symbols of the time- and space-averaging applied in the analysis of the transient CFD simulations presented in this thesis are defined here. Actually, the same averaging definitions are valid for real fluidized bed processes and are closely related also to the averaged parameters applied in the steady-state models of fluidized beds discussed in Chapter 2.2. First, a definition for the local space- and time-average of the general variable f over time period Δt is given as

$$\langle f \rangle_{\Delta t}^{(x,y,z)} = \frac{1}{\Delta t \delta V} \int_0^{\Delta t} \int_{\delta V} f \mathrm{d}V \mathrm{d}t, \tag{4.1}$$

where the coordinates (x, y, z) present a center point of the specific calculation cell. In the analysis of CFD simulations, δV is defined as a volume of the calculation cell. Secondly, a cross-sectional time-average of the general variable f over time period of Δt is defined as

$$\langle f \rangle_{\Delta t} = \frac{1}{\Delta A \Delta z} \int_{\Delta A} \int_{\delta z} \langle f \rangle_{\Delta t}^{(x,y,z)} \mathrm{d}z \mathrm{d}A, \tag{4.2}$$

where Δz is the height of the calculation cells and ΔA is the cross-sectional area under concern for averaging. In this work, cross-sectional time-averages are studied. Thus, Δz is defined here as the height of the calculation cells and ΔA as the cross-sectional area of the reactor, which for two-dimensional cases is the width of the reactor W times the unit depth of 1 m. The cross-sectional time-average is the most commonly referred to parameter in this thesis. The last, general time- and space-average term defined here is a time-average of the general variable f in the dense bed region, which is given by

$$\bar{f} = \bar{f}_{\Delta t} = \frac{1}{H_{bed}} \int_0^{H_{bed}} \langle f \rangle_{\Delta t} \mathrm{d}z. \tag{4.3}$$

The height of the dense bed H_{bed} is defined as the lower bed region where the cross-sectional time-average of the solid volume fraction $\langle a_{\mathrm{C}} \rangle_{20\mathrm{s}} > 0.15$. The limit average solid volume fraction value of 0.15 has been selected from the axial solid volume fraction profiles (Figs. 3.4, 3.5 and 3.6) to represent the boundary between the dense lower and dilute upper bed. Furthermore, the time-average over $\Delta t = 20$ s is considered to represent the average and stabilized conditions in the dense bed, and thus $\bar{f}$ is used in the following chapters to represent also $\bar{f}_{\Delta t=20s}$. The same principle is applied also for the cross-sectional time-average (Eq. 4.2), if the time-period is long enough to represent the stabilized conditions. For these cases, $\langle f \rangle = \langle f \rangle_{\Delta t}$.

4.1.3 Derivation of the bed Sherwood number

The bed Sherwood number represents the average gas-bed mass transfer coefficient over the fluidized bed. Thus, time- and space-averaged values are used in the definition procedure. First, the axial effective reaction rate coefficient in the bed is defined based on the time-averaged cross-sectional reaction rates and oxygen concentrations (Figs. 3.7, 3.8 and 3.9) as follows

$$\langle k_{\text{eff}} \rangle = \frac{\langle R_{\text{C}} \rangle_{20\text{s}}}{\langle a_{\text{C}} \rangle_{20\text{s}} \langle C_{\text{O}_2} \rangle_{20\text{s}}}. \tag{4.4}$$

The surface area of char per reactor volume a_{C} is given by Eq. 3.2. The cross-sectional time-averages of $\langle R_{\text{C}} \rangle_{20\text{s}}$, $\langle a_{\text{C}} \rangle_{20\text{s}}$ and $\langle C_{\text{O}_2} \rangle_{20\text{s}}$ are defined according to Eq. 4.2. The cross-sectional time-average of gas-bed mass transfer coefficient $\langle h_{\text{m}} \rangle$ is solved from

$$\langle k_{\text{eff}} \rangle = \frac{1}{1/k_{\text{C,sur}} + 1/\langle h_{\text{m}} \rangle}, \tag{4.5}$$

where $k_{\text{C,sur}}$ is the chemical kinetic rate coefficient of char per surface area of the particle. Then, the cross-sectional time-average of the bed sherwood number is given according to its dimensionless definition as

$$\langle Sh_{\text{bed}} \rangle = \frac{\langle h_{\text{m}} \rangle d_{\text{p}}}{D_{\text{O}_2}}. \tag{4.6}$$

The average gas-solid mass transfer coefficient $\bar{h}_{\text{m}}$ in the lower dense bed can be solved from the effective reaction rate coefficient $\bar{k}_{\text{eff}}$, which is integrated according to Eq. 4.3 from the cross-sectional profile of $\langle k_{\text{eff}} \rangle$, as follows

$$\bar{k}_{\text{eff}} = \frac{1}{1/k_{\text{C,sur}} + 1/\bar{h}_{\text{m}}}. \tag{4.7}$$

Here, the bed Sherwood number, which is the main concern in the study, is the time-average in the dense bed region. Consequently, the average value in the dense bed is defined from the lower bed region, where the limit in average solid density $\langle \alpha_{\text{s}} \rangle_{20\text{s}} > 0.15$ is applied as discussed in Chapter 4.1.2. On the other hand, a sensitivity analysis showed that the resulted bed Sherwood numbers were not remarkably sensitive to the choice of this value. Finally, the bed Sherwood number in the lower bed is given by its dimensionless definition as

$$\bar{Sh}_{\text{bed}} = \frac{\bar{h}_{\text{m}} d_{\text{p}}}{D_{\text{O}_2}} = Sh_{\text{bed}}. \tag{4.8}$$

The simplified symbol Sh_{bed} represent the time-averaged bed Sherwood number in the dense bed region in the following chapters.

4.2 Bed Sherwood number

The derived bed Sherwood numbers Sh_{bed} in the dense bed region (Eq. 4.8) show four important parametrical relationships. All the obtained bed Sherwood numbers Sh_{bed} in the lower bed (Eq. 4.8) are shown in Fig. 4.1. The figure shows also the experimental bed Sherwood number data and the emulsion Sherwood number correlation (La Nauze et al., 1984).

4.2.1 Effect of fluidization velocity

Fig. 4.1 shows that the increase of fluidization velocity results in the same, strong exponential increase of Sh_{bed} with the Reynolds number as shown by a number of empirical tests (Fig. 4.1). All the empirical data presented in Fig. 4.1 is based on experiments in bubbling beds with only active solids. However, the same response to fluidization velocity was suggested to continue into the turbulent bed regime by the Eulerian CFD simulations of this work. In the CFD simulated large particle ($1.25\ \mathrm{mm}$) pilot balances, the bed Sherwood numbers correspond to the experimental data based on tests with similar particle sizes conducted by Kettering et al. (1950), while the simulated small particle ($0.5\ \mathrm{mm}$) pilot balances result in similar bed Sherwood numbers as in the tests of Resnick and White (1949). Further, the simulated $0.35\ \mathrm{mm}$ particle diameter balances in the bench scale reactor result in bed Sherwood numbers close to the experimental data of Richardson and Szekely (1961). As a conclusion, all empirical and CFD-based bed Sherwood numbers with other process conditions unchanged, such as particle size, have a similar fluidization velocity response in the $Sh_{\mathrm{bed}} - Re$ diagram.

4.2.2 Effect of reactor size

A second parametrical relationship of the bed Sherwood number shown in Fig. 4.1 is the size of reactor. The Eulerian CFD simulations propose that the average gas-bed mass transfer coefficient, and Sh_{bed}, increase remarkably in smaller diameter reactors. Discussion presented in Chapter 5 shows later that this is due to enhanced interphase mass transfer caused by the decrease of reactor diameter in case of the small-scale fluidized bed reactors. The quantity of this increase can be estimated from Fig. 4.1 by comparing the bench and pilot balances with the particle diameter of $0.5\ \mathrm{mm}$. The operational parameters between these two balances are the same, except the size change of the reactor and fluidization velocity (Tables 3.5 and 3.6). Extrapolation of the exponential trend of the pilot bed Sherwood number to the Reynolds number of 1.8 used in the bench reactor simulation propose an about 2.5 times lower Sh_{bed} in a ten times wider reactor.

4.2.3 Effect of particle diameter

A third parametrical dependence on the bed Sherwood number seen in Fig. 4.1 is the effect of particle diameter. The Eulerian CFD simulations suggest that the level of Sh_{bed} trend is dropping with the increase of particle size in the Sh_{bed} - Re chart (Fig. 4.1). This

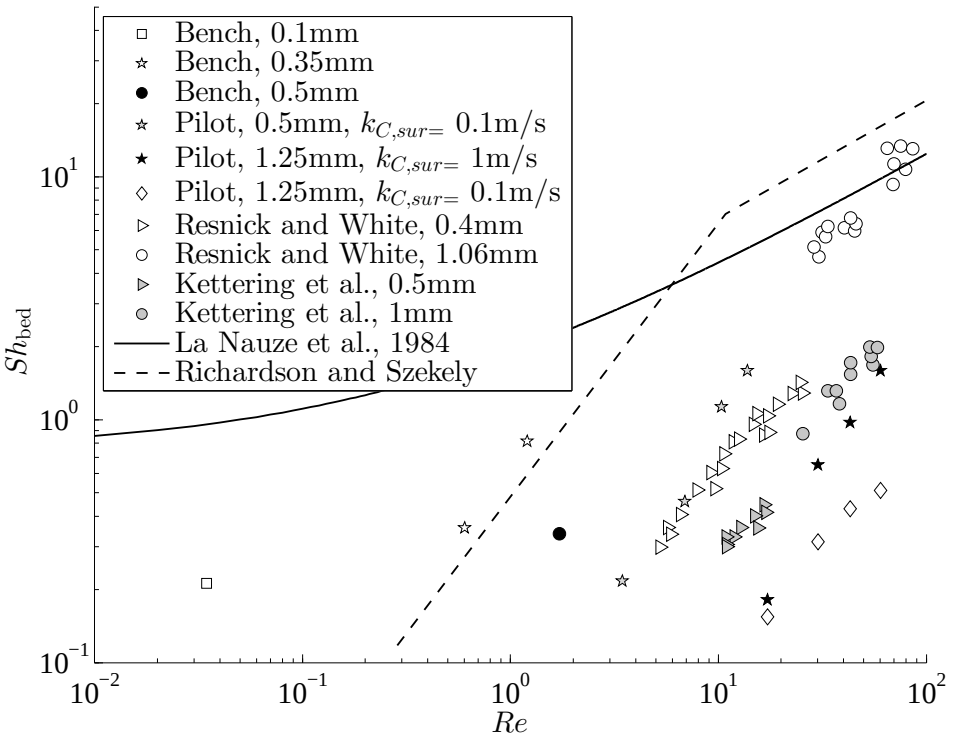

Figure 4.1: Bed Sherwood numbers against particle Reynolds numbers

finding is contradictory to the empirical results of Resnick and White (1949) and Kettering et al. (1950), which clearly propose a slight increase of Sh_{bed} trend in the Sh_{bed} - Re chart. However, in order to achieve comparable axial oxygen profiles in the CFD simulations (Figs. 3.7, 3.8 and 3.9), the char loading had to be remarkably varied between the balances (Tables 3.5 and 3.6). Consequently, any other conclusion than one still relying on the slight enhancement of Sh_{bed} with the particle size as shown by the empirical data is not justified. The effect of char loading is discussed in the following analysis regarding the chemical kinetic coefficient.

4.2.4 Effect of chemical kinetic coefficient

The large particle ($1.25\ \mathrm{mm}$) pilot balances were simulated with two chemical kinetic coefficients $k_{C,sur}$ of 0.1 $\mathrm{m/s}$ and 1 $\mathrm{m/s}$, which represent middle and high reactivity of wood char (Rangel and Pinho, 2011). The oxygen concentration profiles were similar in both balances with the fluidization velocity of 2 $\mathrm{m/s}$, and the bed Sherwood number did not change with the chemical kinetic coefficient. However, to obtain a similar axial oxygen profile in the high kinetic coefficient balance ($k_{C,sur}$ =1 $\mathrm{m/s}$), the char loading

had to be decreased with the same proportion as the kinetic coefficient was increased, to y_c of 0.01. In practice, this means that the product of char volume fraction y_c and kinetic coefficient $k_{C,sur}$ were constant in these balances. It is logical, that the effective reaction rate in beds with both active and inert solids is a combination of the char volume fraction and kinetic coefficient. Thus, the simulations with the constant product of char volume fraction of y_c of 0.1 $\mathrm{m/s}$ and the higher kinetic coefficient of 1 $\mathrm{m/s}$ resulted in a similar fluidization velocity response of the bed Sherwood number than in small particle (0.5 mm) pilot balances with constant char loading. On the other hand, the rise in the effective reaction rate, or product of char volume fraction y_c and kinetic coefficient $k_{C,sur}$, due to an increase of the char volume fraction (Table 3.5) from 0.1 to 0.14 in the case of the lower kinetic coefficient ($k_{C,sur}$ =0.1 $\mathrm{m/s}$) balances resulted a clear drop in the level of the trend of the bed Sherwood number. As a conclusion, the increase of the effective chemical kinetic coefficient, which here was a product of the char volume fraction y_c and kinetic coefficient $k_{C,sur}$, showed a strong decreasing effect to the average mass transfer coefficient, and in these simulations this effect dominated over the particle size influence on the bed Sherwood number discussed above. Actually, reason for the decrease of bed Sherwood number with the increase of kinetic reaction rate is due to a strong decrease of oxygen concentration in regions of emulsion that are close to gas- and oxygen-rich bubbles and voids. Consequently, large regions of emulsion, where reaction rates would be highest, have remarkably lower oxygen concentration than the average oxygen concentration level in the bed proposes. Thus, the decrease of bed Sherwood number is related to the space- and time-averaging of the local and transient process conditions. This issue is later described in details in Chapter 7.

4.2.5 Axial characteristics

The axial behavior of the cross-sectional averaged bed Sherwood numbers $\langle Sh_{\mathrm{bed}} \rangle_{20s}$ observed in the CFD simulations are shown in Fig. 4.2. In principle, three characteristic region-dependent aspects were found. First, the rate of the average gas-solid mass transfer at the region above fluidization gas feeding is relevantly higher than at the bubble region above.

Fig. 4.2 shows the axial bed Sherwood numbers $\langle Sh_{\mathrm{bed}} \rangle_{20s}$ in the fine-particle ($d_{\mathrm{p}} = 0.5$ mm) pilot simulations at the bubbling and turbulent regimes. The average gas-solid mass transfer at the region above gas feeding is higher in all the simulated balances irrespective of the fluidization regime, the particle size or the reactor diameter. This behavior is in accordance with previous research presented in the literature. The interphase mass transfer at just above fluidization gas feeding has been reported to be 40 to 60 times greater than in the dense bubbling region (Behie and Kehoe, 1973). This enhancement is explained by extensive convective throughflow forming bubbles above the grid region. Actually, the design of the air distributor has a strong effect on the rate of heterogeneous mass transfer (Ho, 2003a). The air distributor in the simulation approach was designed straightforwardly as a plane defined as a constant velocity inlet. This approach seems to result in correct enhanced mass transfer behavior in the region above the air distributor. More precise analysis of the average gas-solid mass transfer at the very bottom of bed would

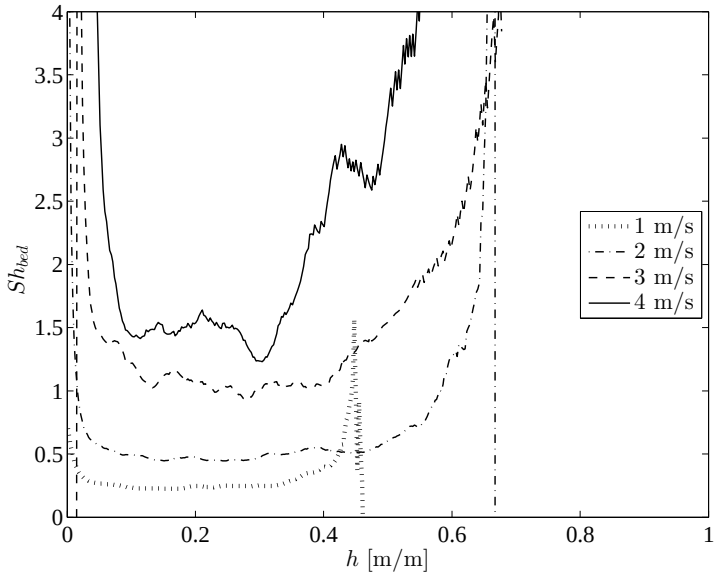

Figure 4.2: Bed Sherwood numbers against dimensionless height of the reactor in fine-particle ($d_\mathrm{p} = 0.5$ mm) pilot simulations.

require simulations with different designs of air distributor. However, the main focus in this thesis is set to the bubble region of the dense bed, which is above the primary effects of the air distributor.

Secondly, in the bubble region of the dense bed, the cross-sectional time-average of the bed Sherwood number $\langle Sh_\mathrm{bed} \rangle_{20s}$ seems to stabilize to a constant level as shown in Fig. 4.2. This behavior was present in all the simulated balances. The bubble region of the dense bed presents the region, where the average bed Sherwood numbers presented in the $Sh_\mathrm{bed} - Re$ diagrams of this thesis have been derived. Finally, the cross-sectional bed Sherwood numbers $\langle Sh_\mathrm{bed} \rangle_{20s}$ above the dense bed seem to rise strongly with the reactor height as shown in Fig. 4.2. Similar behavior of gas-solid mass transfer has been presented in Vepsäläinen et al. (2012), introducing Eulerian CFD simulations of fluidized bed combustion in small-scale reactors used for derivation of axial bed Sherwood numbers. The behavior of the axial bed Sherwood number was very similar to the results of this thesis. Fig. 4.3 shows the bed Sherwood number behavior in turbulent fluidized beds (Vepsäläinen et al., 2012) at region above the dense bubbling bed against fluidization velocity and cross-section averaged solid volume fraction. The region above the dense bubbling bed is commonly called a splashing region. Figs. 3.4, 3.5 and 3.6 show how horizontal and time averages of axial solid volume fractions drop with the reactor height in the splashing region, while the average solid volume fractions in the dense bubbling bed are constant. Contrary to this behavior, the mass transfer research work by Eulerian CFD modeling presented by Chalermsinsuwana et al. (2009) suggests that the bed

Sherwood number decreases slightly with the height of the riser in the lean upper bed of a fine-particle fast fluidized bed. However, this lean upper bed is above the splashing region, which is just above the dense bed surface. An explanation for this could be that in this region, the small and dense fine-particle clusters would form enhanced gas-cluster interphase mass transfer resistance. Actually, the highest velocity simulations at the turbulent regime presented by Vepsäläinen et al. (2012) resulted also in a slightly decreasing trend in the bed Sherwood numbers in the upper lean reactor above the splashing region, while the bed Sherwood numbers increased strongly in the splashing region, as shown in Figs. 4.2 and 4.3. Even more importantly, the experimental work of Kashyap and Gidaspow (2010) supports the results obtained in this thesis. Kashyap and Gidaspow (2010) derived axial Sherwood numbers for fine FCC particles in a pilot reactor operated under the bubbling bed regime. They report low bed Sherwood numbers around 0.0001 in the very bottom bed, the lowest bed Sherwood numbers of around 0.00005 at the dense bubbling bed and the highest bed Sherwood number of 0.0009 at the splashing region above the dense bed. Although, the level of the bed Sherwood numbers for the fine FCC particles is remarkably lower, the axial behavior is same as shown by the bed Sherwood numbers derived in this thesis. Heterogeneous mass transfer in the fine-particle processes is discussed in Chapters 6 and 7.

The heterogeneous mass transfer in the dense bed is the main interest in this research work. However, the axial characteristics discussed above can give guidance for the estimation of gas-bed mass transfer in the different regions of the various and diverse size processes of fluidized beds. It is worth noting, that a limited rate of solid and gas dispersion, and also secondary gas feedings, result in uneven cross-sectional solid, fuel and gas concentrations in larger than pilot scale reactors. Thus, the steady-state fluidized bed models (Chapter 2.2.2) designed for one- and two-dimensional calculation grids should consider the additional resistance to the average gas-solid mass transfer caused by the non-uniformity of the solid and gas concentrations. The three-dimensional fluidized bed models are able to describe the cross-sectional non-uniformity of solids and gaseous species. On the other hand, turbulent and feeding- related fluctuations may cause time-averaging related inaccuracy particularly in the predictions of gaseous emission compounds. In practice, also three-dimensional modeling of large-scale fluidized bed reactors requires the use of a relatively large calculation cell size, thus the modeling is fundamentally based on the space- and time-averages of the properties, conditions and rates describing the process performance. Consequently, the validation simulations of the three-dimensional CFB model (Hyppänen et al., 1991) presented by Vepsäläinen et al. (2009) considering eight large-scale coal combusting CFB boilers and several peat, wood, biomass and waste fired CFB boilers would greatly benefit from the average heterogeneous mass transfer behavior discussed here.

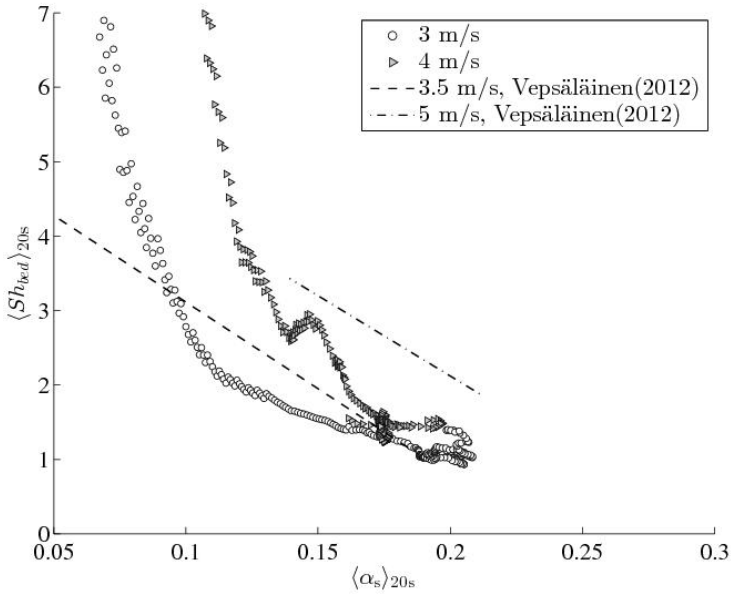

Figure 4.3: Cross-sectional bed Sherwood numbers at the splashing zone against cross-sectionally averaged solid volume fraction in fine-particle ($d_\mathrm{p} = 0.5$ mm) pilot simulations on the turbulent regime. The trendlines of $\langle Sh_\mathrm{bed}\rangle$ obtained from Vepsäläinen et al. (2012) with fluidization velocities of $3.5\mathrm{m/s}$ and $5\mathrm{m/s}$ are based on similar CFD simulations as those presented in Chapter 3 with the coarse particle size of 1.25 mm.

5 Interphase mass transfer in bench and pilot fluidized bed combustors

This chapter presents interphase mass transfer coefficients for the lower dense bed derived from the Eulerian CFD simulations of fluidized bed char combustion presented in chapter 3. First, a steady-state one-dimensional bubble-emulsion fluidized bed char combustor model is formulated, and a method for average bubble size characterization from transient CFD modeling is introduced. This is followed by a fitting of the bubble-emulsion model with the CFD simulations. In the analysis of the results, the effect of fluidization velocity, particle diameter and reactor size to the volumetric interphase mass transfer coefficient $\bar{K}_{\mathrm{be}}$ is presented. Furthermore, the importance of the bubble size and the specific surface area with respect to interphase mass transfer are highlighted. Finally, the average interphase mass transfer coefficient $\bar{K}_{\mathrm{be}}$ is shown to have an exponential relationship with the dimensionless Reynolds number.

5.1 Research approach and methods of analysis

The two-dimensional transient Eulerian CFD simulations presented in Chapter 4 indicated that the transfer of oxygen from the upward flowing gas to the surface of fluidized particles was strongly limited by convective transfer of gas within the bubbles or by the channeling of oxygen-rich low solid concentration plumes and voids at the turbulent regime. Thus, another traditional approach describing the heterogeneous mass transfer in fluidized beds is here used in the analysis of Eulerian CFD simulations to derive the interphase mass transfer coefficients. Consequently, a simple one-dimensional bubble-emulsion fluidized bed char combustor model suitable for bubbling and turbulent beds is formulated. As discussed in Chapter 2, the empirical bubbling and turbulent regime interphase mass transfer correlations are mostly defined for fine (Geldart A) particle fluidized beds. Consequently, the research objective here is to define the interphase mass transfer coefficients for bubbling and turbulent fluidized beds with Geldart B and D solids by Eulerian CFD simulations. The interest is particularly in the effect of fluidization velocity, particle diameter, as well as reactor and bubble size.

5.1.1 Eulerian CFD modeling

The Eulerian CFD simulations of fluidized bed char combustion used in Chapter 5 to derive interphase mass transfer coefficients are the same as the ones presented in Chapter 3.

5.1.2 Bubble-emulsion fluidized bed model

A one-dimensional steady-state fluidized bed model with bubble and emulsion phases has been designed in order to define the interphase mass transfer coefficient from the CFD simulations. The structure of the model is similar to the model presented by Froment and Bischoff (1990, chap. 13). The model describes a one-dimensional continuity equation

for oxygen in the emulsion and bubble phases. The oxygen continuity equation for the bubble phase is given by the convection and interphase mass transfer terms as

$$\alpha_{\mathrm{b}} u_{\mathrm{b}} \frac{\partial C_{\mathrm{O_2,b}}}{\partial z} - \bar{K}_{\mathrm{be}} (C_{\mathrm{O_2,b}} - C_{\mathrm{O_2,e}}) = 0. \tag{5.1}$$

The model assumes that all char is in the emulsion phase. The oxygen continuity equation for the emulsion phase contains also a term of oxygen consumption due to combustion. The oxygen continuity equation is

$$\alpha_{\mathrm{e}} u_{\mathrm{e}} \frac{\partial C_{\mathrm{O_2,e}}}{\partial z} + \bar{K}_{be} (C_{\mathrm{O_2,b}} - C_{\mathrm{O_2,e}}) - R_{\mathrm{C}} W \partial z = 0. \tag{5.2}$$

The combustion reaction is the primary combustion reaction of carbon (Eq. 3.2). The volumetric combustion rate is calculated similarly as in the CFD simulations with

$$R_{\mathrm{C}} = a_{\mathrm{C}} k_{eff} C_{\mathrm{O_2,e}}, \tag{5.3}$$

where the average surface area of char per volume of a reactor a_{C} is taken as the average cross-sectional surface area of char per volume of a reactor $\langle a_{\mathrm{C}} \rangle_{20s}$ given by

$$\langle a_{\mathrm{C}} \rangle_{\mathrm{20s}} = \frac{6 \langle \alpha_{\mathrm{s}} \rangle_{\mathrm{20s}} y_{\mathrm{C}}}{d_{\mathrm{p}}}. \tag{5.4}$$

The average cross-sectional solid volme fraction $\langle \alpha_{\mathrm{s}} \rangle_{\mathrm{20s}}$ is defined according to Eq. 4.2 from the CFD simulations and y_{C} is the volume fraction of carbon in the solids. The effective reaction rate coefficient $\mathrm{k_{eff}}$ is defined with

$$k_{\mathrm{eff}} = \frac{1}{1/(k_{\mathrm{C,sur}}) + 1/h_{\mathrm{m,e}}}, \tag{5.5}$$

where the chemical kinetic reaction rate coefficient per surface area of a char particle $\mathrm{k_{C,sur}}$ is 0.1 $\mathrm{m/s}$ as in the respective CFD simulations. The convection mass transfer coefficient $\mathrm{h_{m,e}}$ in the emulsion phase is defined with the Sherwood number correlation of La Nauze et al. (1984) given by

$$Sh_{\mathrm{e}} = \frac{h_{\mathrm{m,e}} d_{\mathrm{p}}}{D_{\mathrm{O_2}}} = 2\alpha_{\mathrm{g,e}} + 0.69 Re_{\mathrm{e}}^{1/2} Sc^{1/3}. \tag{5.6}$$

The emulsion phase voidage is estimated by the correlation of Delvosalle and Vanderschuren (1985) as

$$\alpha_{\mathrm{g,e}} = \alpha_{\mathrm{g,mf}} (u_{\mathrm{e}}/u_{\mathrm{mf}})^{1/6.7}, \tag{5.7}$$

where the voidage in the minimum fluidization conditions $\alpha_{\mathrm{g,mf}}$ of 0.47 (Kunii and Leven-

spiel, 1991) is applied. The superficial gas velocity in the emulsion phase u_{e} is estimated from the correlation of Hilligardt and Werther (1986) as

$$\frac{u_{\mathrm{e}} - u_{\mathrm{mf}}}{u_{\mathrm{f}} - u_{\mathrm{mf}}} = \frac{1}{8}. \tag{5.8}$$

An average cross-sectional superficial gas velocity is the fluidization velocity u_{f}. Consequently, bubble phase gas velocity u_{b} is defined by

$$u_{\mathrm{f}} = \alpha_{\mathrm{b}} u_{\mathrm{b}} + \alpha_{\mathrm{e}} u_{\mathrm{e}}. \tag{5.9}$$

The volume fraction of the bubble phase is given by

$$\alpha_{\mathrm{b}} = 1 - \frac{\alpha_{\mathrm{s}}}{\alpha_{\mathrm{g,e}}}, \tag{5.10}$$

where the solid volume fraction $\alpha_{\mathrm{s}} = \overline{\alpha}_{\mathrm{s}}$, where the average solid volume fraction in a dense bed is obtained from the CFD simulations according to Eq. 4.2. Here, the height of dense bed H_{bed} is defined as the lower bed region, where the cross-sectional time-average of solid volume fraction $\langle \alpha_{\mathrm{s}} \rangle_{20\mathrm{s}}$ is greater than 75 percent of its maximum value $0.75 \langle \alpha_{\mathrm{s}} \rangle_{20\mathrm{s}}^{max}$. By definition, the volume fraction of the emulsion phase is given by

$$\alpha_{\mathrm{e}} = 1 - \alpha_{\mathrm{b}}. \tag{5.11}$$

Finally, the average oxygen is solved from

$$u_{\mathrm{f}} C_{\mathrm{O_2}} = \alpha_{\mathrm{b}} u_{\mathrm{b}} C_{\mathrm{O_2,b}} + \alpha_{\mathrm{e}} u_{\mathrm{e}} C_{\mathrm{O_2,e}}. \tag{5.12}$$

The two-phase model presented above has been fitted to the CFD simulations by finding the average volumetric interphase mass transfer coefficient $\bar{K}_{\mathrm{be}}$ that results the same average oxygen concentration at the top exit of the reactor for the bubble-emulsion model $(\mathrm{C_{O_2}})_{\mathrm{exit}}$ and for the CFD model $\langle \mathrm{C_{O_2}} \rangle_{\mathrm{exit}}$, respectively. In solution of bubble-emulsion model, the fluidized bed reactors were discretized to 400 differential horizontal elements (axial cells).

5.1.3 Obtaining average bubble sizes

During the CFD simulations, the volume fraction of solid phase α_{s} was stored with 50 ms frequency in every calculation cell. The analysis period of 20 s resulted as 400 two-dimensional solid phase volume fraction profiles. For all the 400 profiles, solid volume fraction contours of 0.2 were formed and the bubble regions were recognized on basis of the solid volume fraction in the center of the contour (mean of x and y coordinates). The volume of bubbles $\bar{V}_{\mathrm{bub}}$ was calculated on basis of the contours. The average bubble diameters were defined by assuming the bubbles to be cylindrical (circle in 2D) with unit depth as follows

$$\bar{d}_{\mathrm{bub}} = 2\sqrt{\frac{\bar{V}_{\mathrm{bub}}}{\pi}}. \tag{5.13}$$

Accordingly, the average bubble surface area for the two-dimensional bubble is given by

$$a_{\mathrm{b}} = \frac{4\alpha_{\mathrm{b}}}{\bar{d}_{\mathrm{bub}}}. \tag{5.14}$$

5.2 Fitting of the bubble-emulsion model

The one-dimensional steady-state model with the bubble and emulsion phases was fitted with the CFD simulations. The simulation matrix and the two-phase model parameters, such as the superficial gas velocity in the bubble and the emulsion phase (u_{b} and u_{e}) and the volume fraction of the bubble phase α_{b}, used in the analysis are shown in Tables 5.1 and 5.2. The principle of the axial oxygen concentration behavior in the bubble and emulsion phases is presented in Fig. 5.1. The fast drop of emulsion phase oxygen concentration to a value between 0.1 $\mathrm{kmol/m^3}$ and 0.3 $\mathrm{kmol/m^3}$ observed in all the fitted balances shows that the rate of char combustion is controlled by the rate of bubble-emulsion phase mass transfer. The oxygen concentrations observed in the bubble and emulsion phases of the CFD simulations were very similar to those presented in Fig. 5.1.

Table 5.1: Modeling balance matrix with two-phase model parameters and average bubble sizes for pilot reactor simulations: balances 1-4 are for the small d_{p} ($0.5\mathrm{mm}$) and balances 5-8 for the large d_{p} ($1.25\mathrm{mm}$).

Balance		1	2	3	4	5	6	7	8
u_{f}	$\mathrm{m/s}$	1	2	3	4	2	3.5	5	7
u_{mf}	$\mathrm{m/s}$	0.12	0.12	0.12	0.12	0.67	0.67	0.67	0.67
y_{C}		0.01	0.01	0.01	0.01	0.1	0.12	0.13	0.14
f_{b}		0.37	0.57	0.67	0.73	0.29	0.5	0.61	0.7
u_{e}	$\mathrm{m/s}$	0.23	0.36	0.48	0.61	0.83	1.0	1.21	1.46
u_{b}	$\mathrm{m/s}$	2.3	3.2	4.3	0.5	5	6.1	7.5	9.2
$\bar{\alpha}_{\mathrm{s}}$		0.33	0.23	0.19	0.16	0.35	0.26	0.2	0.15
$\bar{K}_{\mathrm{be}}$	$1/\mathrm{s}$	2.9	3.2	3.7	4.2	5	10	13	14.5
$\bar{d}_{\mathrm{bub}}$	cm	6.7	8.5	7.4	7.4	4.3	8.2	10.9	8.1

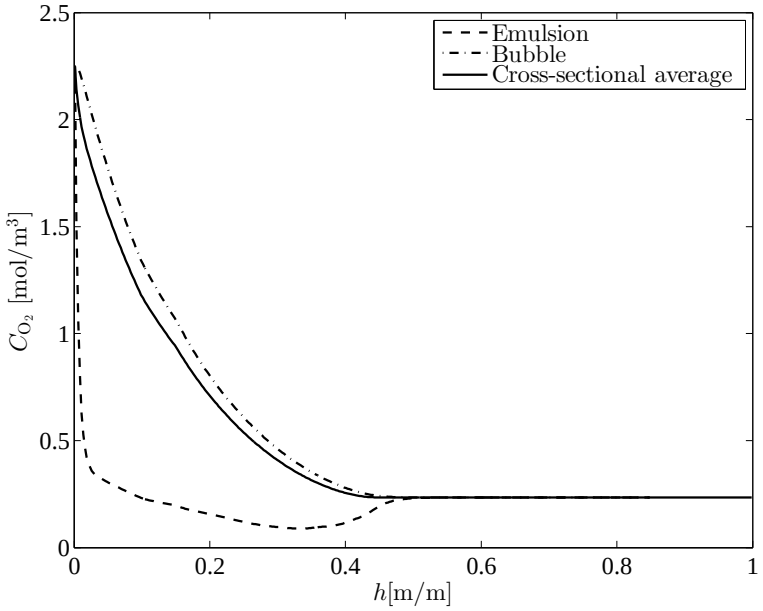

Figure 5.1: Oxygen concentrations in the bubble and emulsion phase, and the cross-sectional average oxygen concentration against the height of reactor in the fitted two-phase model simulation of the pilot balance with the fluidization velocity of 1 m/s.

5.3 Interphase mass transfer coefficients

5.3.1 Effect of fluidization velocity

The obtained average volumetric interphase mass transfer coefficients $\bar{K}_{\mathrm{be}}$ are presented in Tables 5.1 and 5.2. Fig. 5.2 shows that the $\bar{K}_{\mathrm{be}}$ increases with the fluidization velocity. The balances with the same particle diameter have a similar fluidization velocity response of $\bar{K}_{\mathrm{be}}$ than the empirical data reported by Kai et al. (1995) for a turbulent bed with Geldart A solids (55 μm) in a reactor with the diameter of 0.053m. However, $\bar{K}_{\mathrm{be}}$ with Geldart D solids (1.25 mm) seem to have a greater response to fluidization velocity, which corresponds to the empirical correlation of Foka et al. (1996). The empirical correlation of Foka et al. (1996) covers the bubbling and turbulent flow regimes and is based on experiments with Geldart A solids (75-196 μm) in reactors having diameters of 0.1m and 0.2m.

5.3.2 Effect of particle diameter and reactor size

Fig. 5.2 suggests that the level of the average volumetric interphase mass transfer coefficient $\bar{K}_{\mathrm{be}}$ rises with the particle diameter. The figure shows the interphase mass transfer coefficients calculated with the turbulent bed correlation of Miyauchi et al. (1980) with

Table 5.2: Modeling balance matrix with two-phase model parameters and average bubble sizes for bench reactor simulations.

Balance		Bench 1	Bench 2	Bench 3	Bench 4
d_p	mm	0.1	0.35	0.35	0.5
u_f	m/s	0.05	0.25	0.5	0.5
u_mf	m/s	0.005	0.06	0.06	0.12
y_C		0.0001	0.0025	0.0025	0.01
f_b		0.42	0.31	0.45	0.36
u_e	m/s	0.01	0.084	0.12	0.16
u_b	m/s	0.1	0.63	0.97	0.91
$\bar{\alpha}_\mathrm{s}$		0.3	0.34	0.28	0.31
$\bar{K}_\mathrm{be}$	1/s	0.16	2.6	3.2	5
$\bar{d}_\mathrm{bub}$	cm	3.4	1.0	1.2	1.0

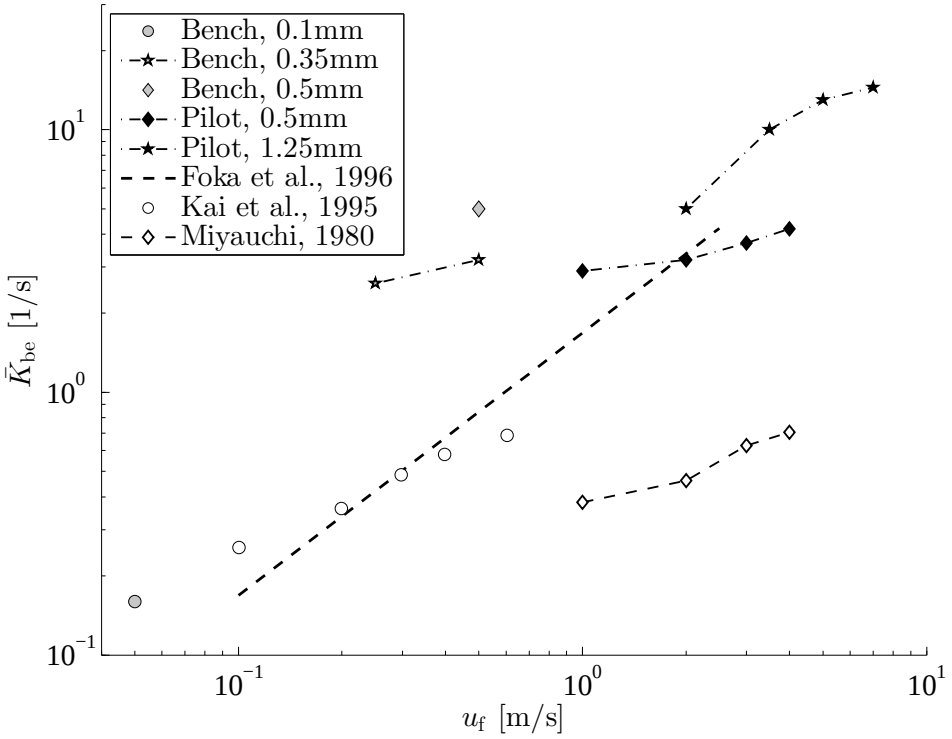

Figure 5.2: Volumetric interphase mass transfer coefficients against fluidization velocities.

parameters of pilot balances with Geldart B solids. The fluidization velocity response trend of $\bar{K}_{\mathrm{be}}$ is the same as in the case of the empirical data of Kai et al. (1995) and the CFD simulations of the pilot balances, although the quantity is one order of a magnitude lower. The correlation of Miyauchi et al. (1980) is based on experiments with particles having the diameter of 53 μm (Geldart A) in a reactor with the diameter of 0.08 m. Furthermore, the correlation of Zhang and Qian (1997) has been calculated with parameters of small particle diameter (0.5 mm) pilot balances. This has resulted in a two orders of magnitude lower $\bar{K}_{\mathrm{be}}$ (0.001-0.04 s^{-1}). The correlation of Zhang and Qian (1997) is based on experimental work with Geldart A solids (77 μm) in a fluidized bed reactor having a width of 0.2 m. Fig. 5.2 shows also that the smallest particle diameter of $0.1\mathrm{mm}$ (close to Geldart group A) bench reactor balance corresponds to the empirical turbulent bed data of Kai et al. (1995) for Geldart A solids. The interphase mass transfer coefficients for the other bench reactor balances with the larger particle diameters are at a relevantly higher level.

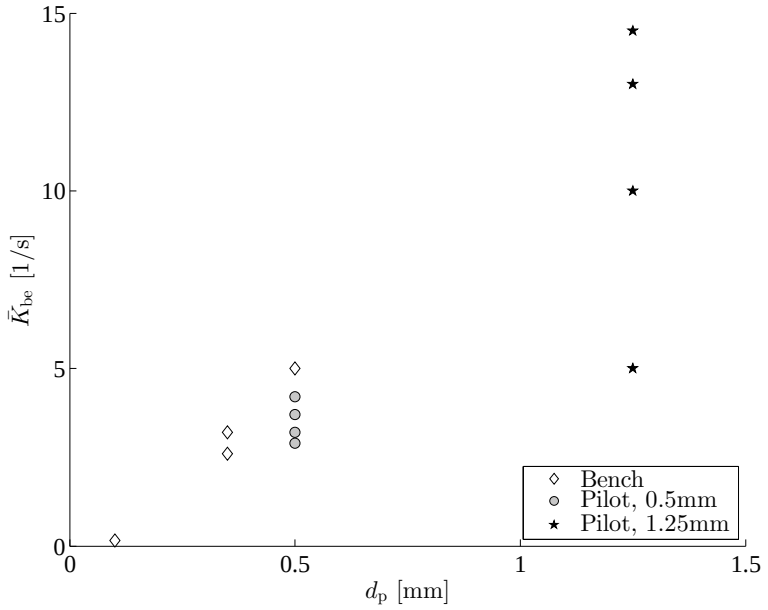

Figure 5.3: Volumetric interphase mass transfer coefficients against particle diameters.

Fig. 5.3 highlights the strong dependence of the average volumetric interphase mass transfer coefficients $\bar{K}_{\mathrm{be}}$ to the particle diameter. For Geldart D particle pilot balances, the interphase mass transfer coefficients are between 5 s^{-1} and 14.5 s^{-1}, while the range is between 2.9 s^{-1} and 4.2 s^{-1} for Geldart B particle pilot balances. A similar enhancement with the particle size is proposed by the bench reactor balances. The enhancement with particle size has been reported to occur in the bubbling bed regime due to enhanced convective throughflow (Sit and Grace, 1981), and seems to apply also in the turbulent

bed regime. It is theoretically reasonable that the interphase mass transfer coefficients increase with the particle size, because the minimum fluidization velocity, which is related to the rate of emulsion throughflow (Murray, 1965), rises exponentially with the particle size (see Tables 5.1 and 5.2).

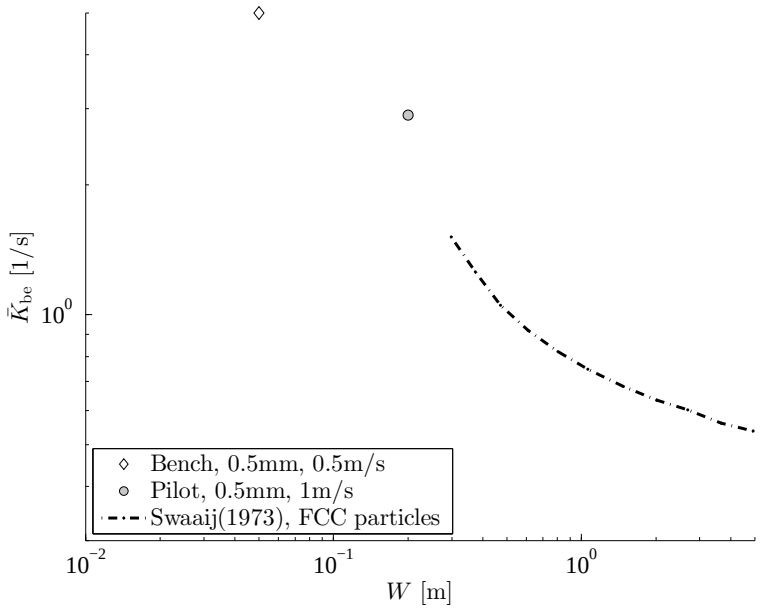

Figure 5.4: Volumetric interphase mass transfer coefficients against reactor width.

Fig. 5.3 shows that the particle size of 0.5 mm in the bench reactor results as a higher $\bar{K}_{\mathrm{be}}$ than the same particle size in the pilot reactor balances. Fig. 5.4 shows that the change from the bench-size to the pilot-size reactor drops the volumetric interphase mass transfer coefficient $\bar{K}_{\mathrm{be}}$ with a trend that corresponds well with the empirical data of van Swaaij and Zuiderweg (1973), when the fluidization velocity effects are considered.

5.3.3 Effect of bubble sizes

The effect of the reactor width to the average volumetric interphase mass transfer coefficient $\bar{K}_{\mathrm{be}}$ is linked to the growth restriction of bubble size due to reactor walls. The average diameter of bubbles $\bar{d}_{\mathrm{bub}}$ detected in the CFD simulations are given in Tables 5.1 and 5.2, and are plotted against the fluidization velocity in Fig. 5.5. In the pilot balances, the bubble diameter rises with fluidization velocity in the bubbling bed regime. Further increase of u_{f} results in as a slight drop of the average bubble size, which indicates also a transition to the turbulent regime. An exception is the u_{f} = 5 m/s pilot balance with Geldart D solids, where the high average bubble size indicates occasional axial slugs in the lower bed area.

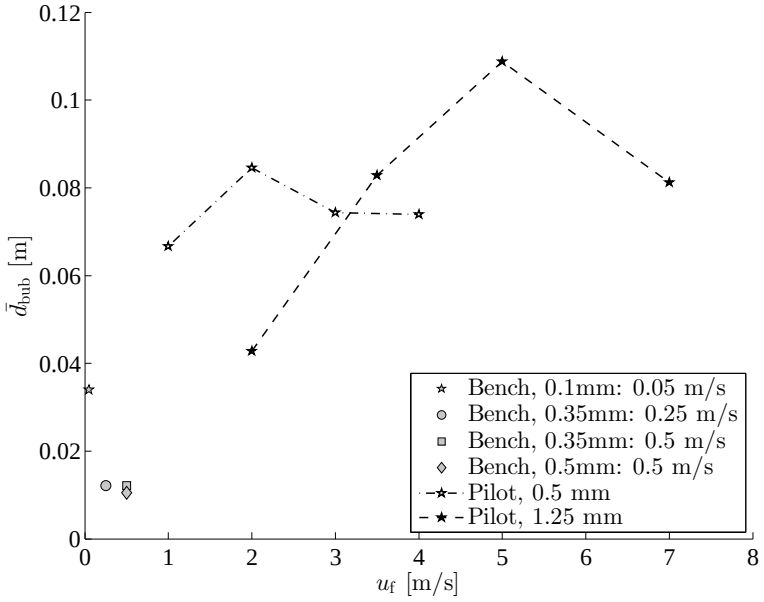

Figure 5.5: Average bubble diameters against fluidization velocities.

Fig. 5.5 underlines the huge difference of the average bubble sizes between the bench and pilot reactors. The average diameter of the bubbles is around 1 cm in the bench-size reactor simulations, while $\bar{d}_{\mathrm{bub}}$ is between 4.5 cm and 11 cm in the pilot balances. Consequently, the average bubble surface area a_{b} per volume may differ even one order of a magnitude between the bench and pilot reactors as shown in Fig. 5.6. In the pilot reactor balances, the average bubble surface area is from 20 m^{-1} to 40 m^{-1}, while it is over 100 m^{-1} in the bench reactor balances. However, the smallest particle diameter (0.1 mm) bench balance has the average bubble diameter of 3.4 cm and the average bubble surface area of 50 m^{-1}.

The two traditional ways of expressing an interphase mass transfer coefficient are linked by the bubble surface area by $\bar{K}_{\mathrm{be}} = a_{\mathrm{b}}\bar{k}_{\mathrm{be}}$. The average interphase mass transfer coefficients $\bar{k}_{\mathrm{be}}$ $(\mathrm{m/s})$ of the balances with the same particle diameters of 0.35 mm, 0.5 mm and 1.25 mm are plotted against the fluidization velocity in Fig. 5.7. The interphase mass transfer coefficients $\bar{k}_{\mathrm{be}}$ of Geldart B solids seem to be independent of the fluidization velocity, which is in accordance with the experimental results of Kai et al. (1995) for Geldart A solids.

Fig. 5.7 indicates that the particle size defines the level of $\bar{k}_{\mathrm{be}}$. The experiments of Kai et al. (1995) with the particle diameter of 0.055 mm, resulted interphase mass transfer coefficients of about 0.013 m/s. The bench-size reactor simulations with the particle diameter of 0.35 mm gave interphase mass transfer coefficients between 0.02 m/s and 0.03 m/s. Furthermore, the pilot reactor simulations with the 0.5 mm particle size resulted

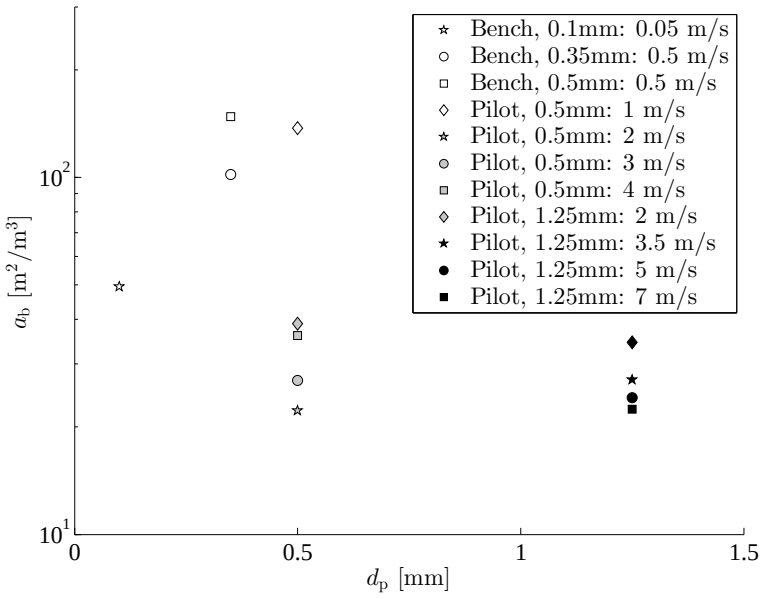

Figure 5.6: Average bubble surface areas per volume of reactor against particle diameters.

in the $\bar{k}_{\mathrm{be}}$ of slightly over 0.1 m/s. In the case of pilot simulations with Geldart D solids (1.25 mm), the interphase mass transfer coefficient ranged from 0.2-0.7 m/s and was also a function of the fluidization velocity.

Fig. 5.7 shows that the bubbling bed interphase mass transfer correlation of Sit and Grace (1981) based on experiments with the particle size of 0.39 mm corresponds with the bench reactor simulations with the diameter of 0.35 mm particles. This suggests that the interphase mass transfer coefficients derived from the CFD simulations are in the correct range. However, the interphase mass transfer correlation of Sit and Grace (1981) seems to underestimate the $\bar{k}_{\mathrm{be}}$ for the larger particle pilot balances with the particle diameters of 0.5 mm and 1.25 mm. Another bubbling bed correlation by Kunii and Levenspiel (1991) proposes a higher level of k_{be} for bench reactor balances, and a relevantly lower level for the pilot reactor (0.5 mm) balances. The correlation of Kunii and Levenspiel (1991) is primarily defined for bubbling beds with Geldart A solids. As the bubbling bed interphase mass transfer correlations predicts the mass transfer per volume of a single bubble, the values shown in Fig. 5.7 were multiplied by the volume fraction of the bubble phase. Also, the correlation of Kunii and Levenspiel (1991) was formulated to a two-dimensional form by multiplying it by the ratio of the surface areas of a cylinder to a sphere. The correlations were calculated with the properties used in the CFD simulations and the bubble properties obtained for each balance (Tables 5.1 and 5.2). The bubble rise velocity in the correlations was estimated according to Davidson and Harrison (1963) with $u_{\mathrm{bub}} = 0.711(gd_{\mathrm{bub}})^{1/2} + (u_{\mathrm{f}} - u_{\mathrm{mf}})$.

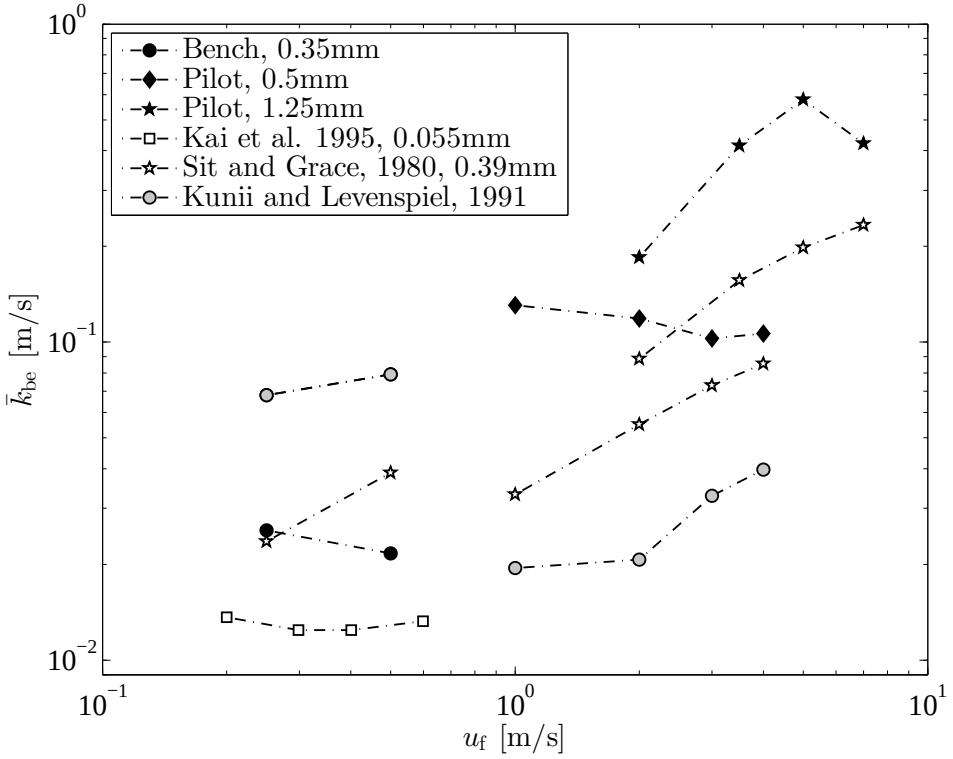

Figure 5.7: Interphase mass transfer coefficients against fluidization velocity (Vepsäläinen et al., 2014).

5.3.4 Relationship with the Reynolds number

Finally, all the obtained volumetric interphase mass transfer coefficients in the lower bed show an exponential dependence to the Reynolds number as shown in Fig. 5.8. The pilot reactor balances with the same order of magnitude average bubble diameters result close to the linear exponential response of the average volumetric interphase mass transfer coefficient $\bar{K}_{\mathrm{be}}$ to the Reynolds number. Similarly, this behavior can be seen in the bench reactor balances, particularly with three balances having similar average bubble sizes. Transition from the bubbling bed to the turbulent regime seems not to have any effect on the trend of the exponential Reynolds response.

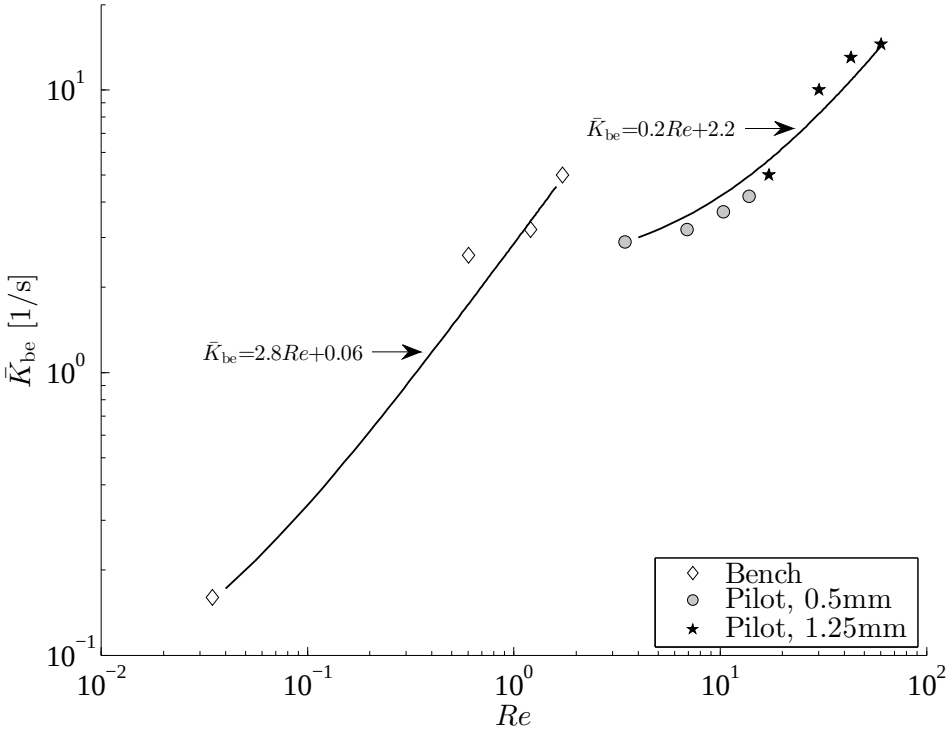

Figure 5.8: Interphase mass transfer coefficients against Reynolds numbers.

6 Bed Sherwood number in fluidized bed chemical looping combustion

This chapter presents the bed Sherwood numbers derived by Eulerian CFD modeling of a pilot fluidized bed fuel reactor in a chemical looping combustion process. First, the principle and the development status of fluidized bed chemical looping combustion technology are introduced briefly with respect to the motivation of this research, heterogeneous mass transfer in fluidized beds. After this, the applied principle of modeling, sub-models, mesh, boundary conditions and properties in CFD modeling are described. As a validative measure, the obtained chemical conversion profiles are compared to the results of reference test balances. Finally, the bed Sherwood numbers derived for the fluidized bed chemical looping combustion process are discussed with respect to the relevant empirical and CFD-based fine-particle data reported in the literature.

6.1 Chemical looping combustion process and research objective

One of the most promising new concepts developed for $\mathrm{CO_2}$ capture for fossil fuel energy conversion is chemical looping combustion (CLC). The process of CLC is a novel and an emerging technology, as in early the 2000s it was not yet technically proven. Even though the chemical looping combustion process can be formed by a number of different concepts, such as alternating fixed beds or rotating reactors, most of the proven pilot CLC plants are based on two interconnected fluidized bed reactors (Adanez et al., 2012).
Chemical looping combustion is based on the transfer of oxygen from air to contact with fuel by means of a metal oxygen carrier without direct contact of air and fuel. Thus, a concentrated $\mathrm{CO_2}$ and $\mathrm{H_2O}$ stream suitable for efficient $\mathrm{CO_2}$ capture is formed. Fluidized bed CLC processes have been developed for both gaseous and solid fossil fuels. In the research of this thesis, only a fuel reactor with gaseous fuel is considered. In practice, the process involves two reactors: a fuel reactor and an air reactor. In the fuel reactor, the gaseous fuel is used to fluidize metal oxygen carriers that oxidize the gaseous fuel to $\mathrm{CO_2}$ and $\mathrm{H_2O}$. The metallic oxygen carrier is circulated to the air reactor, where the oxygen carriers are fluidized by air and oxidized again.
A comprehensive review on the development of the chemical looping combustion technology and metallic oxygen carrier materials has been presented by Adanez et al. (2012). Feasible operation of chemical looping combustion with gaseous fuels has been proven at pilot plant scale. Pröll et al. (2009) reported on stable operation of a 120 $\mathrm{kW_{th}}$ CLC pilot plant based on fluidized bed technology with high conversion rates for gaseous fuel (methane) and a nickel-based oxygen carrier (Fig. 6.1). In the technology development, the next demonstration scale is 1-3 $\mathrm{MW_{th}}$ (Adanez et al., 2012), while large utility concepts have been already pre-designed.
A fluidized bed reactor provides an efficient gas-solid contact required by the chemical looping combustion process. This is beneficial particularly for the operation of a fuel reactor, where slower chemical kinetic coefficients related to the reduction reaction of the oxygen carrier are present (Adanez et al., 2012). In order to analyze the conversion behavior of smaller pilot size chemical looping combustion processes accurately and design

larger demonstration, or industrial size CLC reactors properly, also the reactor size and fluid dynamics dependent rate of gas-solid mass transfer should be known. However, actual heterogeneous mass transfer coefficients for the fluidized bed CLC process are not available in the literature. The objective of the research presented in this chapter is to derive the bed Sherwood numbers by Eulerian CFD modeling for a fluidized bed fuel reactor in a pilot CLC process.

6.2 Eulerian CFD modeling

The Eulerian two-fluid kinetic theory of granular flow was applied in the CFD simulations (Ansys Fluent 14) of a CLC fuel reactor. The approach was the same as the one applied for the CFD modeling of fluidized bed char combustion presented in Chapter 3. The conservation equations and the closure models are the same as the ones described in Chapter 3. However, the fluidization balances, reactor domain and mesh, boundary conditions and properties, as well as heterogeneous chemistry differ from the modeling presented above.

6.2.1 Balances, reactor and calculation mesh

Two chemical looping combustion test balances reported in Pröll et al. (2009) have been chosen as reference balances for the CFD simulations. The modeled 120 $\mathrm{kW_{th}}$ chemical looping combustion prototype is a dual circulating fluidized bed system. Solid flow dynamics and combustion of methane in the fuel reactor are simulated. Fig. 6.1 shows the principle of methane conversion in the dual fluidized bed chemical looping system. One low (60 kW) and one high load (120 kW) balance are studied. The high load balance has been modeled with the fluidization velocity of 0.3 m/s. In the low load balance, the applied fluidization velocity is 0.17 m/s. The fluidization velocities have been defined based on the thermal power of the balance and the lower heat value of methane (48.8 $\mathrm{MW/kg}$). The solid loadings at the fuel reactor in the high and low load balances of experiments were 22 kg and 19 kg, respectively, as reported by Pröll et al. (2009).

The two-dimensional approach has been selected in order to reach appropriate solution times as discussed in the connection of similar two-dimensional CFD simulations by Cloete et al. (2012) for the same fuel reactor balances. The fuel reactor has been dimensioned to the width of 0.159 m and height of 3 m. For the reactor domain, a grid of 80 calculation cells in width and 800 cells in height has been designed. The mesh size is 1.99 $\times$ 3.75 $\mathrm{mm^2}$, which corresponds to 14 and 28 times the particle diameter. The design of the fuel reactor and the used calculation cells are shown in Fig. 6.2. The chosen mesh size should be fine enough to capture the meso-scale structures of gas-solid flow dynamics, which define the average heterogeneous mass transfer characteristics in the system, in a practical accuracy. Justification for this judgment is given in Cloete et al. (2012), who have studied the effect of grid sizes on the total methane conversion in similar Eulerian CFD simulations of fuel reactor balances.

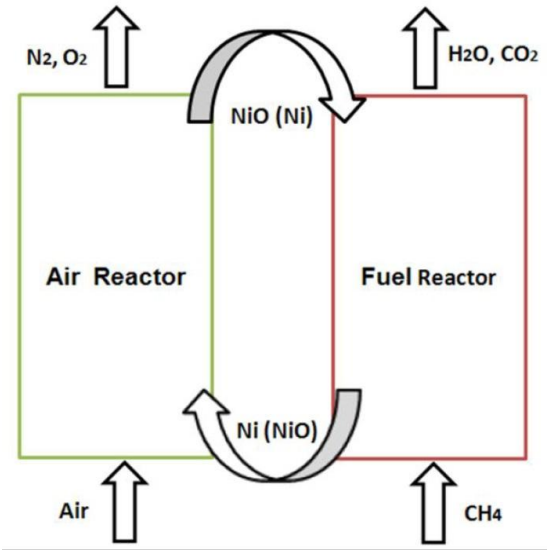

Figure 6.1: The principle of methane combustion in a dual fluidized bed CLC system.

6.2.2 Boundary conditions and properties

The fuel reactor was simulated as a two-dimensional vertical pipe, where the lower opening was defined as a constant velocity inlet for the gaseous methane fuel. In the walls, a no-slip boundary condition was applied for both the gas and solid phases. The upper opening was defined as a pressure outlet. The solids escaped from the top exit were re-circulated back to the reactor during the next time step via a re-circulation inlet. No remarkable solid circulation through the top exit was observed in the simulations. However, this was not a main concern, as the main objective of the simulations was to study the effect of fluctuating solid flow dynamics in the lower dense bed on average gas-solid mass transfer.

Isothermal flow at the constant reactor temperature of 850 °C, which corresponds well with experimental conditions (Pröll et al., 2009), was assumed in the simulations. The constant diffusivity of methane $D_{\mathrm{CH_4}}$ was 1.2×10^{-4} m/s, and the average gas density of $3.6\,\mathrm{kg/m^3}$ and viscosity of $42 \times 10^{-6}\,\mathrm{kg/sm}$ were applied. The mean particle diameter of 0.135 mm and solid density of 3200 $\mathrm{kg/m^3}$ were used for the nickel-oxide oxygen carrier particles. The solids belong to the Geldart group B. The Geldart classification presented in Table 3.2 enlightens that the solids are finer particles of the Geldart group B, like all typical oxygen carriers used in the CLC systems (Abad et al., 2007).

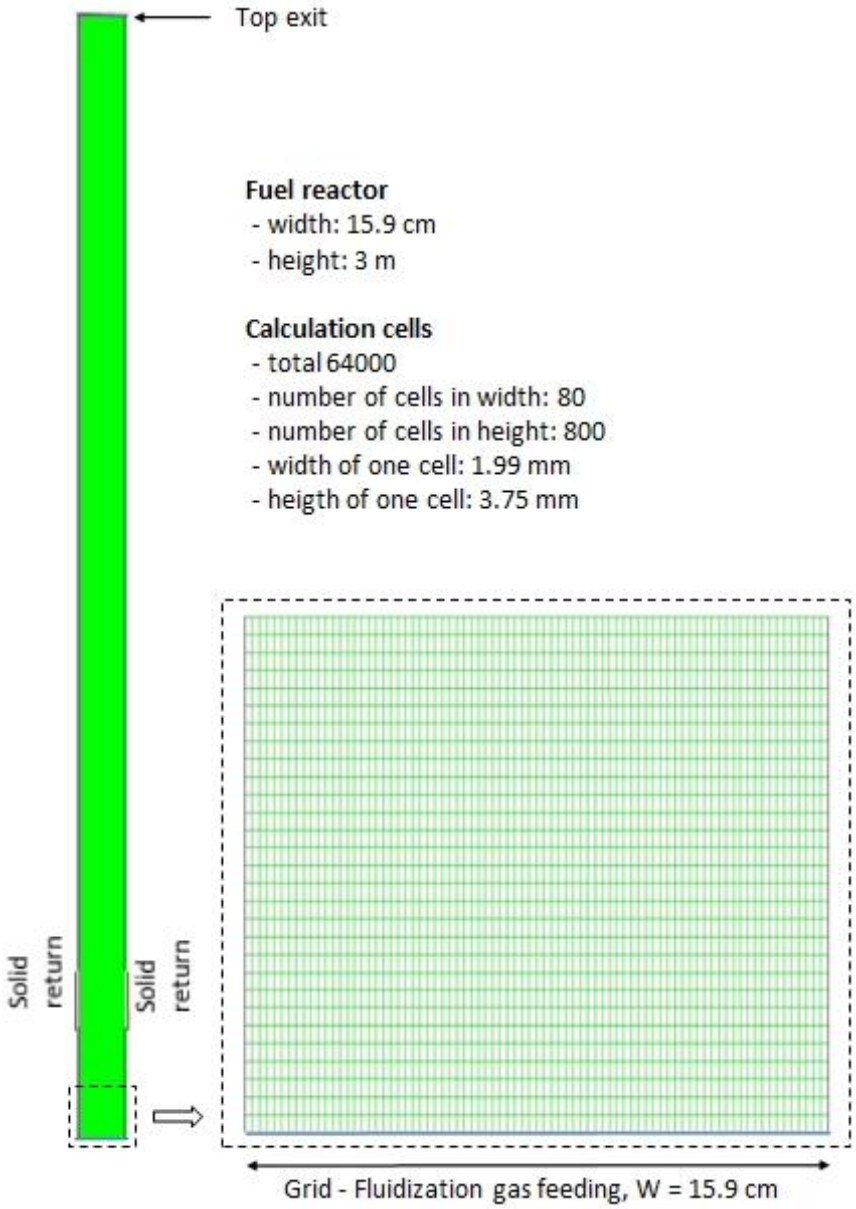

Figure 6.2: Design of the CLC fuel reactor and calculation cells.

6.2.3 Heterogeneous reaction model

The applied heterogeneous reaction model for methane oxidation in the fuel reactor is similar to the char combustion model presented in Chapter 3. The primary reaction, methane combustion, is considered as

$$\mathrm{CH_4(g) + 4NiO(s) \Rightarrow CO_2(g) + 2H_2O(g) + 4Ni(s).} \tag{6.1}$$

The chemical kinetic rate is defined with a first-order rate function as follows

$$R_{\mathrm{CH_4}} = a_{\mathrm{NiO}} k_{\mathrm{eff}} C_{\mathrm{CH_4}}, \tag{6.2}$$

where the specific surface area of the nickel-oxide oxygen carrier is solved from

$$a_{\mathrm{NiO}} = \frac{6\alpha_{\mathrm{s}} y_{\mathrm{NiO}} s_{\mathrm{NiO}}}{d_{\mathrm{p}}}, \tag{6.3}$$

where the volume fraction of the oxygen carrier y_{NiO} is obtained from the CFD solution and the fraction of active NiO in the oxygen carrier s_{NiO} is 0.4 (Pröll et al., 2009). The effective reaction rate coefficient is defined from

$$k_{\mathrm{eff}} = \frac{1}{1/k_{\mathrm{NiO,sur}} + 1/h_{\mathrm{m}}}, \tag{6.4}$$

where $\mathrm{k_{NiO,sur}}$ is the chemical kinetic coefficient of nickel-oxide with methane gas given as per surface area of an oxygen carrier particle. The chemical kinetic coefficients used in the simulations were between 0.3×10^{-3} m/s and 1×10^{-3} m/s. The chemical kinetic coefficients reported in the literature vary with the oxidation degree $X_{\mathrm{O_2}}$. Furthermore, different experimental methods used in the definition of the chemical kinetic coefficient typically results in remarkably different kinetic coefficients as discussed in Chapter 6.3.1 below. The first simulation was performed with the chemical kinetic coefficient 0.3×10^{-3} m/s calculated from the thermogravimetric analysis (TGA) measurements presented by Abad et al. (2007). The local convection mass transfer coefficient $\mathrm{h_m}$ is calculated with the emulsion Sherwood number correlation of La Nauze et al. (1984) given by

$$Sh_e = 2\alpha_{\mathrm{g}} + 0.69(Re/\alpha_{\mathrm{g}})^{1/2} Sc^{1/3}, \tag{6.5}$$

where the local voidage and particle Reynolds number are applied.

6.2.4 Solution and simulation procedure

The applied time step in the simulations was 0.001 s, which has been shown to be proper for fine grid gas-solid simulations as discussed in Chapter 3. In a solution, the first order

implicit method was used for time discretization and the first order upwind method for space discretization. Forty iterations per each time step were used in the solution procedure, and the convergence criteria for continuity and velocity residuals were checked in preliminary calculations to stabilize them with this solution strategy. All simulated balances were started with five-second initialization period, which was simulated by starting from an initial constant solid volume fraction in a reactor, in order to achieve a stabilized state of hydrodynamics, reaction rate and axial gas volume fractions. Simulation of the initial five seconds was enough to result in the same time-average axial solid volume fractions and methane concentrations as the following analysis period. The analysis period consisted of ten seconds of simulation. Averaging of the data used for deriving the bed Sherwood numbers was executed during the 10 s analysis period.

6.2.5 Derivation of the bed Sherwood number

The bed Sherwood numbers for the chemical looping combustion process were calculated with the same principle as defined for the fluidized bed char combustion in Chapter 4. In the derivation, time and cross-section averaged values were used, because the bed Sherwood number represents the average gas-bed mass transfer coefficient. First, the axial volumetric reaction rate in the fuel reactor was defined based on the time-averaged oxygen carrier surface area, oxygen concentration, chemical kinetic coefficient and gas-solid mass transfer coefficient as follows

$$\langle R_{\mathrm{CH_4}} \rangle_{10\mathrm{s}} = \frac{\langle a_{\mathrm{NiO}} \rangle_{10\mathrm{s}} \langle C_{\mathrm{O_2}} \rangle_{10\mathrm{s}}}{1/k_{\mathrm{NiO,sur}} + 1/\langle h_{\mathrm{m}} \rangle}. \tag{6.6}$$

From Equation 6.6, the average gas-solid mass transfer coefficient $\bar{h}_m$ in the lower, dense bed region of interest was solved according to Eq. 4.3 from the cross-sectional average value of $\langle h_{\mathrm{m}} \rangle$. Then, the bed Sherwood number in the dense bed conditions was defined according to its dimensionless definition as follows

$$Sh_{\mathrm{bed}} = \bar{Sh}_{\mathrm{bed}} = \frac{\bar{h}_{\mathrm{m}} d_{\mathrm{p}}}{D_{\mathrm{O_2}}}. \tag{6.7}$$

Here, the dense bed is defined as the lower bed region, where the average solid volume fraction $\langle \alpha_{\mathrm{s}} \rangle_{20\mathrm{s}} > 0.15$, as discussed in Chapter 4.1.2.

6.3 Analysis of fuel reactor performance

6.3.1 Fluidization, conversion and chemical kinetic characteristics

The axial solid volume fraction profiles of the simulations are shown in Fig. 6.3 and Fig. 6.4 presents the instantaneous solid volume fractions of the two fluidization states. The low load (60 kW, 0.17 m/s) balance seems to be in the high velocity bubbling bed regime and the high load balance (60 kW, 0.3 m/s) in the turbulent fluidization regime.

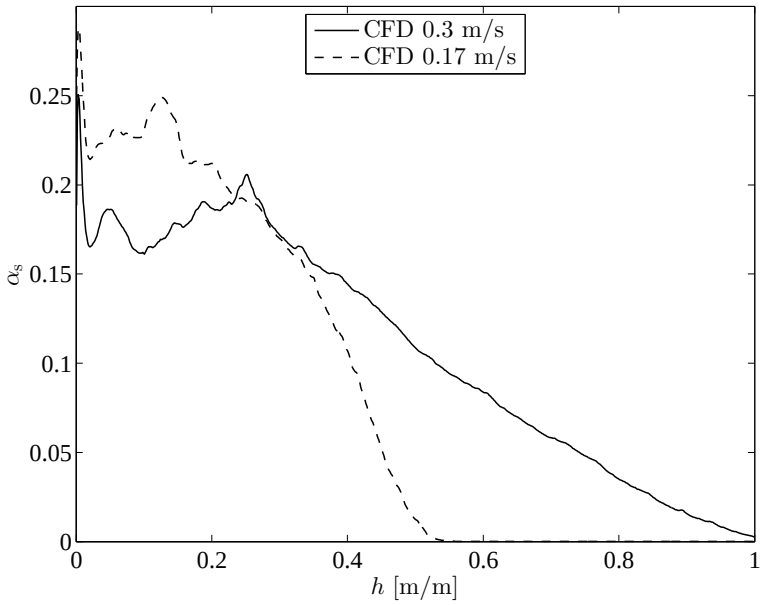

Figure 6.3: Time-averaged axial solid volume fractions at the bubbling bed and turbulent regime balances.

The high load, 0.3 m/s fluidization velocity, balance was simulated with three different chemical kinetic reaction rate coefficients. Fig. 6.5 presents the resulting axial methane volume fractions. First, the chemical kinetic coefficient $k_{\mathrm{NiO,sur}}$ of 0.3×10^{-3} m/s was applied. However, the measured total methane conversion (Pröll et al., 2009) in the balance was relevantly higher as shown in Fig. 6.6. Thus, as the exact value of chemical kinetic coefficient of the nickel-oxygen carrier was not known, the high load balance was simulated with faster chemical kinetic coefficients. The chemical kinetic coefficient $k_{\mathrm{NiO,sur}}$ of 1×10^{-3} m/s resulted exactly in the same total methane conversion $X_{\mathrm{CH_4}}$ of 0.97 as measured (Fig. 6.6). The methane conversion is defined as

$$X_{\mathrm{CH_4}} = 1 - \frac{\dot{n}_{\mathrm{CH_4,out}}}{\dot{n}_{\mathrm{CH_4,in}}}. \tag{6.8}$$

After the high load simulation, the low load balance (60 kW) was simulated with the fluidization velocity of 0.17 m/s and the chemical kinetic coefficient $k_{\mathrm{NiO,sur}}$ of 0.001 m/s. Fig. 6.5 shows that the obtained total methane conversion is higher than measured for this balance. Similar conversion behaviour was shown by Eulerian CFD modeling of the same balances reported in Cloete et al. (2012). Consequently, the low load balance was simulated also with the lower chemical kinetic coefficient $k_{\mathrm{NiO,sur}}$ of 0.0006 m/s, which resulted in a better fit of the total methane conversion compared to the experimental work as shown in Fig. 6.6.

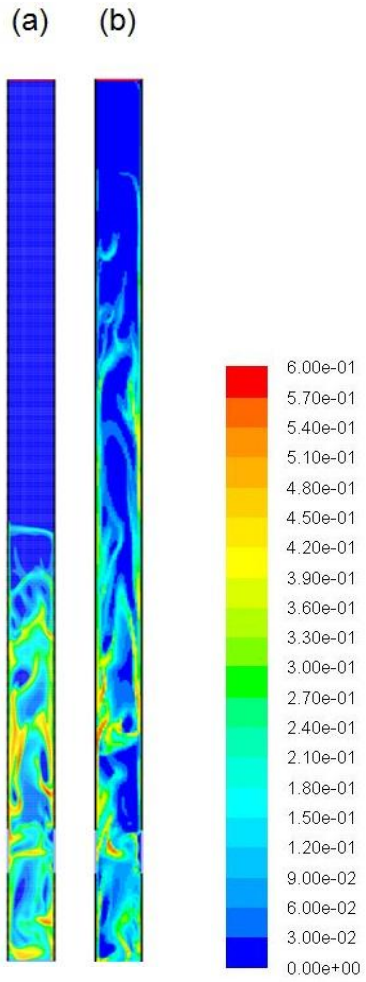

Figure 6.4: Instantaneous solid volume fractions: (a) low load and (b) high load balance.

The lower total methane conversion measured at the low load balance can be explained by the different chemical reaction rate coefficients between the balances due to the different oxidation degree of the NiO particles. Pröll et al. (2009) report that in their experiments the oxidation degree X_{O_2} of the NiO particles was 0.75-0.85 for the low load balance and 0.5-0.6 for the high load balance. Mattisson et al. (2011) have shown that the reaction rate constant of a nickel-based oxygen carrier changes with the oxidation degree X_{O_2} as shown in Fig. 6.7. The behavior of the effective chemical kinetic coefficient originates from the

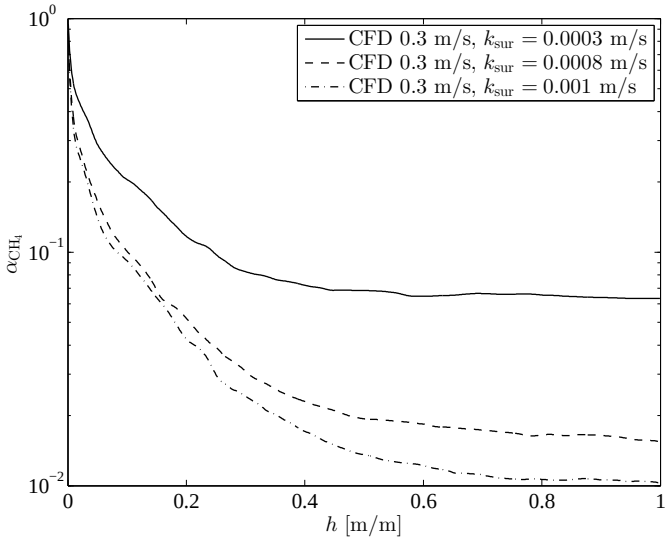

Figure 6.5: Time-averaged axial methane volume fractions at the turbulent regime balance with varied chemical kinetic coefficients.

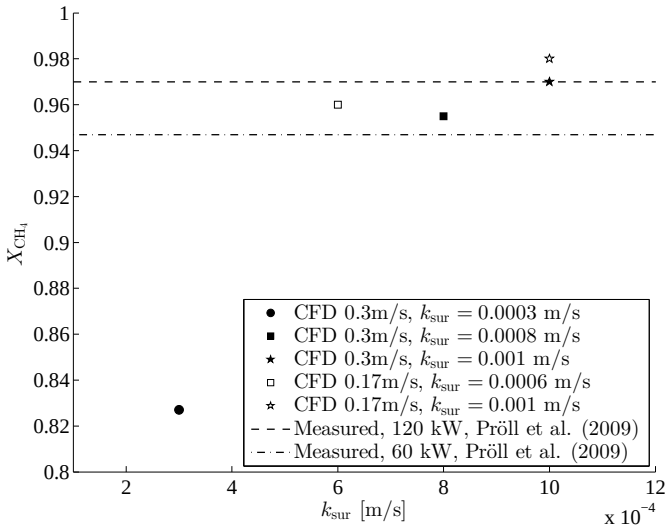

Figure 6.6: Total methane conversions against chemical kinetic coefficients of a NiO oxygen carrier.

variation of grain sizes in NiO particles with the oxidation degree. The kinetic data for NiO particles presented by Mattisson et al. (2011) are based on bench scale fluidized bed (inner diameter 22 mm) experiments, where the mass based kinetic coefficients $k_{\mathrm{NiO,m}}$ varied with the oxidation degree in a range of 0.6-1.7 $\mathrm{mol/(kgbars)}$ at 850 °C.
The tests were carried out close to the minimum fluidization velocity, and deriving the kinetic coefficients the plug flow of gas without heterogeneous mass transfer resistance was assumed. Mattisson et al. (2011) have also presented the effect of temperature in fluidized bed conditions and recalculated TGA reactivity test results of the same particles (Abad et al., 2007). The thermogravimetric analysis reactivity test results showed variance of the kinetic coefficient $k_{\mathrm{NiO,m}}$ from 0.11 to 0.2 $\mathrm{mol/(kgbars)}$. The chemical kinetic coefficient per surface area of spherical NiO particle $k_{\mathrm{NiO,sur}}$ of 0.001 m/s corresponds to $k_{\mathrm{NiO,m}}$ of 0.33 $\mathrm{mol/(kgbars)}$ and $k_{\mathrm{NiO,sur}}$ of 0.0006 m/s to $k_{\mathrm{NiO,m}}$ of 0.2 $\mathrm{mol/(kgbars)}$. As shown in Fig. 6.7, the kinetic coefficients obtained by the Eulerian CFD modeling of the pilot fuel reactor are on the same level than the thermogravimetric analysis reactivity test results presented by Abad et al. (2007). However, the TGA data does not show similar dependence on the oxidation degree as the fluidized bed test data of Mattisson et al. (2011), while the CFD simulations of this research and the experiments of Pröll et al. (2009) indicate that the change of kinetic coefficients would follow the fluidized bed test results presented by Mattisson et al. (2011). Further insights into the Eulerian CFD simulation of pilot CLC fuel reactor balances can be found in Cloete et al. (2012), who discuss the possible issues related to the obtained chemical conversion profiles, particularly the dimensional effects (2D versus 3D) and the boundary condition definition of the fluidization gas inlet in the bubbling bed regime. However, the main objective of this study is to assess gas-bed mass transfer in the lower bed, and a minor change in the simulation results of chemical conversion does not have remarkable influence on the bed Sherwood numbers as shown in Chapter 7. The discussion above gives background information for the fluid dynamic and chemical conversion characteristics in the CLC fuel reactor balances used in the heterogeneous mass transfer research.

6.3.2 Bed Sherwood numbers

The primary objective of the Eulerian two-phase CFD modeling was to derive the average gas-solid mass transfer coefficients for the pilot scale CLC processes, while the chemical kinetic coefficient discussed above provided additional confidence for the accuracy of the CFD modeling approach. Fig. 6.8 shows the obtained bed Sherwood numbers Sh_{bed} against the Reynolds number. An exponentially increasing trend of Sh_{bed} with the Reynolds number is shown in the simulations with the chemical kinetic coefficients $k_{\mathrm{NiO,sur}}$ of 0.001 m/s. The trend seems to continue to the higher Reynolds number range operation, as suggested by the two-dimensional Eulerian CFD simulations presented by Chalermsinsuwan and Piumsomboon (2011) for the bubbling bed fluid-catalytic cracking (FCC) process with similar chemical kinetic coefficients ($k_{\mathrm{NiO,sur}}$ = 0.0005-0.0025 m/s) and particle size (d_{p}= 0.075 mm).
The total reaction rate in the fuel reactor is under heterogeneous mass transfer control, even though the single particle Sherwood number calculated based on the fluidization ve-

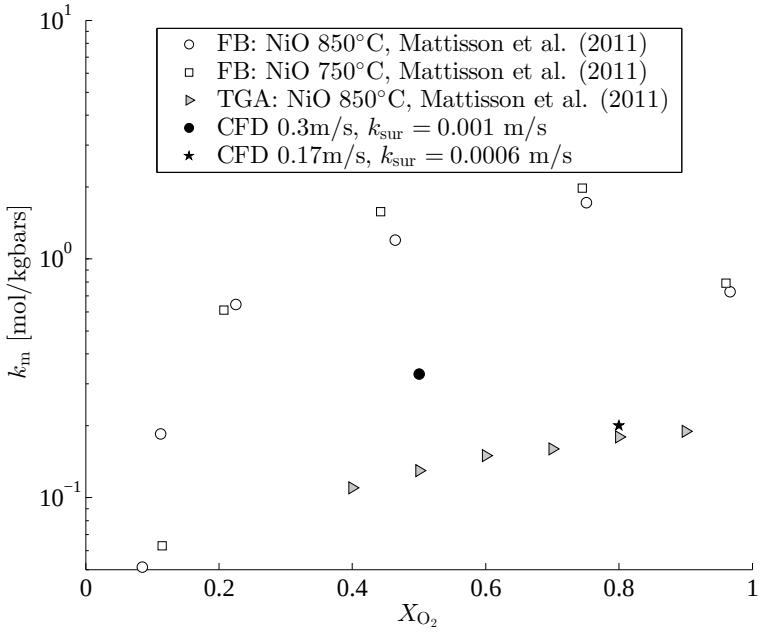

Figure 6.7: Mass-based chemical kinetic coefficients of the NiO oxygen carrier against the degree of oxidation. (CFD data adapted from Vepsäläinen et al. (2013b))

locity is as high as 1.4, which corresponds to the gas-particle mass transfer coefficient of 1.3 m/s. The derived bed Sherwood numbers of 0.0006 and 0.001 correspond to the average gas-solid mass transfer coefficients of 0.00005 m/s and 0.00009 m/s, respectively. The average gas-solid mass transfer coefficients are more than one order of magnitude lower than the kinetic coefficients in the fuel reactor of CLC. Consequently, even a remarkable rise in chemical kinetic coefficients of oxygen carriers would not increase the overall reaction rate, if the heterogeneous mass transfer is not enhanced. Figs. 6.9 a and b highlight the high consumption of methane in the regions of solid-rich emulsion (regions marked with (1) in the figures) and the strong channeling of methane-rich gas flow into the solid lean voids (regions marked with (2) in the figures). Actually, Figs. 6.9 a and b shows clearly that the fine-particle CLC fuel reactor operates under interphase mass transfer control. Recognizing the interphase mass transfer control in fine-particle fluidized beds has practical benefits, as the objective in design development is to reach as high a gaseous fuel conversion in the fuel reactor as possible. However, it is important to note, that the particle size has two opposite effects on the overall conversion. The decrease of particle size slows the rate of interphase mass transfer, while at the same time it enhances the rate of heterogeneous reactions by rising the reactive solid surface area in the fluidized bed.

Fig. 6.8 shows also the effect of small changes in the chemical kinetic coefficient on the bed Sherwood number. Both the CLC and FCC process CFD simulations indicate that

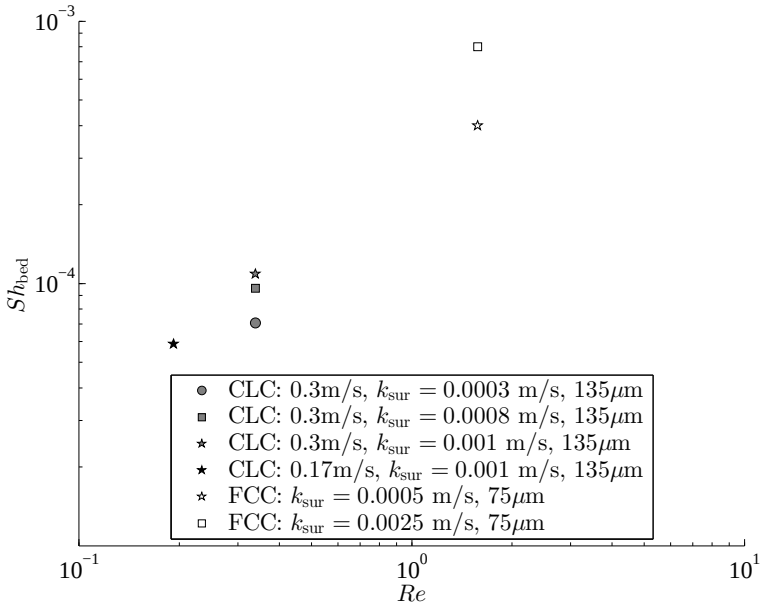

Figure 6.8: Bed Sherwood numbers in chemical looping combustion (CLC) and fluid-catalytic cracking (FCC) processes derived by Eulerian CFD modeling: CLC data adapted from Vepsäläinen et al. (2013a) and FCC data from Chalermsinsuwan and Piumsomboon (2011).

the Sh_{bed} rises slightly with the chemical kinetic coefficient for small particle fluidized bed systems. The same behavior can be seen in the bed Sherwood numbers derived by Chalermsinsuwana et al. (2009) in two-dimensional Eulerian CFD simulations of fast fluidized bed ozone decomposition with similar FCC particles (d_{p}= 0.076 mm) as shown in Fig. 6.10. The reactor width, in these simulations, was 0.2 m and the height 14 m. Even more importantly, the results again indicate that the bed Sherwood number trend presented in Fig. 6.8 continues for the same particle size and kinetics systems to higher Reynolds numbers, and particularly to different fluidization regimes.

Chalermsinsuwan and Piumsomboon (2011) have modeled the bubbling bed ozone decomposition process with FCC particles also with the three-dimensional approach. The width of the simulated bubbling bed was 0.3 m and the depth 0.05 m. The bed Sherwood numbers in Fig. 6.10 represent averaged values in the width and depth direction. The bed Sherwood numbers averaged with the width of the reactor (0.3 m) correspond to the Reynolds number response of same size range reactors (Vepsäläinen et al., 2013a; Chalermsinsuwan and Piumsomboon, 2011). However, the bed Sherwood numbers averaged with the depth of the reactor (0.05 m) indicate enhanced averaged heterogeneous mass transfer for narrower reactors. The reason is most likely a restricted bubble size in the narrow reactors, which results as a higher bubble-emulsion surface area and conse-

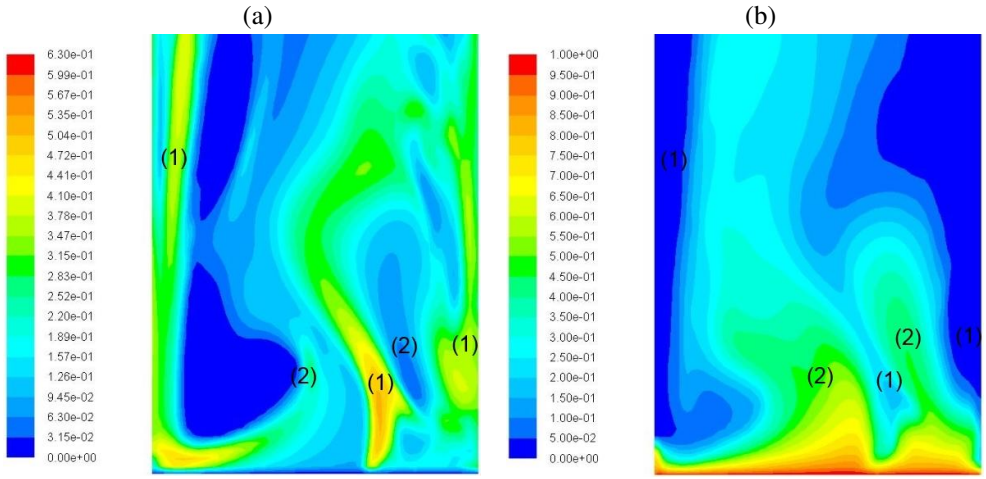

Figure 6.9: Instantaneous (a) volume fraction of oxygen carrier in bed and (b) volume fraction of methane in gas in the bottom bed during the high load balance.

quently a higher interphase mass transfer as discussed in Chapter 5. Fig. 6.10 presents also the experimental bed Sherwood numbers of Kashyap and Gidaspow (2010) for a shallow pilot-scale ozone decomposition reactor (W= 0.3 m, D= 0.05 m, H=1.4 m). The size of the used FCC particles (d_{p}= 0.076 mm) was the same as in the simulations discussed above. The experimental bed Sherwood numbers in the lower dense bed are somewhat lower than in the simulated bubbling bed (Chalermsinsuwan and Piumsomboon, 2011). The level of the bed Sherwood number for the clustering regime, above the dense bubbling bed, is the same as in the lower bed of the simulations. Here, it is worth pointing out that the exact chemical kinetic coefficient in their experiments was unknown.

As a conclusion, the results presented above indicate that the exponential trend of the bed Sherwood number with the Reynolds number for fine particle fluidized bed systems is the same as shown by the experiments and the CFD simulations with the larger particles discussed in Chapter 4 (Fig. 4.1). However, the level of Sh_{bed} is several magnitudes of order lower in chemical looping combustion and fluid-catalytic cracking processes than in e.g. the combustion process (Vepsäläinen et al., 2013b). The explanation is related to (i) lower particle size dependent interphase mass transfer (Chapter 5), (ii) faster reaction rates due to the large reactive surface area in the fine particle systems and the relatively high chemical kinetic coefficients, and (iii) the fraction of active solids in the system, as discussed in Chapter 7 below.

The derived bed Sherwood numbers can be used in various one-, two- and three-dimensional fine particle fluidized bed models in research and engineering tasks related to process scale-up and process analysis. A practical example of such a suitable practical implication has been reported by Peltola et al. (2013). In their research work, a reactivity coefficient correction of a nickel-oxide oxygen carrier obtained by a validation procedure of one-dimensional dynamical fluidized bed model regarding the same pilot chemical looping

balances (Pröll et al., 2009) as modeled in this study shows a similar fluidization velocity response to the Sh_{bed} as presented in Fig. 6.8.

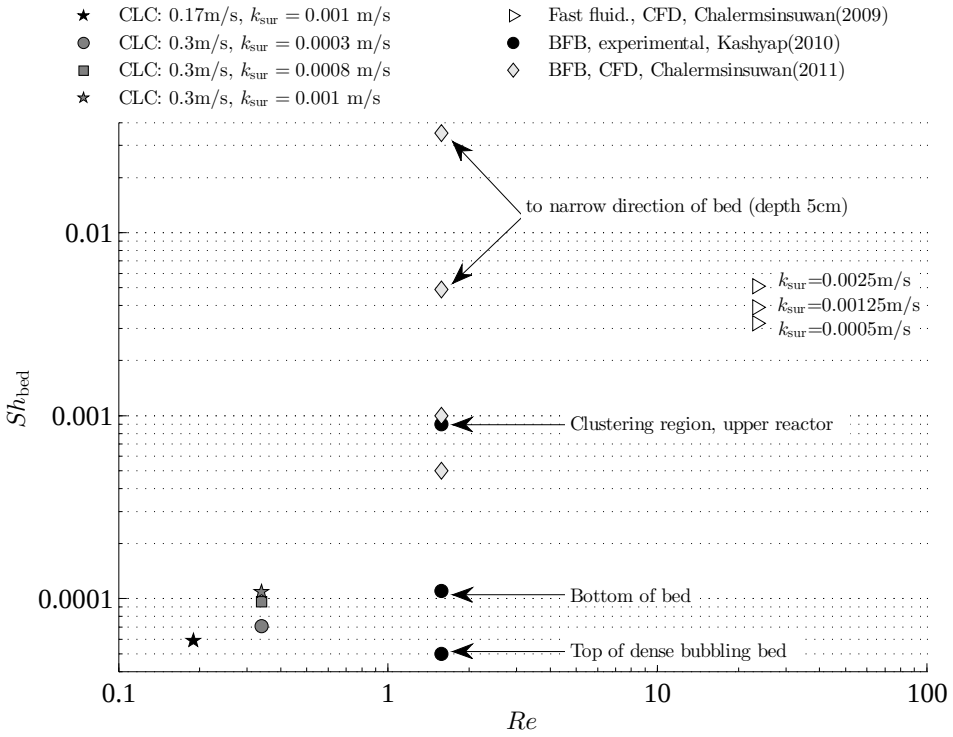

Figure 6.10: Bed Sherwood numbers in chemical looping combustion (CLC) and fluid-catalytic cracking processes (CLC data adapted from Vepsäläinen et al. (2013a)).

7 Specifications to the bed Sherwood number theory

This chapter summarizes the research results of the thesis regarding the theory of the bed Sherwood number, and states new phenomenon-based specifications for the previously presented theoretical framework. In general, the findings on bed Sherwood numbers in this thesis follow the traditional theory presented by Kunii and Levenspiel (1968). This theory is based on even earlier experimental work. The two baselines in the Sh - Re chart are set by the Sherwood number correlations of a gas flow over a single sphere (Frössling, 1938) and through a fixed bed (Ranz and Marshall, 1952). Experiments with high Reynolds numbers (>100) and large particle sizes (>1 mm) for the bubbling, slugging and turbulent fluidized beds (Chu et al., 1953; Thodos and Ricetti, 1961) have shown bed Sherwood numbers between single sphere and fixed bed ones. On the other hand, experimental works (Resnick and White, 1949; Kettering et al., 1950; Richardson and Szekely, 1961) in the bubbling bed regime with smaller particles (0.2-1 mm) has shown an exponential drop of Sh_{bed} from the levels of single sphere and emulsion Sherwood numbers with the decrease of the Reynolds number as shown in Fig. 7.1. Furthermore, Kunii and Levenspiel (1968) have shown also theoretically the relation between the bed Sherwood number and particle size by highlighting the principle that Sh_{bed} decreases with the particle diameter, as shown by the experimental data in Fig. 7.2.

All the empirical data discussed above was based on experiments with a fluidized bed, where all solid particles were active in the heterogeneous reaction process. In Chapter 4, the bed Sherwood numbers were derived at the bubbling and turbulent regimes in bench- and pilot-size fluidized bed reactors combusting wood char particles in a bed of sand. In this study, the flow behavior of the char particles was assumed to be the same as the simulated flow dynamics of the bed material. The first important finding was that the Bed Sherwood numbers in the CFD simulations for the same particle sizes had a similar exponential Reynolds number response compared to the experiments of Resnick and White (1949); Kettering et al. (1950); Richardson and Szekely (1961), as highlighted in Fig. 7.2. Furthermore, the obtained bed Sherwood numbers underlined a different level of the average gas-solid mass transfer between narrower bench and wider pilot reactors. The level of the bed Sherwood numbers dropped with the increase of the reactor diameter. The reason for this was explained by the interphase mass transfer coefficients presented in Chapter 5. For the same particle size, the volumetric interphase mass transfer coefficient in the bench reactor was higher than in the pilot reactor (Fig. 5.8). This was explained by the restricted bubble size growth in the small diameter reactor and the consequently high bubble-emulsion interface areas. The same phenomenon could be seen in the Sh_{bed} - Re chart (Fig. 7.3) as an effect of the reactor diameter to the level of the bed Sherwood number. This was also supported by the experiments of Resnick and White (1949) and Kettering et al. (1950). Reactors with diameters of 2.2 cm and 4.4 cm were used in the work of Resnick and White (1949), which resulted in higher Sh_{bed} than in the work of Kettering et al. (1950) based on experiments with a reactor having the diameter of 5.9 cm.

For the middle size particles of 0.25-1.0 mm, the drop of the bed Sherwood number from the level of the emulsion Sherwood number was at its maximum one order of magnitude for the available data, as shown in Fig. 7.1. The figure presents bed Sherwood numbers

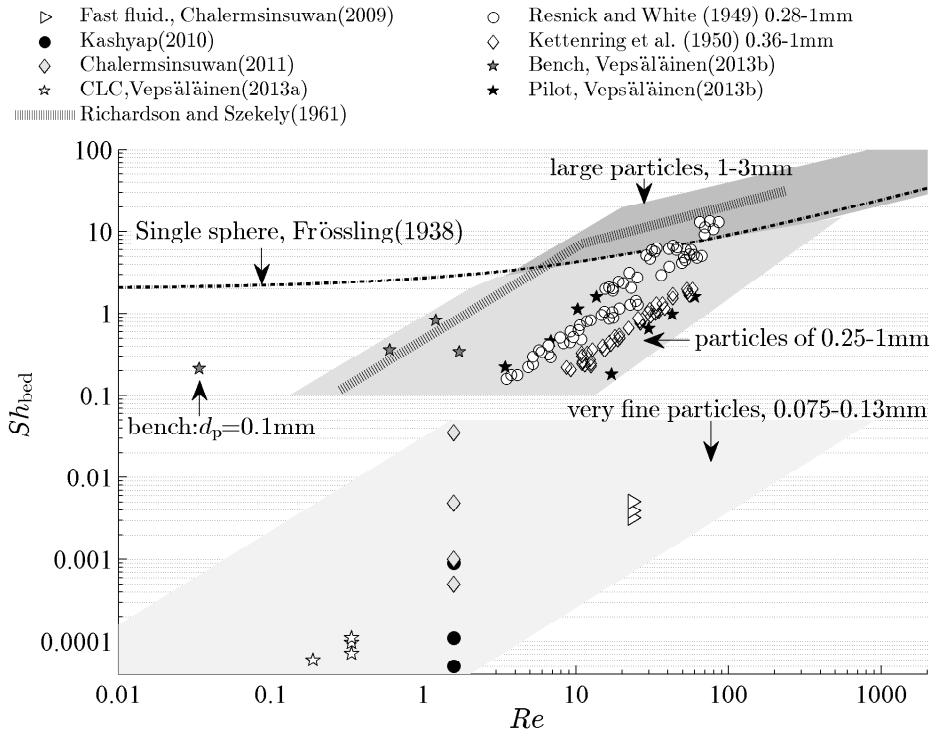

Figure 7.1: Bed Sherwood numbers against particle Reynolds numbers

for middle size particles in experiments in bubbling beds consisting of only active particles operated with a particle diameter range of 0.3-1 mm and in the CFD simulations of this thesis for char combustion in an inert bed of sand with a particle range of 0.1-1.25 mm. However, in the fine particle fluidized beds with only active solids the bed Sherwood numbers are on a remarkably lower level as highlighted in Fig. 7.1. In chapter 6, the bed Sherwood numbers were derived for the fuel reactor in a chemical looping combustion system in the bubbling and turbulent regimes. The bed Sherwood numbers obtained for the CLC process were more than four orders of magnitude lower than the emulsion mass transfer correlations for the same Reynolds number suggests. The particle diameter in the CFD simulations of chemical looping combustion process was 0.13 mm and the chemical kinetic coefficient k_{sur} was 0.001 m/s. On the other hand, the same exponential response of Sh_{bed} to Reynolds number as shown by the experiments of Resnick and White (1949); Kettering et al. (1950); Richardson and Szekely (1961) and the CFD simulations of char combustion in this thesis seems to be valid for the small particle fluidized beds consisting only active particles as shown by Fig. 7.2. This is supported further by the CFD

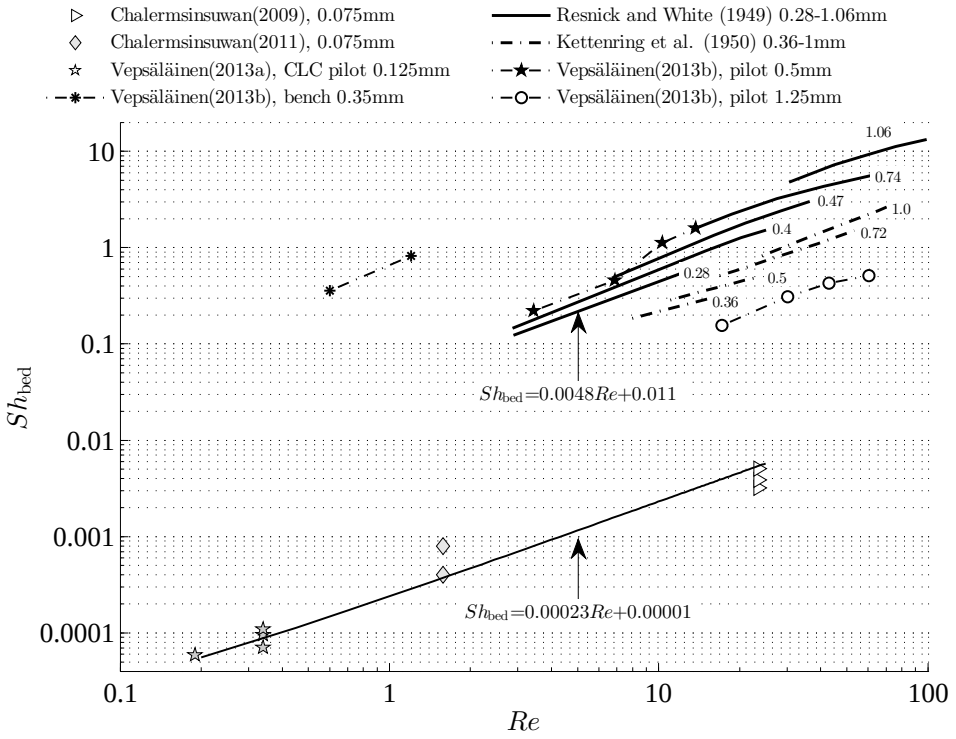

Figure 7.2: Bed Sherwood numbers of different particle diameters against the Reynolds number (CLC data adapted from Vepsäläinen et al. (2013b) and FCC data from CLC data from Chalermsinsuwan and Piumsomboon (2011)).

simulations of Chalermsinsuwan and Piumsomboon (2011) for the fluid-catalytic cracking (FCC) process operated at higher Reynolds number range with the similar chemical kinetic coefficients (k_{sur} = 0.0005-0.0025 m/s) and particle size (d_{p} = 0.075 mm).

Besides the effects of the fluidization velocity and the reactor diameter via the bubble size restriction discussed above, the bed Sherwood number in the Sh_{bed} - Re chart (Fig. 7.3) seems to be defined by the particle size, the chemical kinetic coefficients and the fraction of active solids in the bed. Chapter 5 highlighted that the interphase mass transfer coefficient is greatly influenced by the particle sizes. This indicates that the particle size dependence on Sh_{bed} (Fig. 7.2) can be explained by interphase mass transfer control. The heterogeneous reactions and the average gas-bed mass transfer in bubbling and turbulent fluidized beds seem to be increasingly under interphase mass transfer control with the decreasing particle size starting from the particle diameter of about 1 mm. Consequently, the small particle systems, the chemical looping combustion and the fluid-catalytic crack-

ing have very small bed Sherwood numbers (Fig.7.2). In these processes, also another phenomenon resisting the average gas-bed mass transfer plays an important role. As the small particle systems have a high specific surface area and the local convection to the surface of particles is fast, the local reaction rates in the small particle fluidized beds, where all particle are active, can be very fast. Thus, the local rate of the heterogeneous reaction can be higher than the local rate of interphase mass transfer, which restricts the reactive gas components from bubbles or voids to reach the whole active surface area in the solid-dense emulsion phase, as shown in Fig. 6.9 presenting a fine-particle fluidized bed, the fuel reactor of a CLC plant. In practice, this means that the reactive gas components would be mostly consumed in the interface regions of the bubble and emulsion phases. For the fine particle fluidized beds, this results in a huge drop of the bed Sherwood number. The approximate effects of the kinetic coefficient and the reactor diameter on the bed Sherwood number are presented in Fig. 7.3. The effect of the kinetic coefficient is directly proportional to the fraction of the active particles in the bed. Particularly, the huge effect of chemical kinetic coefficient on close to 0.1 mm particle diameter fluidized bed systems is highlighted in Fig. 7.3. For fine particle fluidized beds, also a slight rise of the bed Sherwood number with the increase of chemical kinetic coefficients occurs simply due to the increased reaction rates within the limited solid surface area as discussed in Chapter 6. However, the combined effect of the low rate of interphase mass transfer and high rate of heterogeneous reaction is the most important controlling mechanism in the characteristics of heterogeneous reactions in fine particle fluidized beds.

As a summary, the average gas-bed mass transfer coefficients for small-scale fluidized bed reactors of conventional and chemical looping combustion operated under the bubbling and turbulent bed conditions can be estimated from the bed Sherwood numbers presented in the thesis. All the bed Sherwood numbers follow the original theory of Kunii and Levenspiel (1968) that explains particularly the fluidization velocity response and the particle size behavior. The analysis of the results provided phenomenon-based specifications into the traditional theory of the bed Sherwood number. Most importantly, interphase mass transfer, chemical kinetic and reactor size related process-specific insights were found and highlighted.

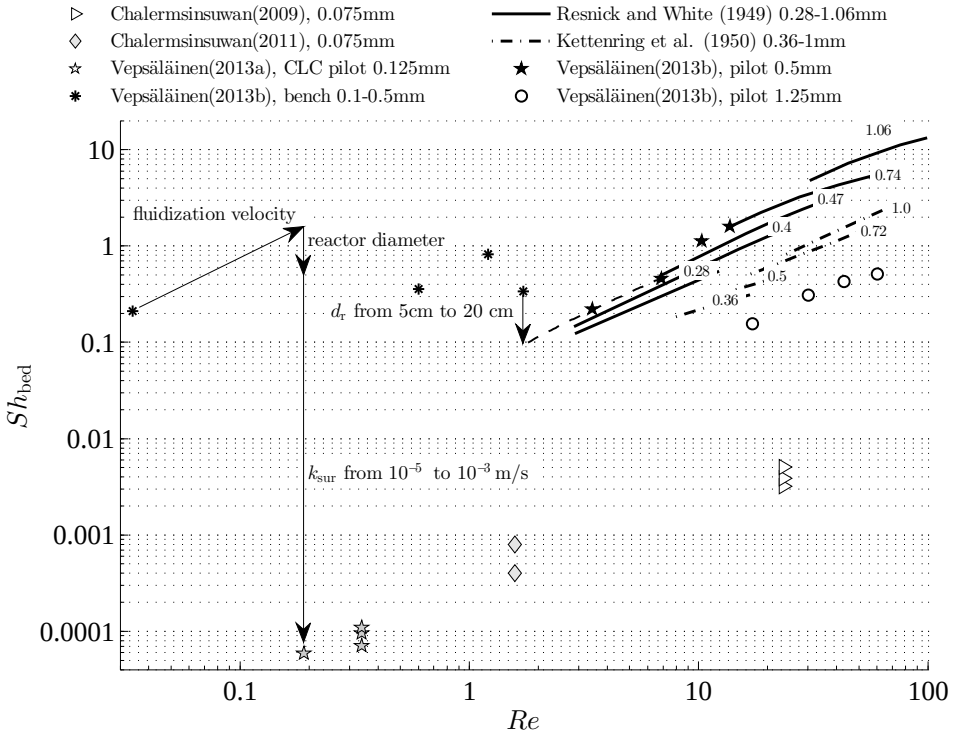

Figure 7.3: Effect of reactor diameter and chemical kinetic coefficient on the level of the bed Sherwood number.

8 Conclusions

8.1 Scientific contribution

The thesis presented an evaluation of the average gas-bed and interphase mass transfer coefficients in the dense bed region predicted by an Eulerian multiphase CFD model in the conditions prevailing in bench- and pilot-scale bubbling and circulating fluidized bed combustors. Particularly, the five research questions raised in the introduction section were answered by the theoretical review and the model-based analyses presented in the thesis. Two-fluid, gas-solid phase, Eulerian CFD simulations proposed a level for the average gas-bed mass transfer coefficient in bench and pilot scale combustors, which was approximately 2 to 5 times lower than the emulsion Sherwood number correlations with the same Reynolds number suggest. The work also showed that the Eulerian CFD model was able to predict the same response of the bed Sherwood number to the Reynolds number as the empirical results proposed, and suggested further that the response was similar in the bubbling and turbulent regimes. Furthermore, the research underlined and quantified the drop of the bed Sherwood number with increase of reactor width from the bench to the pilot scale, which is a very important aspect in the scale-up of fluidized bed reactor-related modeling and design activities. From a fundamental phenomenon research point of view, the research highlighted that the bed Sherwood number is a function of the Reynolds number, as well as the rate of interphase mass transfer, fraction of reactive material and rate of chemical kinetics.

The thesis presented also interphase mass transfer coefficients in the dense bed region derived from CFD simulations of bubbling and turbulent fluidized beds in bench- and pilot-scale combustors. The level and characteristics of the obtained interphase mass transfer coefficients corresponded with the empirical data. Simulations of large-particle fluidized beds underlined that the rate of heterogeneous reactions in fluidized beds operated with Geldart B and D particles is under combined control of the rates of interphase mass transfer and emulsion mass transfer. As a contribution to the fundamental phenomenon research, the results highlighted a strong dependence of the volumetric interphase mass transfer coefficient on the particle, bubble and reactor size, as well as on fluidization velocity. Particularly, the findings considering the particle size dependence of interphase mass transfer coefficient at the turbulent regime created new scientific knowledge. However, it was recognized that an exact definition of bubble-emulsion, or void-cluster, phases in the turbulent regime is a challenge. Consequently, an exact definition of the interphase mass transfer coefficient at the turbulent bed leaves room for further research. For the development of steady-state CFB models towards more accurate predictions of conversion performance, the analysis of the research work proposed a modelling approach with three phases, as a void-dilute emulsion-cluster, which is analytical to the bubble-cloud-emulsion description commonly applied in bubbling bed models. Of course, this approach could also be applied as sub-grid mass transfer models in Eulerian CFD models used in simulations of CFB reactors.

The analysis of all the findings regarding heterogeneous mass transfer presented in this thesis provided an extension to the theory of the bed Sherwood number (Fig. 7.1: Sh_{bed}

- Re chart) presented originally by Kunii and Levenspiel (1968). An important contribution in this was the CFD analysis of heterogeneous mass transfer in the fine-particle fluidized bed applied for chemical looping combustion. The bed Sherwood numbers in the dense bed for a fuel reactor in a pilot-scale CLC system were found to be several orders of magnitudes lower compared to the combustion process operated with larger particles. However, the bed Sherwood numbers for CLC process corresponded to the bed Sherwood numbers obtained for the fluid-catalytic cracking (FCC) process operating with similar small particle sizes and fast heterogeneous chemical kinetics. The drop of the bed Sherwood number could be explained by the different controlling mechanisms in heterogeneous mass transfer in a process having all solids active (CLC, FCC) and in a process with inert and active particles (combustion). The findings highlighted the fact that the limited rate of interphase mass transfer is a dominating phenomenon in fine-particle fluidized beds.
From the point of view of phenomenon scaling (principle in Fig. 1.1), both qualitative and quantitative changes of the derived bed Sherwood numbers and interphase mass transfer coefficients regarding the size of the reactor, bench-scale or pilot, were analyzed and explained. The scale-up aspect is important, as the empirical data on heterogeneous mass transfer coefficients presented in the literature are traditionally based on small particle sizes and low fluidization velocities in a narrow reactor. A general validity range for the heterogeneous mass transfer correlations was presented in Table 1.1. The table underlines that only a limited number of experimental data is available in the turbulent fluidization regime and of pilot size reactors. Thus, the benchmarking of the Eulerian multiphase CFD model regarding heterogeneous mass transfer provided a possibility to extend the validity range of correlations for larger reactors, coarser particle sizes and higher fluidization velocities.

8.2 Reliability and validity

Two major limitations concerning the validity of the results presented in this thesis are worth noting:

- The applied CFD modeling approach includes some uncertainties, as do all CFD models. The modeling approach was discussed in details in Chapter 3 also from the perspective of validation, but two aspects are worth mentioning here:
  (1) A two-dimensional approach was applied in the CFD modeling. As Cloete et al. (2013) report, two- and three-dimensional simulations of reactive fluidized bed result as somewhat different conversion profiles. Particularly, the different specific surface area of the bubbles (or voids) between the approaches has an effect on the rate of heterogeneous mass transfer due to changes in the rate of interphase mass transfer. An approximation for the variation of the interphase mass transfer coefficient caused by the differences of the two-to-three dimensional approaches could be achieved by correcting the two-dimensional coefficients by the ratio of specific surface areas: eg. area of sphere / area of cylinder. On the other hand, most of the CFD-based mass transfer research published in the literature suggests that the

two-dimensional approach gives about the same results as the three-dimensional approaches. Consequently, it can be concluded that the heterogeneous mass transfer results presented are valid qualitatively, and quantitatively they represent at least a close-to-realistic approximation.
(2) Thermal effects were neglected. However, it is unlikely that the inclusion of local temperature effects on the Eulerian CFD modeling would have remarkable influence on the heterogeneous mass transfer coefficients. On the other hand, the validity range of the dimensionless bed Sherwood number and dimensional interphase mass transfer coefficient correlations could be extended for a larger temperature range by simulations of different thermal and gas property conditions.

- Direct validation data was not available: only CFD simulation of a fuel reactor in a CLC plant has been compared with the available experimental data. Of course, validation of Eulerian CFD models regarding axial solid profiles has been under extensive research during the last decade. In recent years, also some CFD-based research work concerning heterogeneous mass transfer coefficients has been published. These and the experimental data on heterogeneous mass transfer coefficients presented in the literature formed the validation data of the thesis, which was characteristically indirect.

8.3 Theoretical and practical implications

Within a theoretical framework, the thesis provides beneficial knowledge in two research fields of fluidized bed technologies:

- Phenomenology of heterogeneous mass transfer: the theory of the bed Sherwood number presented originally by Kunii and Levenspiel (1968) was extended to a process-specific Sh_{bed} - Re chart. Furthermore, new knowledge regarding interphase mass transfer especially in the conditions of a fluidized bed combustor and in the turbulent regime was introduced.

- Eulerian CFD modelling of fluidized bed systems: the thesis serves as a part of Eulerian CFD model development and validation process towards more accurate predictions of reactive fluidized processes, also for large-scale reactors. While validation work of Eulerian CFD modelling has been carried out regarding solid flow dynamics, heterogeneous mass transfer coefficients by the Eulerian CFD modeling in fluidized bed combustion conditions have not been presented earlier. On the other hand, the thesis presents a methodology to derive heterogeneous mass transfer coefficients from CFD simulations, which can be applied also in cost-efficient research of other phenomenona in fluidized beds, e.g. solid dispersion.

A direct practical implication of the thesis is a possibility for more accurate design and optimization of fluidized bed reactors, especially in the phase of designing scale-up of a proven reactor size (see Fig. 1.1). The interpreted bed Sherwood numbers in the dense

bed region can be applied for the steady-state one-, two- and three-dimensional circulating fluidized bed models (e.g. Hyppänen et al. (1991), Pallares and Johnsson (2008)), which utilize the plug flow approach in a calculation cell, to describe the average gas-to-particle mass transfer. With a correct bed Sherwood number, these models can use the real heterogeneous chemical kinetic coefficients. This is a huge benefit, as it is commonly known that the heterogeneous reactivity tests in different size devices result in different effective kinetic coefficients, and a main reason for this is the different gas-solid contact between the tests. Besides bench-to-pilot scaling, the knowledge of gas-bed mass transfer is relevant also for pilot-to-industrial CFB reactor scale-up as discussed in Vepsäläinen et al. (2009). The importance of the interphase mass transfer coefficient is similar, as it has to be applied in bubble-emulsion (void-cluster) phase models, and it could provide additional accuracy to predictions of chemical reactions in fluidized beds, e.g. as the formation of gaseous emissions.

8.4 Recommendations for further research

The multiphase Eulerian CFD model provides a versatility of research opportunities from the concept of phenomenon scaling to the performance of fluidized bed processes.

- Fundamental phenomenon research of heterogeneous mass transfer with Eulerian CFD model should be combined with experimental research by validation and verifications of benchmark tests. After experimental validation, the CFD approach provides a possibility for extensive expansion of the validity ranges of mass transfer correlations. This would enhance the related phenomenon scaling work and prediction accuracy in process scale-up.

- Regarding the bed Sherwood number, a precise process-dependent Sh_{bed} - Re chart is proposed to be formulated with information on the size of the reactor, chemical kinetics, the fraction of active solids, and the diameter of solids.

- Further CFD-based research in the field of heterogeneous mass transfer should consider the effect of particle size distribution and the expansion of thermal validity range, as currently proper scientific knowledge on these issues is not available in the literature. In addition, mass transfer research could be focused on other specific regions of the fluidized bed, such as the region above fluidization gas feeding, splashing region, wall layer and upper lean region.

- In order to increase the prediction accuracy of reaction rates and paths, a new modeling approach is suggested for steady-state CFB reactor models with three separate phases as void-dilute emulsion-emulsion. This approach would be analytical to the fluidization models of bubbling bed models, which commonly have bubble-cloud-emulsion phases.

- Both the bed Sherwood number and the interphase mass transfer coefficient provide opportunities for establishing further analogical relationships with heat transfer and

momentum exchange in different flow structures of fluidized beds, such as gas-bed, bubble-emulsion or void-cluster.

- Similar research methodology to the one presented in the thesis can be applied for fundamental research of other phenomenona in fluidized beds e.g. gas and solid dispersion.
- Development of a reacting solid particle model with low CPU time consumption and a heterogeneous mass transfer model for large calculation grid sizes in the Eulerian CFD model would offer a totally new practical analysis tool for large-scale fluidized bed reactors .

At a general, fluidized bed research community level, it is proposed that public electrical databases for the results of phenomenon experiments and benchmarking process tests were developed. Also, simple steady-state one-dimensional (1D) BFB and 1.5D CFB model codes that have reached a certain academic maturity could be available for a fast-to-benchmark capability for scientists working in the various research fields of fluidized bed technologies.

References

Abad, A., et al. (2007). Mapping of the range of operational conditions for Cu-, Fe-, and Ni-based oxygen carriers in chemical-looping combustion. *Chemival Engineering Science*, 62, pp. 533–549.

Abba, I.A., Grace, J., Bi, H.T., and Thompson, M.L. (2003). Spanning the flow regimes: Generic fluidized-bed reactor model. *AICHE Journal*, 49, pp. 1838–1848.

Abdulally, I., et al. (2012). *ALSTOM's chemical looping combustion prototype for CO_2 capture from existing pulverized coal fired plants*. Technical report. DOE, NETL project NT0005286.

Adanez, J., et al. (1995). A model for prediction of carbon combustion efficiency in circulating fluidized bed combustors. *Fuel*, 74, pp. 1049–1056.

Adanez, J., et al. (2012). Progress in chemical-looping combustion and reforming technologies. *Progress in Energy and Combustion Science*, 38, pp. 215–282.

Agrawal, K., Loezos, P., Syamlal, M., and Sundaresan, S. (2001). The role of meso-scale structure in rapid gas-solid flows. *Journal of Fluid Mechanics*, 445, pp. 151–185.

Andrews, A., Loezos, P., and Sundaresan, S. (2005a). Coarse-Grid Simulation of Gas-Particle Flows in Vertical Risers. *Industrial & Engineering Chemistry Research*, 44, pp. 6022–6037.

Andrews, A., Loezos, P., and Sundaresan, S. (2005b). Coarse-grid simulation of gas-particle flows in vertical risers. *Industrial and Engineering Chemistry Research*, 44, p. 6022.

Anthony, E. and Hack, H. (2013). Oxy-fired fluidized bed combustion: technology, prospects and new developments. In: Scala, F., ed., *Fluidized bed technologies for near-zero emission combustion and gasification*, pp. 867–894. Woodhead Publishing, ISBN 978-0-85709-541-1.

Avedesian, M. and Davidson, J. (1973). Combustion of carbon particles in a fluidised bed. *Transactions of Institution of Chemical Engineers*, 51, pp. 121–131.

Basu, P. (1999). Combustion of coal in circulating fluidized-bed boilers: a review. *Chemical Engineering Science*, 54, pp. 5547–5557.

Basu, P. (2013). *Biomass gasification, pyrolysis and torrefaction - practical design and theory*, chap. Design of biomass gasifiers, pp. 420–459. Academic Press, ISBN 0123964881.

Behie, I. and Kehoe, P. (1973). The grid region in a fluidized bed reactor. *AIChE Journal*, 19, pp. 1070–1072.

Benyahia, S. (2012). Fine-grid simulations of gas-solids flow in a circulating fluidized bed. *AIChE Journal*, 58, pp. 3589–3592.

Benyahia, S., Arastoopour, H., Knowlton, T., and Massah, H. (2000). Simulation of particles and gas flow behavior in the riser section of a circulating fluidized bed using the kinetic theory approach for the particulate phase. *Powder Technology*, 112, pp. 24–33.

Bi, H.T., Ellis, N., Abba, I.A., and Grace, J.R. (2000). A state-of-the-art review of gas-solid turbulent fluidization. *Chemical Engineering Science*, 55, pp. 4789–4825.

Breault, R.W. (2006). A Review of gas-solid dispersion and mass transfer coefficient correlations in circulating fluidized beds. *Powder Technology*, 163, pp. 9–17.

Chalermsinsuwan, B. and Piumsomboon, P. (2011). Computation of the mass transfer coefficient of FCC particles in a thin bubbling fluidized bed using two- and three-dimensional CFD simulations. *Chemical Engineering Science*, 66, pp. 5602–5613.

Chalermsinsuwana, B., Piumsomboona, P., and Gidaspow, D. (2009). Kinetic theory based computation of PSRI riser, Part II: Computation of mass transfer coefficient with chemical reaction. *Chemical Engineering Science*, 64, pp. 1212–1222.

Chiba, T. and Kobayashi, H. (1970). Gas exchange between the bubble and emulsion phases in gas-solid fluidized Beds. *Chemical Engineering Science*, 25, pp. 1375–1385.

Chu, J., Kalil, J., and Wetteroth, W. (1953). Mass transfer in a fluidized bed. *Chemical Engineering Progress*, 49, pp. 141–149.

Cloete, S., Johansen, S.T., and Amini, S. (2012). An assessment of the ability of computational fluid dynamic models to predict reactive gas-solid flows in a fluidized bed. *Powder Technology*, 215-216, pp. 15–25.

Cloete, S., Johansen, S.T., and Amini, S. (2013). Investigation into the effect of simulation a 3D cylindrical fluidized bed reactor on a 2D plane. *Powder Technology*, 239, pp. 21–35.

Davidson, J.F. and Harrison, D. (1963). *Fluidised particles*. University Press, Cambridge, ISBN 0521047897.

Davidson, J., Paul, R., Smith, M., and Duxbury, H. (1959). Rise of bubbles in fluidized Beds. *Transactions of the Institution of Chemical Engineers*, 37, p. 323.

Delvosalle, C. and Vanderschuren, J. (1985). Gas-to-particles and particle-to-particle heat transfer in fluidized beds of large particles. *Chemical Engineering Science*, 40, pp. 769–779.

Dong, W., Wang, W., and Li, J. (2008a). A multiscale mass transfer model for gas-solid riser flows, Part I: Sub-grid model and simple tests. *Chemical Engineering Science*, 63, pp. 2798–2810.

Dong, W., Wang, W., and Li, J. (2008b). A multiscale mass transfer model for gas–solid riser flows, Part II: Sub-grid simulation of ozone decomposition. *Chemical Engineering Science*, 63, pp. 2811–2823.

Enwald, H., Peirano, E., and Almstedt, A. (1996). Eulerian two-phase flow theory applied to fluidization. *International Journal of Multiphase Flow*, 22, pp. 21–66.

Farag, H., Ege, P., Grislingås, A., and De Lasa, H. (1997). Flow patterns in a pilot plant-scale turbulent fluidized bed reactor: Concurent application of tracers and fiber optic sensors. *Canadian Journal of Chemical Engineering*, 75, pp. 851–860.

Foka, M., Chaouki, J., and Klvana, D. (1996). Gas phase hydrodynamics of a gas-solid turbulent fluidized bed reactor. *Chemical Engineering Science*, 51, pp. 713–723.

Froment, G. and Bischoff, K. (1990). *Chemical Reactor Analysis and Design*, 2nd edn. Wiley Series in Chemical Engineering, ISBN 0-471-51044-0.

Frössling, N. (1938). The evaporation of falling drops. *Gerlands Beiträge zur Geophysik*, 52, pp. 170–216.

Fryer, C. and Potter, O. (1972). Countercurrent backmixing model for fluidized bed catalytic reactors. Applicability of simplified solutions. *Industrial & Engineering Chemistry Fundamentals*, 11 (3), p. 338.

Furuzaki, S., Nozaki, Y., and Nakagiri, K. (1984). Mass transfer coefficients and amounts of direct-contact-catalyst in fluidized catalyst beds. *The Canadian Journal of Chemical Engineering*, 62, Issue 5, pp. 610–616.

Gidaspow, D., Bezburuah, R., and Ding, J. (1992). Hydrodynamics of Circulating Fluidized Beds, Kinetic Theory Approach. In: Potter, O., ed., *Proceedings of the 7th Engineering Foundation Conference on Fluidization*, pp. 75–82. May 1992, Brisbane, Australia.

Gómez-Barea, A. and Leckner, B. (2010). Modeling of biomass gasification in fluidized bed. *Progress in Energy and Combustion Science*, 36, pp. 444–509.

Grace, J.R. (1986a). Contacting modes and behaviour classification of gas-solid and other two-phase suspensions. *The Canadian Journal of Chemical Engineering*, 64, pp. 353–363.

Grace, J.R. (1986b). Fluid beds as chemical reactors. In: Geldart, D., ed., *Gas fluidization technology*, pp. 285–339. Chichester: John Wiley & Sons, ISBN 0471908061 9780471908067.

Gungor, A. and Eskin, N. (2008). Two-dimensional coal combustion modeling of CFB. *International Journal of Thermal Sciences*, 47, pp. 157–174.

Gunn, D. (1978). Transfer of heat or mass to particles in fixed and fluidized beds. *International Journal of Heat and Mass Transfer*, 21, pp. 467–476.

Halder, P., Datta, A., and Chattopadhyay, R. (1993). Combustion of single char particles in a turbulent fluidized bed. *The Canadian Journal of Chemical Engineering*, 71, pp. 3–9.

Hannes, J., Bleek, C., and Renz, U. (1995). The IEA model for circulating fluidized bed combustion. In: Heinschel, K., ed., *Proceedings of the 13th International Conference on Fluidized Bed Combustion*, pp. 287–296. May 1995, Orlando, Florida.

Harris, A., Thorpe, R., and Davidson, J. (2002). Characterization of the annular film thickness in circulating fluidized-bed risers. *Chemical Engineering Science*, 57, pp. 2579–2587.

Hatano, H. and Ishida, M. (1986). Interphase mass transfer in a three-dimensional fluidized bed. In: Ostergaard, K. and Soorensen, A., eds, *Proceedings of the 5th Engineering Foundation conference on fluidization*, pp. 119–127. May 1986, Elsinore, Denmark.

Hayhurst, A.N. and Parmar, M.S. (2002). Measurement of the Mass Transfer Coefficient and Sherwood Number for Carbon Spheres Burning in a Bubbling Fluidized Bed. *Combustion and Flame*, 130, pp. 361–375.

Higbie, R. (1935). The rate of absorption of a pure gas into a still liquid during short periods of exposure. *Transactions of the Institution of Chemical Engineers*, 35, pp. 36–60.

Hilligardt, K. and Werther, J. (1986). Local bubble gas-holdup and expansion of gas/solid fluidized beds. *German Chemical Engineering*, 9, pp. 215–221.

Ho, T.C. (2003a). Mass Transfer. In: Yang, W.C., ed., *Handbook of Fluidization and Fluid-particle Systems*. Marcel Dekker, ISBN 9780824702595.

Ho, T.C. (2003b). Modeling. In: Yang, W.C., ed., *Handbook of Fluidization and Fluid-particle Systems*. Marcel Dekker, ISBN 9780824702595.

Horio, M. (1997). Hydrodynamics. In: Grace, J., Avidan, A., and Knowlton, T., eds, *Circulating fluidized Beds*. Blackie Academic & Professional, London, ISBN 0751402710.

Hotta, A., et al. (2008). CFB technology provides solutions to combat climate change. In: Yue, G., Zhang, H., Zhao, C., and Luo, Z., eds, *Proceedings of the 9th International Conference on Circulating Fluidized Beds*, pp. 11–17, keynote. May 2008, Hamburg, Germany.

Hou, B., Li, H., and Zhu, Q. (2010). Relationship between flow structure and mass transfer in fast fluidized bed. *Chemical Engineering Journal*, 163, pp. 108–118.

Hovmand, S. and Davidson, J. (1971). Pilot plant and laboratory scale fluidized reactors at high gas velocities: the relevance of slug flow. In: Davidson, J. and Harrison, D., eds, *Fluidization*. Academic Press, London and New York, ISBN 0-12-2055504.

Hua, Y., Flamant, G., Lu, J., and Gauthier, D. (2004). Modelling of axial and radial solid segregation in a CFB boiler. *Chemical Engineering and Processing*, 43, pp. 971–978.

Huilin, L., et al. (2000). A coal combustion model for circulating fluidized bed boilers. *Fuel*, 79, pp. 165–172.

Hulme, I., Clavelle, E., Lee, L., and Kantzas, A. (2005). CFD Modeling and Validation of Bubble Properties for a Bubbling Fluidized Bed. *Industrial & Engineering Chemistry Research*, 44, pp. 4254–4266.

Hyppänen, T., Lee, Y., and Rainio, A. (1991). A Three-Dimensional Model for Circulating Fluidized Bed Boilers. In: Anthony, E., ed., *Proceedings of the 11th International Conference on Fluidized Bed Combustion*, pp. 439–448. September 1991, Montreal, Canada.

Igci, Y., andrews, A., Sundaresan, S., and Pannala, S. (2008). Filtered two-fluid models for fluidized gas-particle suspensions. *AIChE Journal*, 54 (6), pp. 1431–1448.

Jain, M., Sathiyamoorthy, D., and Govardhana, R. (2013). A new model for bubbling fluidized bed reactors. *Chemical Engineering Research and Design*, Article in Press.

Johnsson, F., Andersson, S., and Leckner, B. (1991). Expansion of a freely bubbling fluidized bed. *Powder Technology*, 68 (2), pp. 117–123.

Johnsson, F. and Leckner, B. (1995). Vertical distribution of solids in a CFB-furnace. In: Heinschel, K., ed., *Proceedings of the 13th International Conference on Fluidized Bed Combustion*, pp. 671–679. May 1995, Orlando, Florida, USA.

Kai, T., Imamura, T., and Takahashi, T. (1995). Hydrodynamic influences on mass transfer between bubble and emulsion phases in a fine particle fluidized bed. *Powder technology*, 83, pp. 105–110.

Kallio, S. (2005). Comparison of simulated and measured voidage and velocity profiles and fluctuations in a CFB riser. In: *Proceedings of the 8th International Conference on the Circulating Fluidized Beds*, pp. 105–112. May 2005, Hangzhou, China.

Kashyap, M. and Gidaspow, D. (2010). Computation and measurements of mass transfer and dispersion coefficients in fluidized beds. *Powder Technology*, 203, pp. 40–56.

Kato, K. and Wen, C. (1969). Bubble assemblage model for fluidized bed catalytic reactors. *Chemical Engineering Science*, 24, p. 1351.

Kettering, K., Manderfield, E., and Smith, J.M. (1950). Heat and Mass Transfer in Fluidized System. *Chemical Engineering Progress*, 46, pp. 139–145.

Knoebig, T., Luecke, K., and Werther, J. (1999). Mixing and reaction in the circulating fluidized bed - A three-dimensional combustor model. *Chemical Engineering Science*, 54, pp. 2151–2160.

Kunii, D. and Levenspiel, O. (1968). Bubbling bed model for kinetic processes in fluidized beds. *I&EC Process Design and Development*, 7, pp. 481–492.

Kunii, D. and Levenspiel, O. (1990). Entrainment of solids from fluidized beds I. Hold-up of solids in the freeboard II. Operation of fast fluidized beds. *Powder Technology*, 61, pp. 193–206.

Kunii, D. and Levenspiel, O. (1991). *Fluidization Engineering*. Butterworth-Heinemann series in chemical engineering, ISBN 0-409-90233-0.

La Nauze, R. and Jung (1983b). Mass transfer of oxygen to a burning particle in a fluidized bed. In: *Proceedings of the 8th Australian fluid mechanism conference*, pp. 5C.1–5C.4. November 1983, New South Wales, Australia.

La Nauze, R. and Jung, K. (1982). The kinetic of combustion of petroleum coke particles in a fluidized-bed combustor. In: *The 19th international symposium on combustion*, pp. 1087–1092. The Combustion Institute, Pittsburg.

La Nauze, R., Jung, K., and Kastl, J. (1984). Mass transfer to large particles in fluidised beds of smaller particles. *Chemical Engineering Science*, 39, Issue 11, pp. 1623–1633.

Li, J. (1994). *Particle-Fluid Two-Phase Flow: The Energy-Minimization Multi-Scale Method*. Metallurgical Industry Press, ISBN 7502415726.

Li, J. and Wang, L. (2002). Concentration distributions during mass transfer in circulating fluidized beds. In: *Proceedings of the 7th International Conference on Circulating Fluidized Beds*. May 2002 , Niagra Falls. Ontario, Canada.

Luecke, K., Hartge, E.U., and Werther, J. (2004). A 3D Model of Combustion in Large-Scale Circulating Fluidized Bed Boilers. *International Journal of Chemical Reactor Engineering*, 2, p. Article A11.

Mattisson, T., Jerndal, E., Linderholm, C., and Lyngfelt, A. (2011). Reactivity of a spray-dried NiO/NiAl2O4 oxygen carrier for chemical-looping combustion. *Chemical Engineering Science*, 66, pp. 4636–4644.

Miyauchi, T., Furusaki, S., Yamada, K., and Matsumura, M. (1980). Experimental determinations of the vertical distribution of contact efficiency inside fluidized catalysts. In: Grace, J.R. and Matsen, J.M., eds, *Proceedings of the 1980 International Fluidization Conference*, pp. 571–585. August 1980, Newhampshire, England.

Mori, S. and Wen, C. (1975). Estimation of bubble diameter in gaseous fluidized beds. *AIChe Jounal of Chemical Engineering Research and Development*, 21, pp. 642–655.

Murray, J. (1965). On the mathematics of fluidization: Part1. Fundamental equations and wave propagation. *Journal of Fluid Mechanics*, 21, pp. 465–493.

Myöhänen, K. (2011). *Modelling of combustion and sorbent reactions in three-dimensional flow environment of a circulating fluidized bed furnace*. Ph.D. thesis. Lappeenranta University of Technology.

Myöhänen, K. and Hyppänen, T. (2011). A Three-Dimensional Model Frame for Modelling Combustion and Gasification in Circulating Fluidized Bed Furnaces. *International Journal of Chemical Reactor Engineering*, 9, p. Article A25.

Myöhänen, K., Hyppänen, T., and Loschkin, M. (2005). Converting measurement data to process knowledge by using three-dimensional furnace model. In: *Proceedings of the 8th International Conference on Circulating Fluidized Beds*, pp. 306–312. May 2005, Hangzhou, China.

Myöhänen, K., Hyppänen, T., Miettinen, J., and Parkkonen, R. (2003). Three-dimensional modeling and model validation of circulating fluidized bed combustion. In: *Proceedings of the 17th International Conference on Fluidized Bed Combustion*, pp. 293–304. May 2003, Jacksonville, Florida, USA.

Myöhänen, K., Hyppänen, T., and Vepsäläinen, A. (2006). Modelling of circulating fluidized bed combustion with a semi-empirical three-dimensional model. In: *Proceedings of the 47th Conference on Simulation and Modelling*, pp. 194–199. September 2006, Helsinki, Finland.

Nikolopoulos, A., et al. (2010). An advanced EMMS scheme for the prediction of drag coefficient under a 1.2 MWth CFBC isothermal flow - Part II: Numerical implementation. *Chemical Engineering Science*, 65 (13), pp. 4089–4099.

Nozaki, Y., Furuzaki, S., and Miyauchi, T. (1985). Determination of the parameters of a fluidized bed of fine catalyst particles by gas absorption. *International Chemical Engineering*, 35, pp. 499–506.

Pallares, D. and Johnsson, F. (2008). Modeling of fuel mixing in fluidized bed combustors. *Chemical Engineering Science*, 63, pp. 5663–5671.

Patridge, B. and Rowe, P. (1966). Chemical reaction in a bubbling gas-fluidized bed. *Transactions of the Institution of Chemical Engineers*, 44, pp. 335–348.

Peltola, P., et al. (2013). One-dimensional modelling of chemical looping combustion in dual fluidized bed reactor system. *International Journal of Greenhouse Gas Control*, 16, pp. 72–82.

Preto, F. (1986). *Studies and modelling of atmospheric fluidized bed combustion of coal*. Ph.D. thesis. Queens University, Ontario, Canada.

Prins, W. (1987). *Fluidized bed combustion of a single carbon particle*. Ph.D. thesis. Twente University, The Neatherlands.

Prins, W., Casteleijn, W.D., and van Swaaij, W. (1985). Mass transfer from a freely moving single sphere to the dense phase of a gas fluidized bed of inert particles. *Chemical Engineering Science*, 40, pp. 481–497.

Pröll, T., Kolbitsch, P., Bolhár-Nordenkampf, J., and Hofbauer, H. (2009). A novel dual circulating fluidized bed system for chemical looping processes. *Environmental and Energy Engineering*, 55, pp. 3255–3265.

Qi, H., Li, F., Xi, B., and You, C. (2007). Modeling of drag with the Eulerian approach and EMMS theory for heterogeneous dense gas-solid two-phase flow. *Chemical Engineering Science*, 62, 6, pp. 1670–1681.

Rangel, N. and Pinho, C. (2011). Kinetic and diffusive data from batch combustion of wood chars in fluidized bed. *Biomass and bioenergy*, 35, pp. 4124–4133.

Ranz, W. and Marshall, W. (1952). Evaporation from drops, Part I. *Chemical Engineering Progress*, 48, pp. 141–146.

Resnick, W. and White, R. (1949). Mass transfer in systems of gas and fluidized solids. *Chemical Engineering Progress*, 45, pp. 377–390.

Rhodes, M., et al. (1992). Similar profiles of solids flux in circulating fluidized bed riser. *Chemical Engineering Science*, 47, pp. 1635–1643.

Richardson, J.F. and Szekely, J. (1961). Mass transfer in a fluidized bed. *Transactions of Chemical Engineers*, 39, pp. 212–222.

Ross, I., B. and Davidson, J., F. (1981). The Combustion of Carbon Particles in a Fluidized Bed. *Trans IChemE*, 59, pp. 108–114.

Rowe, P., Claxton, K., and Lewis, J. (1965). Heat and mass transfer from a sphere in a extensive flowing fluid. *Transactions of the Institution of Chemical Engineers*, 43, pp. T14–T31.

Saraiva, P., Azevdo, J., and Carvalho, G. (1993). Mathematical simulation of a circulating fluidized bed combustor. *Combustion Science and Technology*, 93, p. 233.

Scala, F. (2007). Mass transfer around freely moving active particles in the dense phase of a gas fluidized bed of inert particles. *Chemical Engineering Science*, 62, pp. 4159–4176.

Scala, F. (2013). Particle-fluid mass transfer in multiparticle systems at low Reynolds numbers. *Chemical Engineering Science*, 91, pp. 90–101.

Schoenfelder, H., Kruse, M., and Werther, J. (1996). Two-dimensional model for circualting fluidized-Bed reactors. *AIChe Jounal of Chemical Engineering Research and Development*, pp. 1875–1888.

Shah, S. (2012). *Analysis and validation of space averaged drag model for numerical simulations of gas-solid flows in fluidized beds*. Ph.D. thesis. Lappeenranta University of Technology.

Shah, S., Ritvanen, J., Hyppänen, T., and Kallio, S. (2012). Space averaging on a gas-solid drag model for numerical simulations of a CFB riser. *Powder Technology*, 218, pp. 131–139.

Sit, S.P. and Grace, J.R. (1981). Effect of bubble interaction on interphase mass transfer in gas fluidized beds. *Chemical Engineering Science*, 36, Issue 2, pp. 327–335.

Smolders, K. and Baeyens, J. (2001). Hydrodynamic modelling of the axial density profile in the riser of a low-density circulating fluidized bed. *The Canadian Journal of Chemical Engineering*, 79, pp. 422–429.

Souza-Santos, M.L.d. (2010). *Solid Fuels Combustion and Gasification - Modeling, Simulation, and Equipment Operations*, 2nd edn. CRC Press, Taylor & Francis Group, ISBN 1420047493.

Stamatelopoulos, G.N. and Darling, S. (2008). Alstom's CFB technology. In: Yue, G., Zhang, H., Zhao, C., and Luo, Z., eds, *Proceedings of the 9th International Conference on Circulating Fluidized Beds*, pp. 3–9. keynote. May 2008, Hamburg, Germany.

Stephens, G., Sinclair, R., and Potter, O. (1967). Gas exchange between bubbles and dense phase in a fluidised bed. *Powder Technology*, 1, pp. 157–166.

Stewart, P. and Davidson, J. (1967). Slug flow in fluidized Beds. *Powder Technology*, 1, pp. 61–80.

van Swaaij, W. and Zuiderweg, F. (1973). Investigation of ozone decomposition in fluidized beds on the basis of a two-phase model. In: *Proceedings of the International Symposium on Fluidization and its Applications*, pp. B9: 25–36. October 1973, Toulouse, France.

Syamlal, M., Rogers, W., and O'Brien, T.J. (1993). *MFIX Documentation - Theory Guide*. Technical report. U.S. Department of Energy, Office of Fossil Energy, DOE/METC-94/1004 (DE94000087).

Thodos, G. and Ricetti, R. (1961). Mass transfer in the flow of gases through fluidized beds. *AIChe Jounal*, 7, pp. 442–444.

Toomey, R. and Johnstone, H. (1952). Gas fluidization and solid particles. *Chemical Engineering Progress*, 48, pp. 220–226.

Vepsäläinen, A., Shah, S., and Hyppänen, T. (2012). Heterogeneous mass transfer characteristics in char combustion at fluidized bed reactor with laboratory to pilot size fluidization scaling approach - Eulerian multiphase CFD model study. In: *Proceedings of the 21th international conference on fluidized bed combustion*, pp. 938–945. June 2012, Naples, Italy.

Vepsäläinen, A., Shah, S., Peltola, P., and Hyppänen, T. (2013a). Bed Sherwood number and chemical kinetic coefficient in a fuel reactor of chemical looping combustion by Eulerian CFD Modeling. In: *Proceedings of Fluidization XIV: From Fundamentals to Products*, pp. 275–282. May 2013, Noordwijkerhout, The Netherlands.

Vepsäläinen, A., Shah, S., Ritvanen, J., and Hyppänen, T. (2013b). Bed Sherwood number in Fluidised Bed Combustion by Eulerian CFD Modelling. *Chemical Engineering Science*, 93, pp. 206–213.

Vepsäläinen, A., Shah, S., Ritvanen, J., and Hyppänen, T. (2014). Interphase mass transfer coefficient in fluidized bed combustion by Eulerian CFD modelling. *Chemical Engineering Science*, 106, pp. 30–38.

Vepsäläinen, A., et al. (2009). Development and validation of a 3-dimensional CFB furnace model. In: *Proceedings of the 20th International Conference on Fluidized Bed Combustion*, pp. 757–763. May 2009, Xian, China.

Wang, J. and Liu, Y. (2010). EMMS-based Eulerian simulation on the hydrodynamics of a bubbling fluidized bed with FCC particles. *Powder Technology*, 197 (3), pp. 241–246.

Wang, Q., et al. (1999). A mathematical model for a circulating fluidized bed (CFB) boiler. *Energy*, 24, pp. 633–653.

Wang, S., et al. (2009). CFD studies on mass transfer of gas-to-particle cluster in a circulating fluidized bed. *Computers and Chemical Engineering*, 33, pp. 393–401.

Wang, W. and Li, J. (2007). Simulation of gas-solid two-phase flow by a multi-scale CFD Approach - Extension of the EMMS model to the sub-grid level. *Chemical Engineering Science*, 62, pp. 208–231.

Wang, W., et al. (2010). A review of multiscale CFD for gas-solid CFB modeling. *International Journal of Multiphase Flow*, 36, pp. 109–118.

Werther (1980). Modeling and scale up of industrial fluidized bed reactors. *Chemical Engineering Science*, 35, pp. 372–379.

Werther, J. and Wein, J. (1994). Expansion behaviour of gas fluidized beds in the turbulent regime. *AIChE Symposium Series*, 301 (90), pp. 31–44.

Yang, N., Wang, W., Ge, W., and Li, J. (2003). CFD simulation of concurrent-up gas–solid flow in circulating fluidized beds with structure-dependent drag coefficient. *Chemical Engineering Journal*, 96, 1-3, pp. 71–80.

Zhang, D. and van der Heyden, W. (2002). The effects of mesoscale structures on the macroscopic momentum equations for two-phase flows. *International Journal of Multiphase Flow*, 28, p. 805–822.

Zhang, N., Lu, B., Wang, W., and Li, J. (2010). 3D CFD simulation of hydrodynamics of a 150 MWe circulating fluidized bed boiler. *Chemical Engineering Journal*, 162 (2), pp. 821–828.

Zhang, X. and Qian, Y. (1997). Mass transfer between the bubble and emulsion phase in a turbulent fluidized bed with FCC particles. In: Yu, Q. and Huanqin, C., eds, *Advances in Environmental Engineering and Chemical Engineering*, pp. 190–193. Guangzhou, China: South China University of Technology Press, ISBN 7562312184.

ACTA UNIVERSITATIS LAPPEENRANTAENSIS

563. MARTIKKA, OSSI. Impact of mineral fillers on the properties of extruded wood-polypropylene composites. 2013. Diss.

564. AUVINEN, SAMI. Computational modeling of the properties of TiO2 nanoparticles. 2013. Diss.

565. RAHIALA, SIRPA. Particle model for simulating limestone reactions in novel fluidised bed energy applications. 2013. Diss.

566. VIHOLAINEN, JUHA. Energy-efficient control strategies for variable speed controlled parallel pumping systems based on pump operation point monitoring with frequency converters. 2014. Diss.

567. VÄISÄNEN, SANNI. Greenhouse gas emissions from peat and biomass-derived fuels, electricity and heat – Estimation of various production chains by using LCA methodology. 2014. Diss.

568. SEMYONOV, DENIS. Computational studies for the design of process equipment with complex geometries. 2014. Diss.

569. KARPPINEN, HENRI. Reframing the relationship between service design and operations: a service engineering approach. 2014. Diss.

570. KALLIO, SAMULI. Modeling and parameter estimation of double-star permanent magnet synchronous machines. 2014. Diss.

571. SALMELA, ERNO. Kysyntä-toimitusketjun synkronointi epävarman kysynnän ja tarjonnan toimintaympäristössä. 2014. Diss.

572. RIUNGU-KALLIOSAARI, LEAH. Empirical study on the adoption, use and effects of cloud-based testing. 2014. Diss.

573. KINNARINEN, TEEMU. Pressure filtration characteristics of enzymatically hydralyzed biomass suspensions. 2014. Diss.

574. LAMMASSAARI, TIMO. Muutos kuntaorganisaatiossa – tapaustutkimus erään kunnan teknisestä toimialasta. 2014. Diss.

575. KALWAR, SANTOSH KUMAR. Conceptualizing and measuring human anxiety on the Internet. 2014. Diss.

576. LANKINEN, JUKKA. Local features in image and video processing – object class matching and video shot detection. 2014. Diss.

577. AL-SAEDI, MAZIN. Flexible multibody dynamics and intelligent control of a hydraulically driven hybrid redundant robot machine. 2014. Diss.

578. TYSTER, JUHO. Power semiconductor nonlinearities in active d*u*/d*t* output filtering. 2014. Diss.

579. KERÄNEN, JOONA. Customer value assessment in business markets. 2014. Diss.

580. ALEXANDROVA, YULIA. Wind turbine direct-drive permanent-magnet generator with direct liquid cooling for mass reduction. 2014. Diss.

581. HUHTALA, MERJA. PDM system functions and utilizations analysis to improve the efficiency of sheet metal product design and manufacturing. 2014. Diss.

582. SAUNILA, MINNA. Performance management through innovation capability in SMEs. 2014. Diss.

583. LANA, ANDREY. LVDC power distribution system: computational modelling. 2014. Diss.

584. PEKKARINEN, JOONAS. Laser cladding with scanning optics. 2014. Diss.

585. PELTOMAA, JYRKI. The early activities of front end of innovation in OEM companies using a new FEI platform as a framework for renewal. 2014. Diss.

586. ROZHANSKY, IGOR. Resonant tunneling effects in semiconductor heterostructures. 2014. Diss.

587. PHAM, THUY DUONG. Ultrasonic and electrokinetic remediation of low permeability soil contaminated with persistent organic pollutants. 2014. Diss.

588. HOKKANEN, SANNA. Modified nano- and microcellulose based adsorption materials in water treatment. 2014. Diss.

589. HINKKANEN, JUHA. Cooperative strategy in emerging markets – analysis of interfirm R&D cooperation and performance in Russian manufacturing companies. 2014. Diss.

590. RUSKOVAARA, ELENA. Entrepreneurship education in basic and upper secondary education – measurement and empirical evidence. 2014. Diss.

591. IKÄHEIMONEN, TUULI. The board of directors as a part of family business governance – multilevel participation and board development. 2014. Diss.

592. HAJIALI, ZUNED. Computational modeling of stented coronary arteries. 2014. Diss.

593. UUSITALO, VILLE. Potential for greenhouse gas emission reductions by using biomethane as road transportation fuel. 2014. Diss.

594. HAVUKAINEN, JOUNI. Biogas production in regional biodegradable waste treatment – possibilities for improving energy performance and reducing GHG emissions. 2014. Diss.

595. HEIKKINEN, JANNE. Vibrations in rotating machinery arising from minor imperfections in component geometries. 2014. Diss.

596. GHALAMCHI, BEHNAM. Dynamic analysis model of spherical roller bearings with defects. 2014. Diss.

597. POLIKARPOVA, MARIIA.Liquid cooling solutions for rotating permanent magnet synchronous machines. 2014. Diss.

598. CHAUDHARI, ASHVINKUMAR. Large-eddy simulation of wind flows over complex terrains for wind energy applications. 2014. Diss.

599. PURHONEN, MIKKO. Minimizing circulating current in parallel-connected photovoltaic inverters. 2014. Diss.

600. SAUKKONEN, ESA. Effects of the partial removal of wood hemicelluloses on the properties of kraft pulp. 2014. Diss.

601. GUDARZI, DAVOOD. Catalytic direct synthesis of hydrogen peroxide in a novel microstructured reactor. 2014. Diss.

602. VALKEAPÄÄ, ANTTI. Development of finite elements for analysis of biomechanical structures using flexible multibody formulations. 2014. Diss.

603. SSEBUGERE, PATRICK. Persistent organic pollutants in sediments and fish from Lake Victoria, East Africa. 2014. Diss.

604. STOKLASA, JAN. Linguistic models for decision support. 2014. Diss.